THE HALL EFFECT IN TIN

by

R. C. Barklie

Churchill College, Cambridge.

Dissertation submitted to the University of Cambridge in application for the degree of Doctor of Philosophy.

P R E F A C E

This dissertation describes work carried out in the Magnetic Laboratory, Cambridge, between October 1966 and April 1969.

Until September 1968 I was fortunate to have Dr. R. C. Young as my supervisor. I am very grateful to him for suggesting the project, being a source of helpful ideas and encouragement, and providing me with some of his apparatus for which acknowledgement is made in the text. I was equally fortunate in having as his successor Professor A. B. Pippard. I am very grateful for his interest, encouragement and ideas, many of which led to an explanation of my results and acknowledgement is made for them in the text. It is a pleasure to thank D. D. Stewart, E. G. Collins and K. Franklin who have made much of my apparatus and whose good company contributed much to making my stay enjoyable. My thanks are also due to F. Sadler and P. Booth who supplied many litres of liquid helium, and to many others of the assistant staff. I would also like to thank T. Brown for allowing me to use his crystal puller and for his help and advice. I must also thank Mrs. M. Brown and Miss J. Bland for typing the thesis and Mr. W. H. Andrews for preparing the photographs.

For financial assistance I would like to thank the University of Cambridge for a Robert Gardiner Memorial scholarship and Trinity College,

Dublin, for a research exhibition.

The experimental work is essentially original and due acknowledgement has been made in the test of all sources of information used.

Finally, I declare that this dissertation is not substantially the same as any other I have submitted for a degree or diploma or other qualification at any other university.

Churchill College, Cambridge.
August, 1969.

R. C. Barklie.

CONTENTS

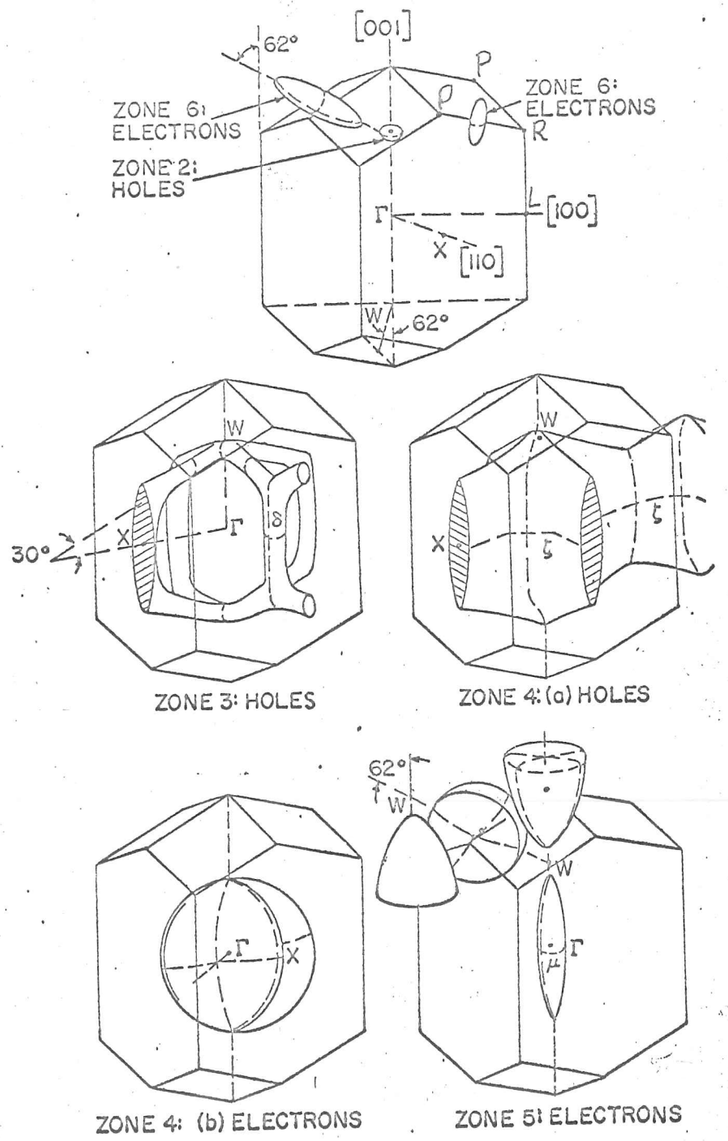

Fig. 1-1 The nearly-free-electron Fermi surface in the reduced zone scheme.

$\Gamma L = \frac{2\pi}{a}$, $\Gamma X = \frac{1}{\sqrt{2}}\left(\frac{2\pi}{a}\right)$. $a = 5.82$ Å.

Chapter 1

Introduction

A description is given of the Fermi surface of tin and some of the open orbits it can support. The phenomenon of magnetic breakdown is then discussed and the reason it might be expected to occur in tin is explained. The evidence of other workers for magnetic breakdown in tin is summarized. Finally, the aims of the present experiments are listed.

1.1) The Fermi surface of tin and some open orbits it can support

Fig. 1-1 shows the Brillouin zone for tin and the nearly-free-electron (N.F.E) model of the Fermi surface as constructed by Gold and Priestley (1). In appendix I, various cross sections of the Fermi surface are constructed using Harrison's method. Weisz(2) has also calculated the Fermi surface using an orthogonalized-plane-wave method, the parameters being determined by fitting to the size effect data of Gantmaker (3). His model is topologically similar except in a few ways which are listed

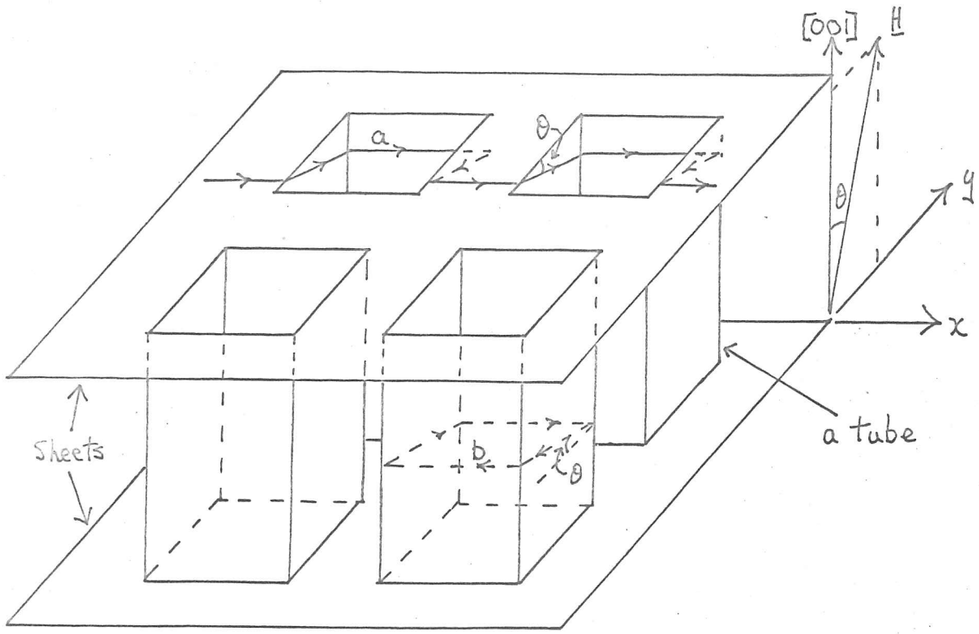

Fig. 1-2. An open surface formed by two parallel sheets pierced by tubes. It can support open orbits such as a; there is a similar open orbit going in the opposite direction on the bottom of the lower sheet. It can also support closed orbits, b. When the field is tipped sufficiently far from [001] for it to be no longer possible to have a closed orbit, b, in the connecting tube, then an open orbit on the top sheet can pass down a tube to the lower sheet where it goes in the opposite direction and eventually closes.

For the 4th zone open hole surface, $x \parallel [\bar{1}10]$ and b is the electron orbit $\mathfrak{I}$.

For the 5th zone open electron surface, $x \parallel [00]$ and b is the hole orbit λ.

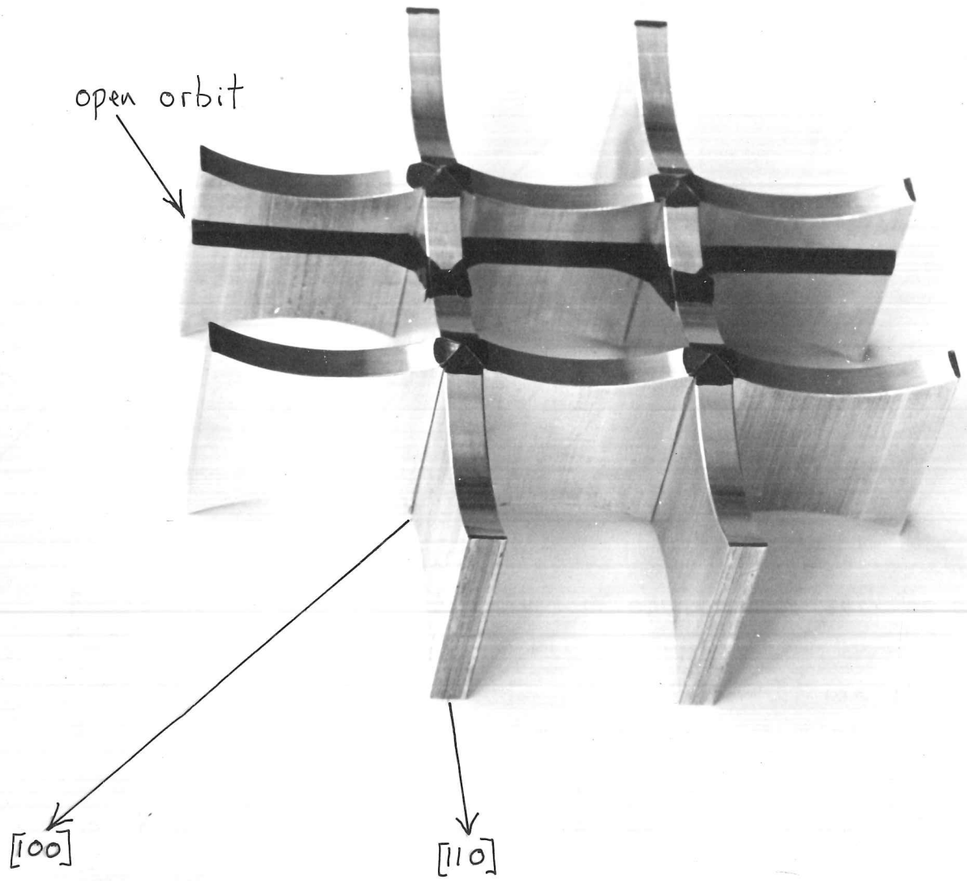

Fig. 1-3. A model of the fourth zone open hole surface showing a typical periodic open orbit which occurs when $\underline{H}$ is tipped from [001] towards $[\bar{1}\,\bar{1}\,0]$.

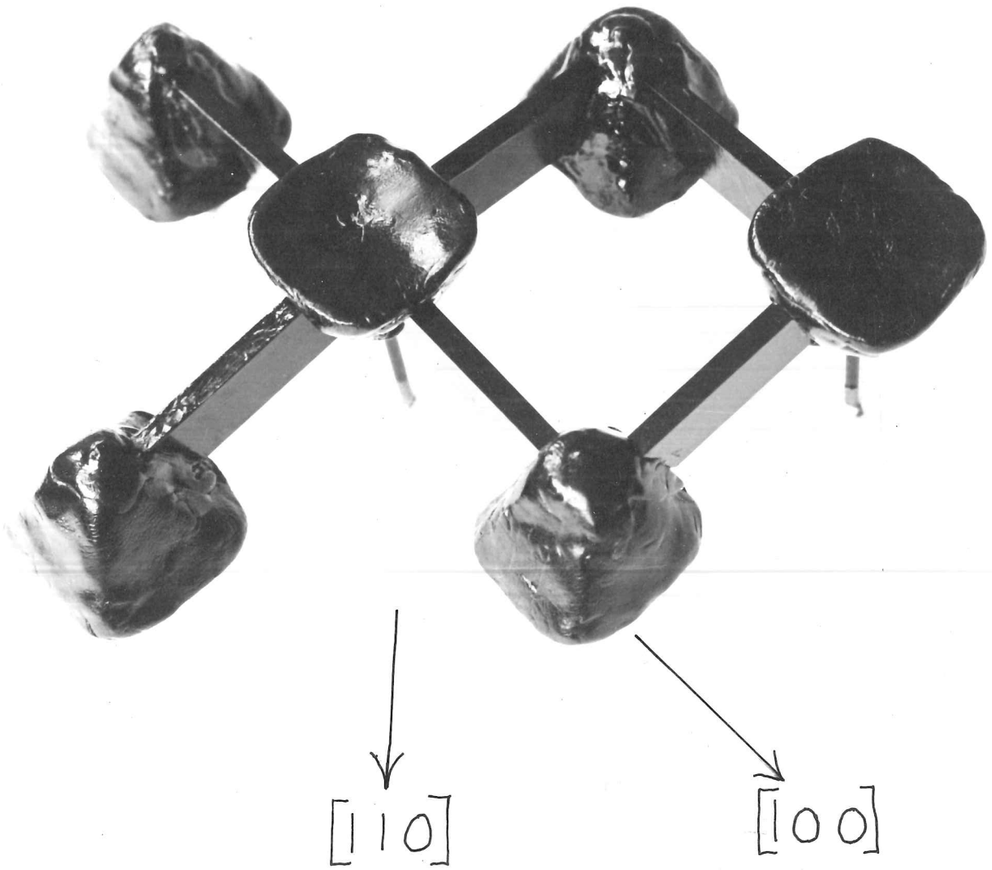

Fig. 1-4. A model of the fifth zone open electron surface. The doubles pancakes have been replaced by rectangular strips.

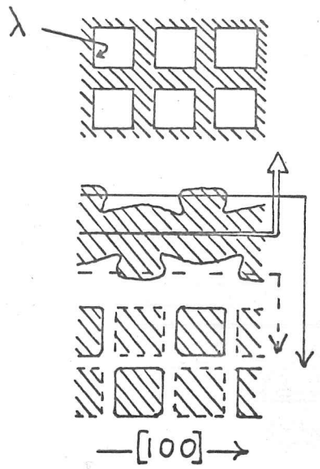

Fig. 1-5. Schematic diagram of cross sections of the fifth zone electron regions. The cross sections in the ΓLR plane (middle diagram), and cross section in two horizontal planes (upper and lower diagrams). The electron regions are shaded. The hole orbit λ is shown.

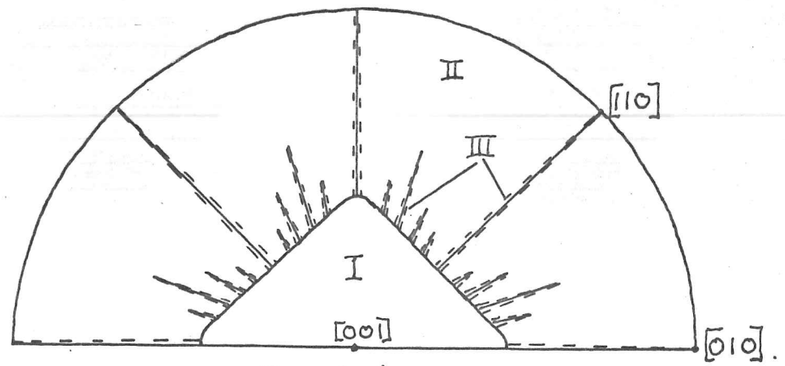

Fig. 1-6.

Stereogram of Alekseevskii et al.

Open orbits occur for magnetic field directions inside I and along the axial lines. No open orbits occur in region II. Elongated trajectories occur in regions III.

in appendix I, and we will use it as a basis for discussion.

Fortunately, for the present experiments, we will only be concerned with four of the surfaces shown in fig 1-1, namely the third zone hole surface, the fourth zone open hole surface, and the fifth zone electron surfaces of pears and double pancakes which link up to form an open electron surface. The third zone surface of Weisz differs from the N.F.E. model of Fig 1-1 in that the part near W is pinched off destroying the multiple connectivity, so that the surface consists of hole cylinders running parallel to [001]. The two open surfaces are in the form of sheets in the (001) plane each sheet being pierced by tubes, as shown in fig 1-2. A model of the fourth zone open hole surface is shown in fig. 1-3. The open electron surface formed by the fifth zone pears and double pancakes is topologically similar. The pancakes merely act as arms joining the pears and the only major difference between this open surface and the open hole surface is that in this case the two sheets are puckered rather than plane. A model of this surface in which the double pancakes have been replaced by rectangular blocks is shown in fig. 1 - 4. Some cross sections of this surface, as constructed by Weisz, are shown in fig. 1-5.

Two classes of open orbit - periodic and aperiodic - can occur in tin. The former occur in some directions of high symmetry when the magnetic field, $\underline{H}$, is perpendicular to those directions and successive elements of the open orbit are identical. Aperiodic open orbits occur for field directions around a direction of high symmetry. As Anderson and Young (4) point out, the criterion for the existence of an aperiodic open orbit in tin is that a closed orbit can be found in the connecting tube (see fig. 1-2) mentioned above. In this case it is impossible for an electron to travel from one sheet to the other, where it would travel in the opposite direction and eventually close on itself to form an extended closed orbit. The open orbits run in a direction given by the intersection of the plane perpendicular to $\underline{H}$ and the (001) plane.

The fourth zone open hole surface can support periodic open orbits when $\underline{H}$ is perpendicular to [110] as illustrated in fig. 1-3. Weisz (2) suggests that it can also support a narrow band of them when $\underline{H}$ is perpendicular to [100]. It can also support aperiodic open orbits for all field directions for which the closed electron orbit $\mathcal{S}$ exists. Similarly, the fifth

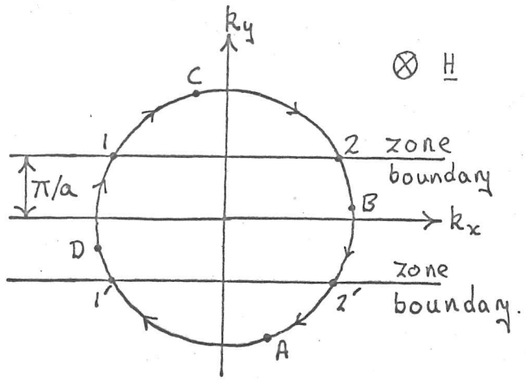

Fig. 1-7
A Fermi surface which intersects only one zone boundary, $k_y = \pm \frac{\pi}{a}$. Section taken at $k_z = 0$.

Fig 1-8 . Possible trajectories in the x-y plane :-

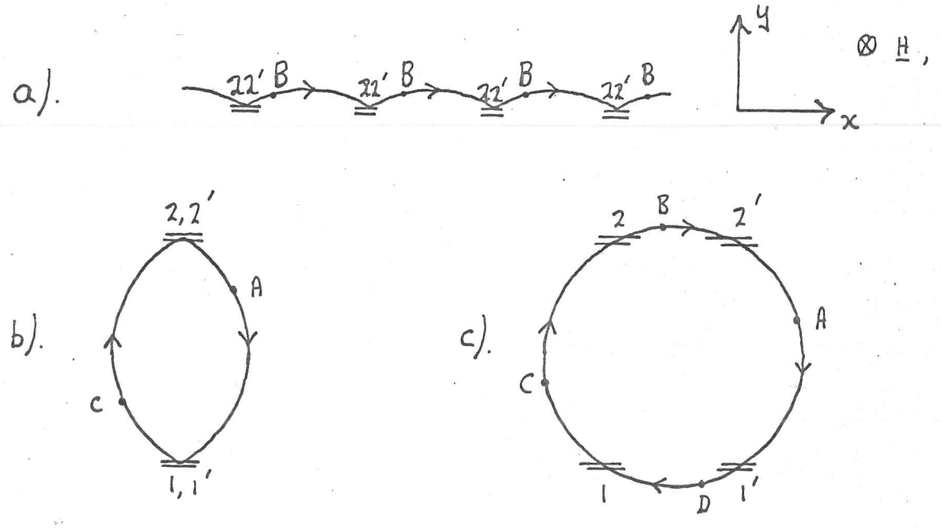

a). an open orbit.
b). a closed orbit.
c). The free electron orbit which occurs when the lattice potential is zero or when breakdown takes place.

zone surface can support periodic open orbits when H is perpendicular to [100] and Weisz (2) suggests that it can also support a narrow band of them when H is perpendicular to [110]. It can support aperiodic open orbits for all field directions for which the closed hole orbit λ exists.

Alekseevskii et al (5) have made a study of the magnetoresistance of tin and from their results have determined the extent of open orbits in tin. A stereogram illustrating the range of field directions for which open orbits occur, as found by them, is shown in fig 1 - 6.

1.2) The phenomenon of magnetic breakdown and why it is expected to occur in tin

Stark and Falicov (6) consider a hypothetical metal whose unperturbed Fermi surface is such that it intersects only one pair of zone boundaries, $k_y = \pm \frac{\pi}{a}$ where Bragg diffraction can occur (see fig. 1-7). If the zone boundaries were not there i.e. the electron-lattice interaction was zero, then only one trajectory would occur - the free electron orbit (see fig. 1-8c). Introduction of the zone boundaries with the consequent

Bragg diffraction at points 1, 1', 2, 2' leads to a splitting apart in energy of the trajectories at these points and an electron on arm B will go on an open orbit as shown in fig. 1-8a. A closed electron orbit is also formed (see fig. 1-8b). If the electron-lattice interaction is very weak, it is intuitively obvious that an intermediate regime should exist such that an electron has a probability greater than zero but less than one of being Bragg diffracted at points 1, 1', 2, 2' of Fig. 1-7. This effect which depends on the magnetic field is known as magnetic breakdown. It has been shown (7) that the transition or breakdown probability, P, at all fields is given by

$$P = \exp.\left(-H_0/H\right) \qquad (1-1)$$

where

$$H_0 \doteq \frac{m\Delta^2}{E_F \hbar e} \qquad (1-2)$$

E_F is the Fermi energy and Δ is the relevant energy gap. This result may be derived in a number of ways. Stark and Falicov (6) employ a diffraction approach and Ziman (8) shows how the result may be derived by analogy to Zener breakdown.

Let us now see whether magnetic breakdown is likely to occur in tin. Consider the cross section of the Fermi surface

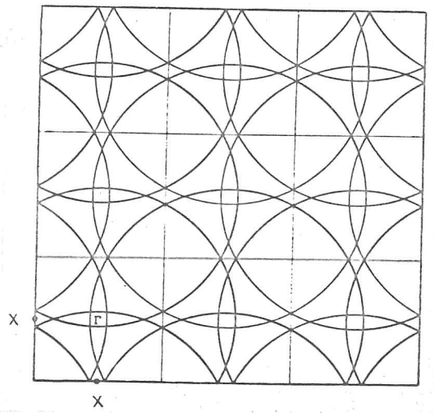

Fig. 1-9a . Sections of free-electron Fermi surfaces for a metal having the same crystal structure and same electron density as tin.

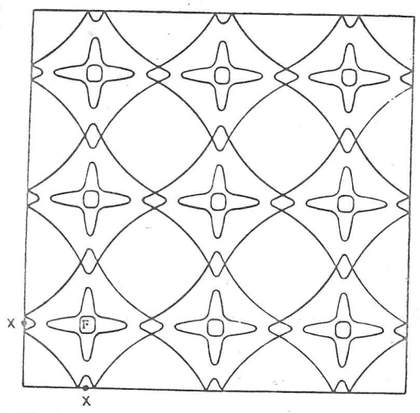

Fig. 1-9b

The effect of including the electrostatic lattice potential. (schematic).

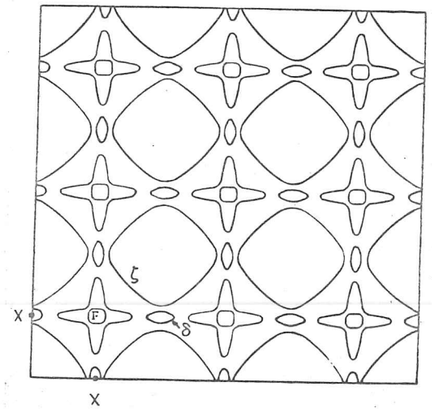

Fig. 1-9c.

The effect of including the spin-orbit interaction. (schematic).

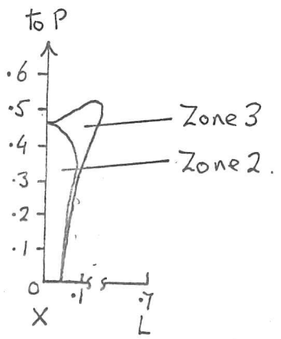

(units of 1.08×10^8 cm^{-1}).

Fig. 1-10 . The intersection of the 3rd and 4th zone hole surfaces of Weisz' model with the zone face XPL. The zone numbers for the two regions refer to the highest zone containing electrons there.

lying in the central (001) plane of the Brillouin zone as shown in fig. 1-9. In Fig. 1-9a no account is taken of the interaction of the electrons with the lattice and the surface consists of free-electron constant-energy spheres with radii fixed by the electron density in tin. The effects of including the electrostatic interaction between the electrons and the periodic potential of the lattice are shown in fig. 1-9b. The degeneracy at X is not removed, although outside the central plane, the band gap increases with height above the central plane as shown in fig. 1-10. When spin-orbit interaction is taken into account(2) the degeneracy is removed and the resulting section of the Fermi surface is shown in fig. 1-9c. As the field strength is increased breakdown becomes probable first near X since the band gap due to spin-orbit interaction is much less than the gaps introduced by the electrostatic interaction. When breakdown does occur, and with H parallel to [001], the orbits ζ and δ link up to form a two dimensional network similar to Fig. 1-9b.

Weisz (2) estimated that the splitting of the energy levels would allow magnetic breakdown to occur when a field of about 4 kg. is directed along [001].

Pippard (9, 10) shows how a network of orbits coupled by breakdown can be analyzed by treating the electron wave packets as being narrowly confined in real space to a network obtained by rotation of the k-space network through 90° about the field direction and by scaling its linear dimensions by the factor $\hbar c/eH$. Partial transmission along two paths occurs at each intersection with transmission coefficients that depend on H. When interference effects of the electron waves around the network are taken into account it is found that the transmission coefficients vary in an oscillatory manner (9, 10) with the de Haas-van Alphen frequencies of the orbits concerned. This leads to an oscillatory coupling between the orbits and thus the trajectory of an electron varies periodically and hence also the conductivity in accordance with the expression

$$\beta_{ij} = \frac{e^2}{4\pi^3 \hbar} \int L_i \, dS_j \qquad (1\text{-}3)$$

where L_i is the effective path (11) or mean distance travelled by an electron created on an element dS_j of the Fermi surface. The derivation of this expression is given in Appendix 2.

These oscillations only occur when there is phase coherence of the electrons around the orbits concerned. It needs only a few dislocations enclosed within the orbit for that orbit to suffer a phase shift of several cycles (11). When this happens, the variation of phase shift from one orbit to another leads to the randomization of the phases and results in the disappearance of quantum mechanical effects. Thus, except at very high fields, one would not expect phase coherence to be preserved on any but the smallest orbits i.e. the δ orbit in the case of tin.

1-3) Evidence for magnetic breakdown in tin

(a) When H is parallel to [001]

Strøm-Olsen (12) carried out measurements of the magnetoconductivity of a single crystal specimen (residual resistance ratio = 25,000) at 1.4°K using helicon standing waves. At magnetic field strengths $\simeq$ 120 kG directed along the c - axis, oscillations were observed in the helicon signal. Long period non-sinusoidal oscillations were recorded corresponding

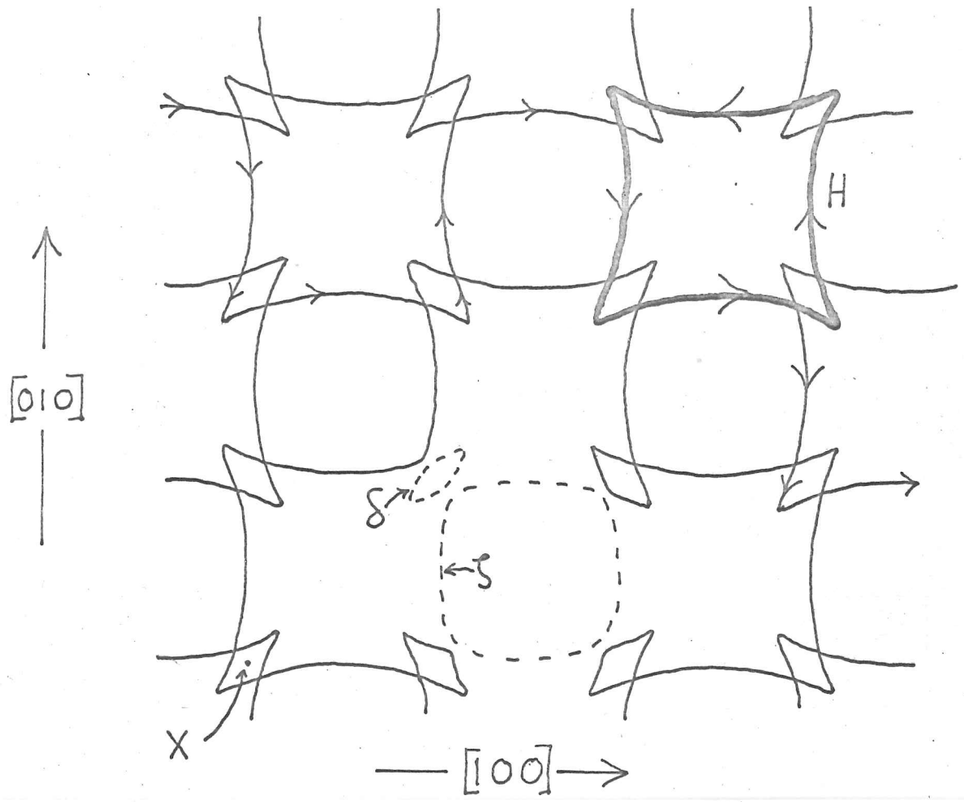

Fig 1-11. The two dimensional network of coupled orbits in the central (001) plane, with H along [001]. The dashed lines indicate the δ- and ς- orbits in low fields (no breakdown); the thick curve is a typical orbit at high fields (complete breakdown).

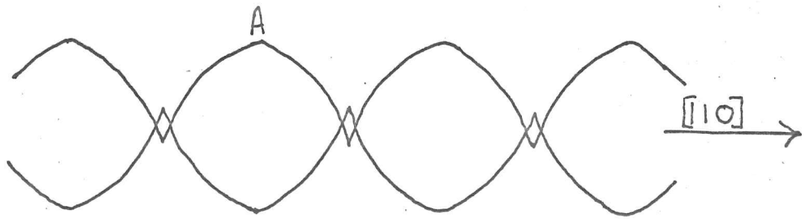

Fig. 1-12. Network formed when breakdown links ς and δ into a linear chain along [110]. H is tipped from [001] towards [$\bar{1}$10]. A is too far above the central (001) plane for breakdown to occur.

to phase coherence round the orbit δ . Superimposed on these were short period oscillations of two periods which were found to give areas within 2% of those found by Stark and Craven (13) for orbits ς and H (see fig 1 - 11) from de Haas-van Alpehn measurements. The observations were explained in terms of the linking of orbits δ and ς by magnetic breakdown to form a two dimensional network as shown in fig 1 - 11.

b) H a few degrees from [001]

Young (14) has measured the transverse magnetoresistance of a [110] single crystal ($R_{290°K}/R_{4.2°K}$ = 20,000) at 1.1°K. Magnetic fields ≒ 90 kG were applied in a direction perpendicular to [110] and 5° from [001]. Long period non-sinusoidal oscillations (f = 0.17 x 10^7G) were observed in the magneto-resistance due to phase coherence round δ . Superimposed on these were short period oscillations (f = 1.2 x 10^8 G) whose amplitude was greatest at the peak of the slow oscillations; their period corresponded to the electrons having phase coherence round orbit ς .

These results were interpreted in terms of the linking by magnetic breakdown of the δ and ξ orbits into a linear chain in the [110] direction as shown in fig. 1 - 12.

c) H more than a few degrees from [001]

Anderson and Young (4) have made measurements of the transverse magnetoresistance (i.e. E_x/J_x, where x is parallel to the crystal axis) of single crystal specimens ($R_{290^\circ K}/R_{4.2^\circ K}$ = 20,000) as the crystals were rotated about their axis in a constant magnetic field applied perpendicular to the crystal axis. Using a specimen with $\alpha = 85^\circ$, $\beta = 44^\circ$ (where α = polar angle of the specimen axis from [001] and β = azimuthal angle from [100] to the plane containing the specimen axis and [001] they obtained rotation diagrams as shown below. For clarity, the zeros for different fields are displaced.

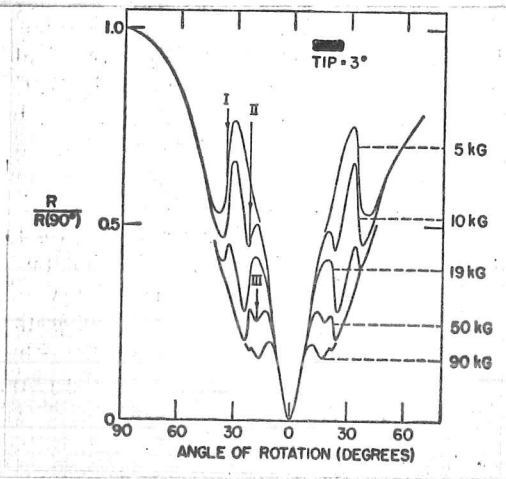

Fig 1-13. Rotation diagram of R/R(90°) (the resistance anisotropy) for the above specimen when the field passes 3° from [001], showing how the anisotropy develops between 5 and 90 kg. Anomalies I, II and III are marked.

The angle of tip is the angle between [001] and the field at its closest approach to [001], while the zero of rotation is the point of closest approach.

Although only anomalies II and III have been attributed to the effect of magnetic breakdown, it is worthwhile to explain also at this stage the occurrence of anomaly I as one of the aims of the present experiment is to look for anomalies in the Hall voltage corresponding to I, II and III.

To see how these anomalies arise, it is helpful to have an expression for the conductivity tensor. Now we have seen that the Fermi surface of tin consists of both open, and closed electron and hole, orbits. To see what the conductivity tensor looks like, consider the following simple model - a Fermi surface which consists of two spherical surfaces - one filled, the other empty - and a cylindrical surface (infinite in length in the extended zone scheme), as shown below:-

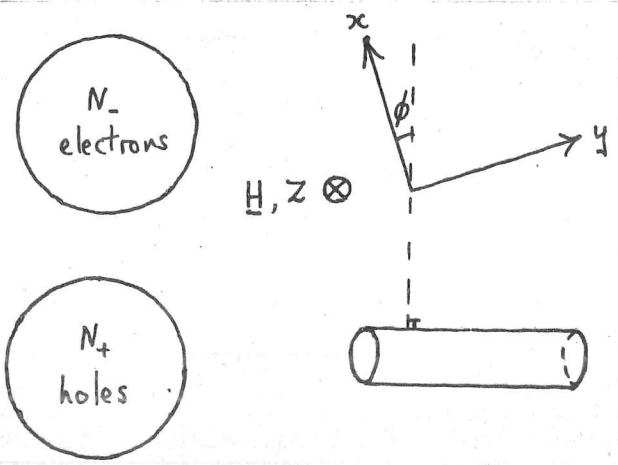

Fig. 1-14.

A model Fermi surface.

Suppose that $\underline{H}$ is applied parallel to the z-axis and that x, y are mutually perpendicular axes in a plane perpendicular to $\underline{H}$, the x-axis making an angle ϕ with the normal to the cylinder.

Electrons on the cylinder are confined to move in a direction parallel to the cylinder axis in $\underline{k}$-space and can therefore conduct only in a direction perpendicular to the cylinder axis.

Also, suppose that for the spherical sheets, the filled one contains n_- electrons of mass m_- and relaxation time τ_- and the empty one contains n_+ holes of mass m_+ and relaxation time τ_+.

To find σ_{xy} we apply an electric field along y and measure the current density along x. This gives

$$(\sigma_{xy})_{\text{closed orbits}} = \frac{e}{H}\left(\frac{n_- X_-^2}{1+X_-^2} - \frac{n_+ X_+^2}{1+X_+^2}\right)$$

where $X_+ = e\tau_+ H/m_+$, $X_- = e\tau_- H/m_-$

$$(\sigma_{xy})_{\text{open orbits}} = \sigma' \cos\phi \sin\phi$$

where σ' is the zero field conductivity of the open orbits.

The other components may be found in a similar manner to

give

$$\sigma_{ij} = \begin{bmatrix} \frac{e}{H}\left(\frac{n_- X_-}{1+X_-^2} + \frac{n_+ X_+}{1+X_+^2}\right) + \sigma' \cos^2\phi, & \frac{e}{H}\left(\frac{n_- X_-^2}{1+X_-^2} - \frac{n_+ X_+^2}{1+X_+^2}\right) + \sigma' \cos\phi \sin\phi, & 0 \\ -\frac{e}{H}\left(\frac{n_- X_-^2}{1+X_-^2} - \frac{n_+ X_+^2}{1+X_+^2}\right) + \sigma' \cos\phi \sin\phi, & \frac{e}{H}\left(\frac{n_- X_-}{1+X_-^2} + \frac{n_+ X_+}{1+X_+^2}\right) + \sigma' \sin^2\phi, & 0 \\ 0, & 0, & c \end{bmatrix} \quad (1\text{-}3)$$

where c is a constant.

Now, if the direction of the crystal axis is taken as being parallel to the x-axis, then the angle ϕ will be closely related to the angle of rotation as defined above. This can be shown as follows:-

For the model, when $\phi = 0$, the open orbit direction in k-space is perpendicular to the x-axis and when $\phi = 90^\circ$, it is parallel to it. Also, for tin, the direction of open orbits in k-space is given by the intersection of the plane perpendicular to H and the (001) plane. Thus when the angle of rotation, ϕ',

is zero, the open orbit direction in k-space is perpendicular to the crystal axis. As the angle of rotation, ϕ', is increased, the angle between the open orbit direction, $\underline{d}_k$, in k-space and the crystal axis (parallel to $\underline{J}$, the current density) decreases, as is shown in the stereograms below (fig. 1-15):-

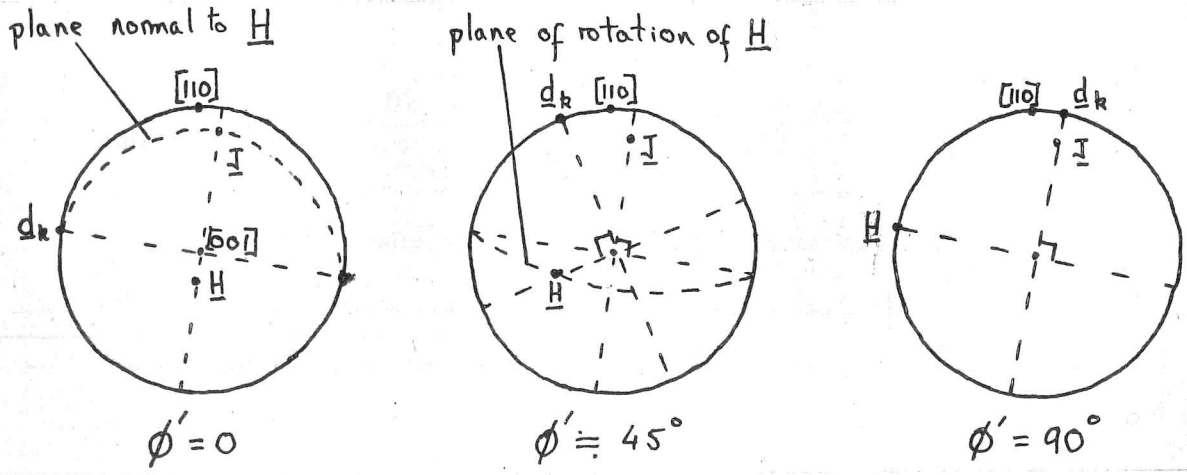

If $\underline{J}$ makes an angle α' with [001], then when $\phi' = 90^\circ$, the angle between the open orbit direction in k-space and $\underline{J}$ is $(90 - \alpha')$. Thus provided α' is close to 90°, the variation of magnetoresistance with ϕ as given by the model should closely represent the way in which it varies with angle of rotation, ϕ', in the real case.

If X_- , X_+ are both $\gg 1$ at the fields considered, then (1-3) gives

$$\rho_{xx} = \frac{(n_- Y_- + n_+ Y_+) + \beta' H^2 \sin^2 \phi}{\beta'(n_- Y_- + n_+ Y_+) + e^2 (n_- - n_+)^2} \qquad (1-4)$$

where $Y_- = \frac{m_-}{\tau_-}$, $Y_+ = \frac{m_+}{\tau_+}$

This shows why there is a steady increase in ρ_{xx} as ϕ' increases, since as ϕ increases from zero the H^2 term is introduced and the coefficient of H^2 slowly increases as ϕ increases.

Anomaly I occurs when the field is tilted 37° away from [001]. When $\underline{H}$ is tilted towards [100], anomaly I is taken to mark the range of open orbits on the fourth and fifth zone open surfaces i.e. the closed orbits ζ and λ can no longer occur. This is in agreement with Weisz' model of the Fermi surface which predicts that both ζ and λ can occur for field directions up to 37° from [001] towards [100]. Towards

[110], anomaly I is taken to mark the limit of open orbits on the fifth zone surface only. A further anomaly, O, occurs as shown below (fig 1 - 16) when H is about 44° from [001] and is taken to mark the limit of open orbits on the fourth zone open surface.

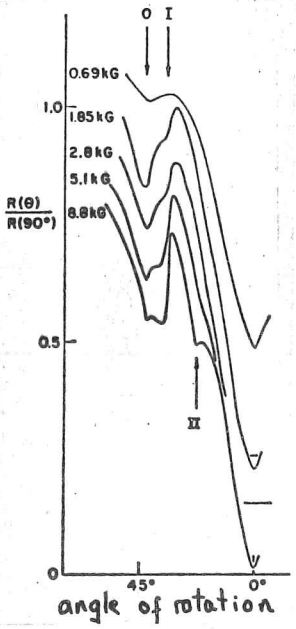

Fig. 1-16. Rotation diagrams at low fields with the field nearly perpendicular to [110] where an extra anomaly O occurs.

Weisz' model predicts that orbit 5 can occur for field directions up to 43° towards [110].

The decrease in ρ_{xx} at anomalies O and I is explained in terms of the reduction in the number of open orbits which causes a decrease in β' and hence in the dominant H^2 term in equation (1-4).

Fig. 1-17.

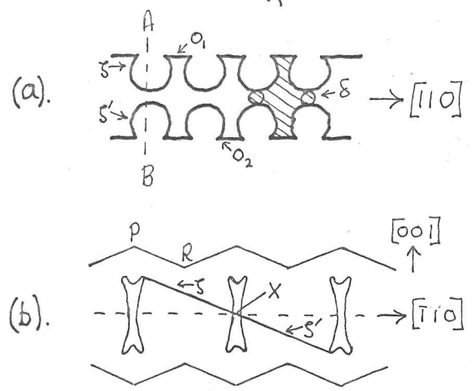

The closing of [110] open orbits on the forth zone surface by breakdown.

(a). When the field is tilted sufficiently far from [001], open orbits O_1 and O_2 may be linked by breakdown via δ to give the closed hole orbit shown (shaded).

(b). The (110) section AB, containing P, R, X (see fig 1-1).

(c). Linking of two aperiodic open orbits to form extended hole orbits by the same mode of breakdown - mode A - as in (a).

Figure 1-18

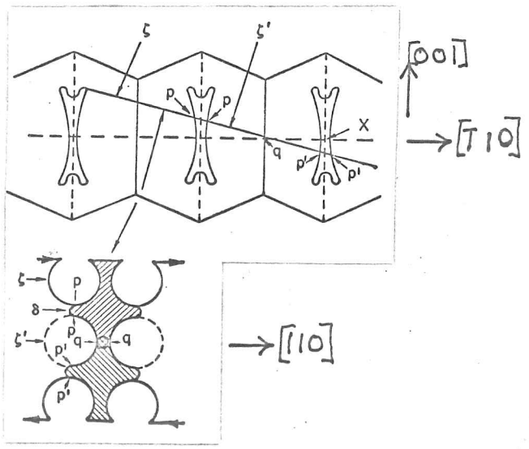

Mode C for closing open orbits along [110] by linking them via a closed orbit ζ and two hole orbits δ.
This occurs when the field is sufficiently high for breakdown to occur some way from the point of lowest energy gap in the central (001) plane.

As H is increased from 5 to 10 kG, anomaly II appears when H is about 22° from [001] and this is also interpreted as being due to a reduction in the number of open orbits, the reduction this time being caused by the linking of some of the open orbits by magnetic breakdown to form closed orbits. According to Weisz' model, when H is tipped 22° away from [001] it is just possible for two open orbits, one on either side of the fourth zone hole surface, to lie in the same plane, both passing close to point X. Fig 17a illustrates how two periodic open orbits may be linked via the δ orbit by magnetic breakdown (mode A) to form closed hole orbits. Fig. 1-17c shows how two aperiodic open orbits may be linked to form extended hole orbits. In the latter case H lies a few degrees outside the (110) plane.

An increase in field from 10 to 19 kg. causes II to increase and I to decrease. This is taken to be due to more open orbits being closed as breakdown occurs further from point X.

It was suggested that anomaly III was due to open orbits being closed by a mode, c, of breakdown as indicated in figure 1-18. the magnetic field now being sufficiently high for magnetic breakdown to occur some way from the central (001) plane.

Further evidence for the occurrence of magnetic breakdown in tin was obtained by Hayes and McLean (15) in a study of helicon propagation in tin single crystals (residual resistance ratio $\simeq$ 20,000) at magnetic fields up to 14 kG and temperatures down to 1.2°K. They observed quantum oscillations ($f = [0.175 \pm 0.001] \times 10^7$ G) in the helicon signal, the amplitude of which varied considerably with the angle between $\underline{H}$ and [001], as is shown in fig. 1-19.

The large oscillation amplitude for $\underline{H} \parallel$ [001] is interpreted in terms of the linking by magnetic breakdown of the closed orbits φ and δ into a two dimensional network. As the field is tipped away from [001], the network breaks up into a set of essentially linear chains and beyond a few degrees from [001] not even a linear chain remains. This, together with the appearance of aperiodic open orbits, leads to a rapid fall in the oscillation amplitude. The sudden increase occurs at the same position as anomaly II, namely when $\underline{H}$ is about $\pm$ 21° from [001] and this adds further evidence for the existence of mode A of magnetic breakdown. At these angles of tip of $\underline{H}$ from [001], the open

θ = angle between [001] and rotation plane of $\underline{H}$
ψ = angle between [100] and the line of intersection of the plane of rotation of $\underline{H}$ and the plane containing [100] and [010].
ϕ' = angle between $\underline{H}$ and the projection of [001] on the rotation plane.

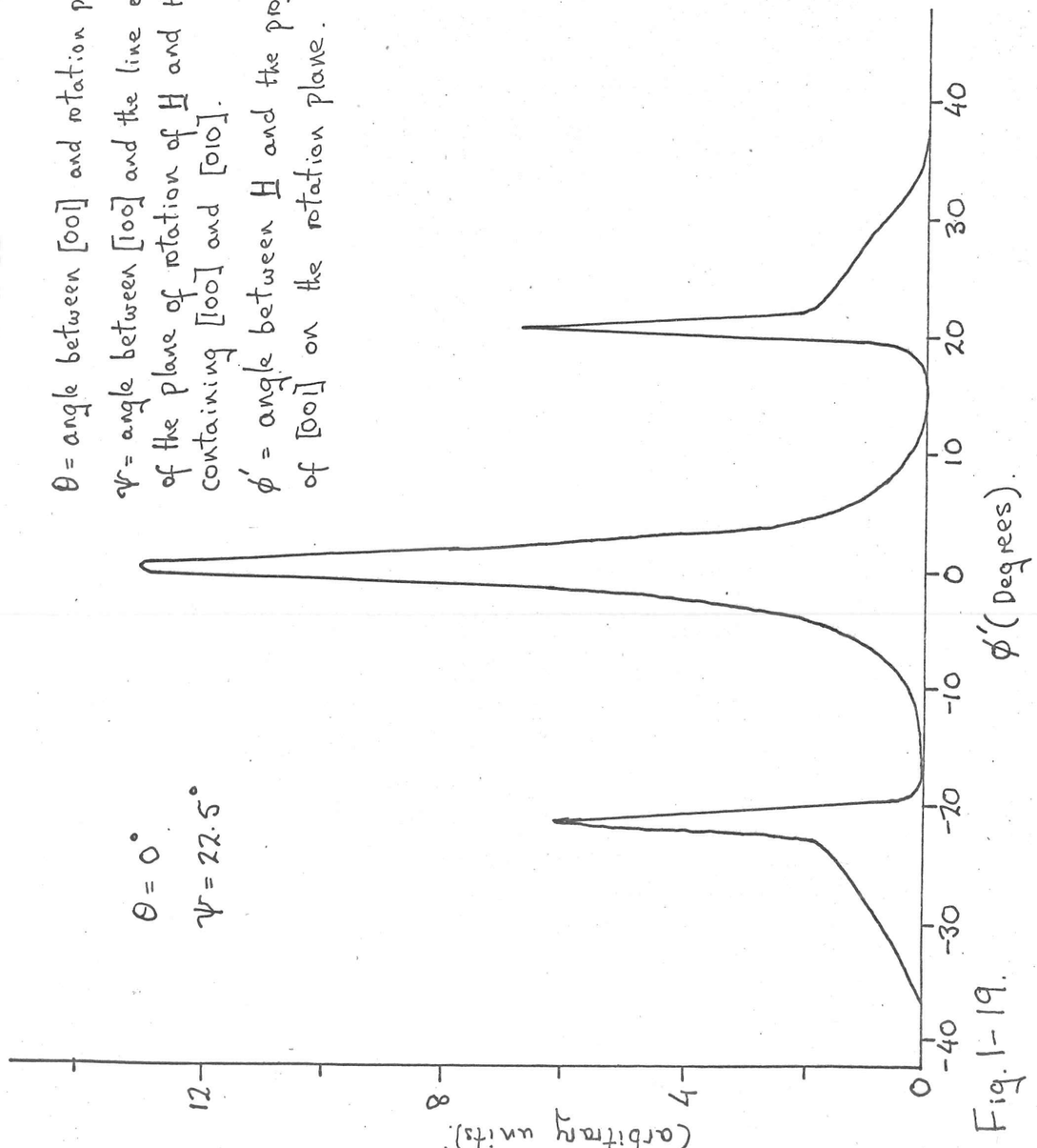

Amplitude of quantum oscillations of helicon signal divided by the steadily varying part of the signal. (arbitrary units)

Fig. 1-19.

orbits dominate the conductive behaviour and when they are linked by breakdown a large oscillatory dependence of the conductivity is to be expected as well as the change in the steadily varying part of the conductivity observed by Young (4). The disappearance of quantum oscillations for $|\emptyset'| > 37^{\circ}$ is explained by Hays and McLean in terms of the disappearance of open orbits.

1-4) Aims of the present experiment

The aim of the present experiment was, firstly, to make a study of the behaviour of the Hall field, $\underline{E}_H$, when $\underline{H}$ was close to [001]. ($\underline{E}_H$ is the field, odd in H, that is in a direction perpendicular to $\underline{H}$ and $\underline{J}$, the current density). It might be expected that the coupling of electron orbits ξ and hole orbits δ to form closed hole orbits would lead to a change in the Hall coefficient, R_H, defined by $\underline{E}_H = R_H \underline{H} \times \underline{J}$, since in the absence of open orbits and at sufficiently large values of $\underline{H}$, R_H depends only on the net number density of carriers of a particular sign. Also, no

oscillations had previously been directly observed in the Hall voltage in tin and it was thought worthwhile to see if they occurred. A further aim of the present experiment was to study how the Hall coefficient behaved as the angle between $\underline{H}$ and [001] was increased from 0° to about 50°, to see whether anomalies corresponding to 0, I, II, III above would be seen.

Chapter 2. Experimental Procedure

2-1 The transverse even voltage - a major obstacle to measuring the Hall voltage

Measurements of the Hall voltage, $V_{\mathcal{H}}$, in tin are made difficult by one major factor. A transverse even voltage, V_{TE}, (i.e. one perpendicular to $\underline{H}$ and $\underline{J}$ and even in H) also occurs when open orbits are present, except when they are in certain directions. The transverse even voltage being proportional to H^2, is in general much larger than the Hall voltage which is proportional to H. The Hall voltage could be found by taking two measurements of the transverse voltage, V_T, (i.e. that perpendicular to $\underline{H}$ and $\underline{J}$) the second being with the field reversed since

$$|V_{\mathcal{H}}| = \tfrac{1}{2} \left| V_{T+} - V_{T-} \right| \qquad (2\text{-}1)$$

where V_{T+}, V_{T-} refer to the transverse voltages obtained for the two field directions. Since in general $V_{TE} \gg V_{\mathcal{H}}$, $V_{\mathcal{H}}$ would be given by the difference between two large nearly equal, quantities and hence the error in measuring $V_{\mathcal{H}}$ would be large. Fortunately, V_{TE} becomes zero for certain directions of open orbits

and it is clearly desirable to measure the Hall voltage when this is the case.

The existence of the transverse even voltage is implied by equation (1-3) for the conductivity tensor for the model Fermi surface since this gives

$$\rho_{yx} = \frac{eH(n_- - n_+) + \beta' H^2 \cos\phi \sin\phi}{\beta'(n_-\gamma_- + n_+\gamma_+) + e^2(n_- - n_+)^2} \qquad (2\text{-}2)$$

assuming $x_- \gg 1$, $x_+ \gg 1$.

It follows from (2-2) that the transverse even voltage is zero whenever $\phi = 0$ or 90°. Since we have taken the crystal axis to be parallel to the x-axis, this means that $V_{TE} = 0$ so long as the crystal axis is perpendicular or parallel to the open orbit direction in $\underline{k}$-space. The transverse even voltage remains zero even if the crystal axis is not parallel to the open orbit direction in real space so long as it remains perpendicular to the open orbit direction in $\underline{k}$-space. Suppose that the latter condition is fulfilled and also that the crystal axis makes an angle $(90 - \theta')$ with the magnetic field as shown below:-

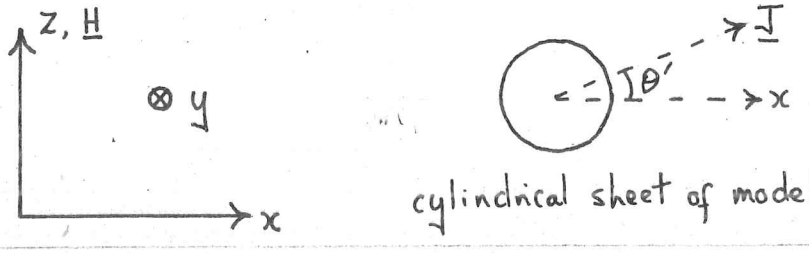

Fig. 2-1.

cylindrical sheet of model Fermi surface (axis // y).

In this case, since $\phi = 0$, (2-2) $\Rightarrow$

$$\rho_{yx} = \frac{eH(n_- - n_+)}{\delta'(n_- \gamma_- + n_+ \gamma_+) + e^2(n_- - n_+)^2} \qquad (2\text{-}3)$$

If we define the Hall coefficient, R_H, by

$$R_H = \frac{(E_y)_{odd}}{H J_x}$$ where $\underline{H} \parallel$ z-axis

and where the Hall voltage $V_H = \dfrac{(E_y)_{odd}}{d}$

(d = crystal diameter)

then $$\frac{(E_y)_{odd}}{H J} = R_H \cos\theta' \qquad (2\text{-}4)$$

It is worth noting that $R_H = \dfrac{1}{(n_- - n_+)e}$ only when

$$(n_- - n_+)^2 e^2 \gg \delta'(n_- \gamma_- + n_+ \gamma_+)$$

It follows from the above that the transverse even voltage is zero when the open orbit direction in $\underline{k}$-space is perpendicular to the crystal axis. In the present experiment we are interested in finding how R_H varies as the angle θ between the magnetic field direction and [001] varies and the question now arises of whether there is a plane in which $\underline{H}$ may be tipped such that the

angle θ varies but the transverse even voltage remains zero. Now, as mentioned before, for tin the direction of open orbits in k-space is given by the intersection of the plane perpendicular to H and the (001) plane. The open orbit direction in real space also lies in the plane perpendicular to H and is perpendicular to its direction in k-space. Consider the stereogram of an (001) projection as shown below with the crystal axis i.e. J, in an arbitrary direction.

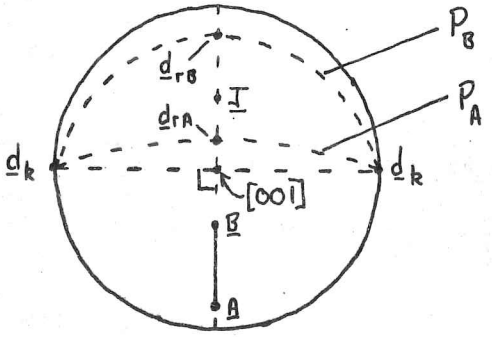

Fig. 2-2

Suppose H lies in the plane containing J and [001], and is changed in direction from A to B. P_A, P_B are the planes perpendicular to H when H is in the directions A and B. The direction of the open orbits in real space moves from d_{rA}

to $\underline{d}_{rB}$ as shown, remaining in the same plane as $\underline{J}$ and $\underline{H}$, while the open orbit direction in k-space remains perpendicular to $\underline{J}$. Thus the transverse even voltage is zero whenever $\underline{H}$ lies in the plane defined by $\underline{J}$ and [001]. By orientating the crystal such that $\underline{J}$, $\underline{H}$ and [001] all lie in the same plane and then tipping the crystal about an axis perpendicular to $\underline{H}$ and $\underline{J}$ as shown in fig. 2-3, the angle θ could be varied while still keeping $\underline{J}$ in the plane defined by $\underline{H}$ and [001] i.e. while V_{TE} remained zero.

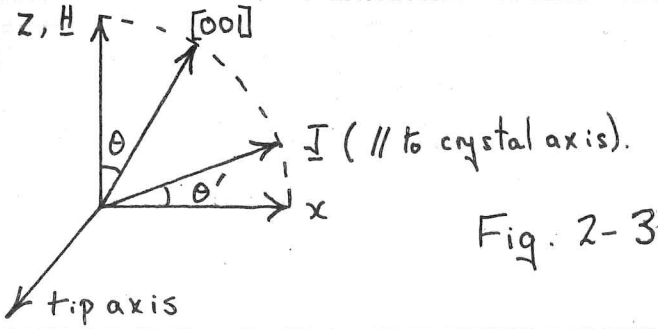

Fig. 2-3

2-2). <u>The reasons for using more than one crystal in studying the angular variation of R_H</u>

In the present experiment we are interested in seeing how R_H alters as the angle θ is changed from 0^o to $\approx 45^o$. There are two reasons why this necessitates the use of more than one crystal. Firstly, we want to keep $\theta' \simeq 0$ so that the change in Cos θ' as the crystal is tipped is small. For example, if we tip

a given crystal such that θ' lies within the range $\pm 10^{\circ}$, then the maximum error that occurs in equating $(E_y)_{odd}/(H\,I)$ to R_{ρ} is $\pm$ 1.5%. This is a bearable error as the change in R_{ρ} observed for a tip angle change of about 10° is much larger than 1½%. However, for greater angles of tip, a correction would have to be made to allow for the change in Cos θ'. Secondly, the angle through which a crystal could be tipped was limited by the fact that there was not room in the set-up used to tip the crystal holder through more than approximately $\pm 10^{\circ}$ about an axis perpendicular to $\underline{H}$ and $\underline{J}$.

The following crystals were therefore used:-

(α = polar angle of specimen axis from [001] β' = azimuthal angle from [110] to the plane containing the specimen axis and [001]).

Specimen	α(degrees)	β'(degrees)	$R_{290^{\circ}}/R_{4.2^{\circ}K}$
$Sn^{[110]}_{1,2,3}$	90 $\pm$ 1	0 $\pm$ 1	(22 $\pm$ 2) x 10^3
$Sn^{[110]}_{4,5}$	90 $\pm$ 1	0 $\pm$ 1	not measured
"Sn^{11}"	79 $\pm$ 1	11 $\pm$ 1	(26 $\pm$ 2) x 10^3
"Sn^{25}"	65 $\pm$ 1	15 $\pm$ 1	(20 $\pm$ 2) x 10^3
"Sn^{37}"	53 $\pm$ 1	12 $\pm$ 1	(17 $\pm$ 2) x 10^3

The residual resistance ratios for $Sn^{[110]}_{4,5}$ are probably about 20×10^3 since they were prepared from the same purity tin as the other crystals.

The range of angle θ between $\underline{H}$ and [001] for which the Hall voltage was measured for each crystal is given below:-

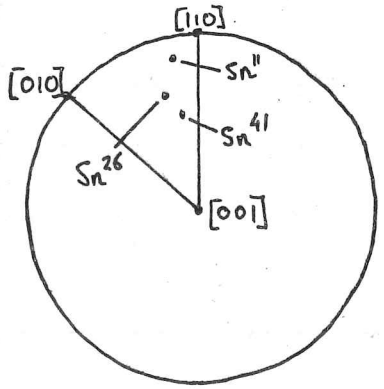

Fig. 2-4.

Specimen	Range of θ
$Sn^{[110]}_{1,2,3}$	$\sim \pm 3^\circ$
Sn''	$\sim 10^\circ \rightarrow \sim 25^\circ$
Sn^{25}	$\sim 22^\circ \rightarrow \sim 36^\circ$
Sn^{37}	$\sim 32^\circ \rightarrow \sim 50^\circ$

The directions of the crystal axes are shown (not to scale) in the stereogram above (fig. 2-4).

The reason for not making $\beta' = 0$ for the latter three crystals is as follows. When $\beta' \neq 0$ the open orbits are aperiodic and will thus traverse all the arcs ζ that are geometrically allowed (see fig 1 - 17C). If one of these is connected by breakdown to ζ' and thus to the other side of the

sheet, the open orbit closes. Thus, at least in the limit of infinite τ, all the aperiodic open orbits are closed for field directions for which the linking of ζ to ζ' connects one sheet to the other. For a periodic open orbit, however, all the arcs ζ are identical, so that only a small band of open orbits will pass sufficiently close to X to break through. As the field increases, orbits further from X can break through but at any finite field there will always be some open orbits which do not get closed by breakdown. Thus if an anomaly is going to occur in the Hall voltage due to the closing of open orbits by breakdown, it is likely that the anomaly will be larger if the orbits are aperiodic rather than periodic and thus more likely to be observed.

To summarize, what we have shown so far is:-

1) Why a transverse even voltage appears in tin
2) For what orientations of $\underline{J}$ relative to $\underline{H}$ it becomes zero
3) How the variation of R_H with angle θ, for θ in the range 0° to about 50° may be studied by using four crystals of appropriate orientation.

The next question that arises is how can each of these crystals be orientated so that H, J and [001] all lie in the same plane.

2-3). The use of rotation diagrams of the transverse magnetoresistance in orientating the specimen such that the transverse even voltage is zero

Now, as shown in fig. 1 - 13, the plot of the transverse magnetoresistance against the angle of rotation exhibits a deep minimum when H, J, and [001] all lie in the same plane. In this case the angle of tip was 3°. The rotation diagrams for tip angles up to at least 45° are similar in that this deep minimum occurs when H , J and [001] lie in the same plane, although for tip angles greater than about 25° anomalies I, II and III are no longer clearly seen. A typical rotation diagram for a tip angle of about 25° is as shown below

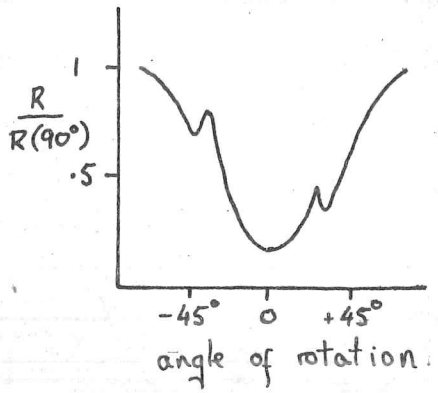

Fig. 2-5

R is the transverse magnetoresistance i.e. E_x / J_x, where the crystal axis is parallel to the x-axis.

The spikes occur when H is perpendicular to [110] and [100] and are due to the appearance of periodic open orbits on the fourth and fifth zone open surfaces. The important point is, however, that by rotating the crystal about its axis, which is close to perpendicular to H, until the transverse magnetoresistance is a minimum, the transverse even voltage can be eliminated.

It is convenient to mention here how, by a study of the rotation diagrams of a [110] crystal for various tip angles, it is possible to tell whether the angle of tip is being increased or decreased and also when H is very close to [001]. Although not shown in the rotation diagrams of fig 1 - 13, a peak occurs in the transverse magnetoresistance when H is perpendicular to [110]. This is due to the appearance of a broad band of periodic open orbits on the fourth zone surface and a narrow band on the fifth zone surface. It is not clear why a peak does not also occur when H is perpendicular to [100]. As the angle of tip is decreased, the peak moves closer to the zero of rotation as is clear from the stereogram below.

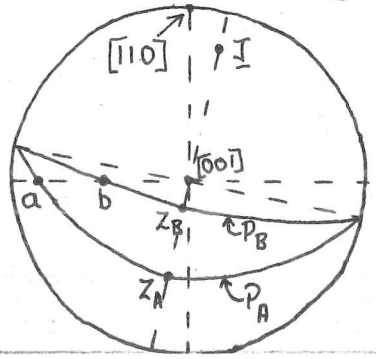

Fig. 2-6.

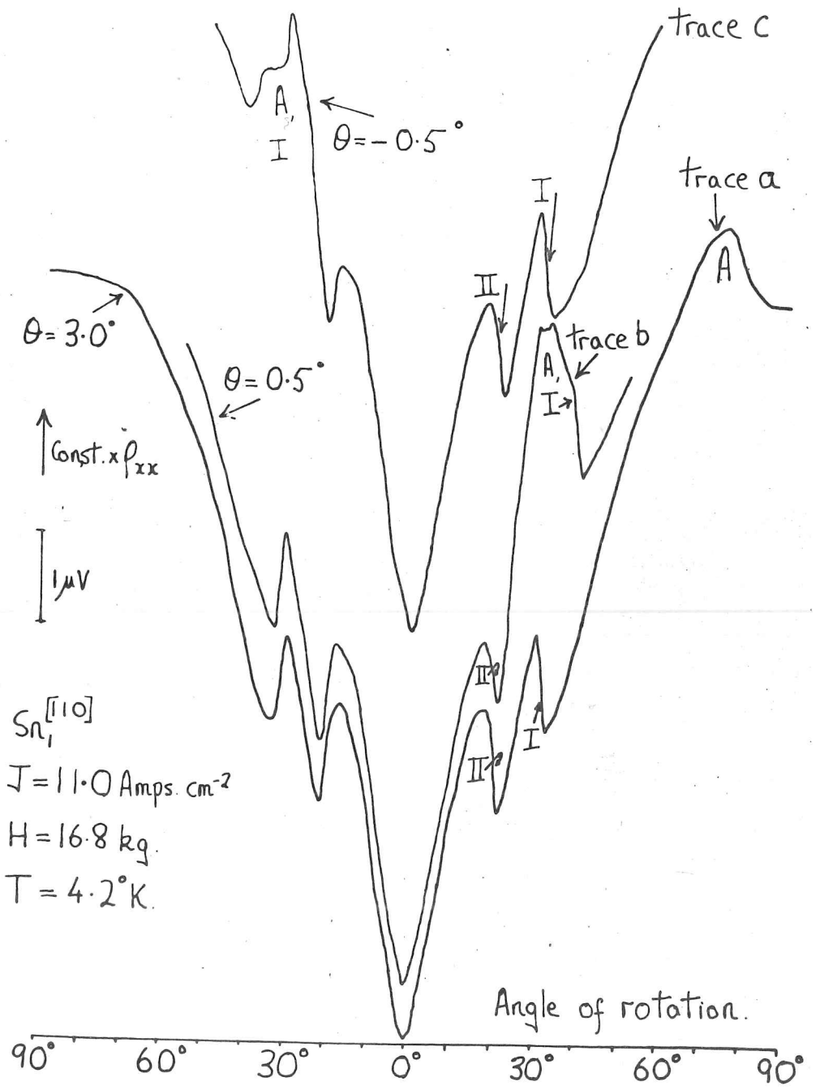

Fig. 2-7 . Rotation Diagram of the Transverse Magnetoresistance.

J represents the direction of the crystal axis which is close to [110]. P_A, P_B represent the planes of rotation of H for two tip angles - LT_A and LT_B, say, where $LT_A > LT_B$. a and b are the directions for which H is exactly perpendicular to [110]. It can be seen that as the tip angle is decreased, the point at which H is perpendicular to [110] moves closer to the zero of rotation represented by the point z. The traces in fig. 2-7 demonstrate this. Changing the tip angle from that for trace a to that for trace b causes the peak A to move closer to the zero of rotation and hence the tip angle must have decreased. In trace c it can be seen that the peak A has moved to the other side of the zero of rotation. Thus for some intermediate tip angle between that for trace b and that for trace c, H will become parallel to [001]. Fig. 2-7 also shows the anomalies I and II observed by Young(4).

2-4). Procedure for taking measurements

The crystal was first rotated about its axis which was approximately perpendicular to H until the transverse magnetoresistance, ρ_{xx}, was a minimum. In practice it was difficult

to locate the minimum to closer than $\pm \frac{1}{2}^{o}$ and the transverse even voltage, V_{TE}, was still appreciable. V_{TE} could be reduced further by making fine adjustments to the angle of rotation until $V_{T+} = - V_{T-}$; V_{T+} and V_{T-} refer to the values of the transverse voltage for two opposite directions of the magnetic field. In this way V_{TE} could be reduced to less than 1% of the Hall voltage, V_{H} , but since V_{TE} was very sensitive to the rotation angle, this was difficult to do.

To find how V_{H} depended on H and on θ, two traces of V_T were recorded, for each value of θ , on an X-Y recorder:-

a) when $\underline{H}$ was decreasing from the maximum field (about 45 kg) to zero.

b) when $\underline{H}$ was increasing from zero to the same maximum field at the same rate by with $\underline{H}$ reversed in direction.

The measured transverse voltage, V_T , for a given value of $\underline{H}$ and θ consists of the Hall voltage, any remaining transverse even voltage, and a voltage in the leads due to the

changing magnetic field. By averaging the values of V_T for the two traces, the latter two voltages were eliminated, the Hall voltage being given by

$$|V_H| = \frac{1}{2} | V_{T+} - V_{T-} |$$

The plotting of two traces for each value of θ may seem a lengthy procedure for finding the Hall voltage, but the following information could also be extracted:-

a) The variation of the Hall voltage with $\underline{H}$ at constant θ.

b) The variation of the oscillation amplitude of the Hall voltage with $\underline{H}$ at constant θ.

c) The period of the oscillations.

There was another reason for continuously recording the transverse voltage as the field was changed. The change in field produced a change in the force (proportional to $\underline{J} \times \underline{H}$) experienced by the crystal and this sometimes caused the crystal to slip slightly in its holder. This in turn caused a change in the orientation of the crystal and hence also in the magnitude

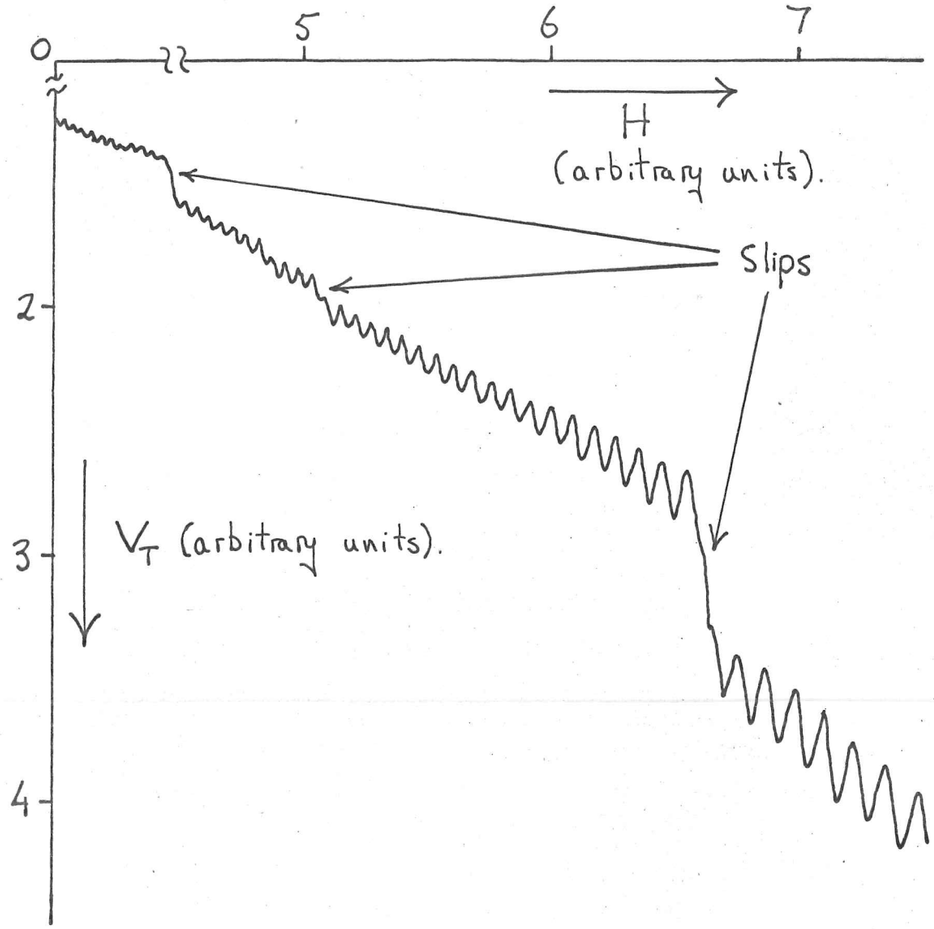

Fig. 2-8. Experimental trace of transverse voltage against magnetic field strength illustrating the discontinuities that occur when the crystal moves slightly in its holder.

of the transverse even voltage present. On a trace of V_T against $\underline{H}$ the slip is clearly marked by a sharp discontinuity as is shown in fig 2 - 8. If a continuous recording were not made, it is unlikely that the change would be noticed and an incorrect value would be given to the Hall voltage, since the amount of transverse even voltage would be different for the two readings V_{T+} and V_{T-} of the transverse voltage.

The angle θ was varied by altering the tip angle. Since the axis about which the crystal was tipped was approximately perpendicular to $\underline{H}$ and $\underline{J}$ a small alteration of tip angle still left $\underline{H}$, $\underline{J}$ and [001] approximately in the same plane. If necessary, before taking another pair of traces at the new value of θ, a slight alteration could be made to the rotation angle to reduce V_{TE}.

Measurements were also made of the variation of transverse magnetoresistance, ρ_{xx}, with angle θ. Most of these measurements were made at a constant value of $\underline{H}$, the angle θ being varied as described above. However in these sets of measurements no alteration was made to the rotation angle after it had been initially

set such that $V_{TE} = 0$.

Measurements were also made to find out how the transverse even voltage varied with angle θ when $\underline{H}$ was close to [001]. In this case the variation of V_T with angle θ at constant field, $\underline{H}$, was recorded ; the field was then reversed and the values of V_T corresponding to the same values of θ were noted. V_{TE} was given by

$$V_{TE} = \frac{1}{2} \left[V_{T+} + V_{T-} \right]$$

In this set of measurements the rotation angle was left unchanged.

2-5). The Apparatus

a) The crystal holder

As has been pointed out, it is important to keep small the number of dislocations present. It was thus desirable that the method of holding the crystal should be such that the crystal was not damaged. Fixing the crystal to a firm base would be unsuitable as it would lead to straining of the crystal by differential

Fig. 2-9. A crystal mounted in its holder.

contraction between it and the base. The method of support finally adopted is as shown in fig 2-9. The loops, which served the dual purpose of supports and contacts for measuring the transverse magnetoresistance, ρ_{xx}, were of 44 S.W.G. copper and when the crystal was absent were sprung shut by the 24 S.W.G. Copper-Beryllium wires to which they were attached. (I am indebted to Professor Pippard for suggesting this means of support). Attachment of the 'Hall contacts' was also a problem. It was desirable that the area of contact should be small and that the line joining the contacts should be perpendicular to the crystal axis. The latter condition was required if no component of the transverse magnetoresistance, ρ_{xx}, was to be picked up by the 'Hall contacts'. Attempts were made to solder on the 'Hall contacts' but difficulties in aligning the contacts and in preventing the solder from spreading led to the abandonment of the idea. The Hall contacts finally used consisted of two pieces of 32 S.W.G. Cu-Be wire which were araldited into a groove, as shown in fig 2-9, at one end, and were free to move in a parallel groove, whose width was just greater than the wire diameter, at the other end. The grooves were cut perpendicular

to the plane containing the ends of the loops.

The transverse even voltage could be reduced to less than 1% of the Hall voltage and thus any transverse even voltage larger than this which might be measured could be ascribed to the even component of ρ_{yx} and not a component of ρ_{xx}.

Although the line joining the 'Hall contacts' was thus very close to perpendicular to $\underline{J}$, it was not easy to mount the crystal so that this line was perpendicular to [001]. The [110] crystals could be mounted in the correct position fairly easily since the (001) planes were clearly visible after the crystal had been etched in conc. HCl. For the other crystals, the plane containing $\underline{J}$ and [001] could only be distinguished for certain by X-raying the crystal.

If, having got $\underline{H}$, $\underline{J}$ and [001] all in the same plane, the line joining the 'Hall contacts' makes an angle δ with the axis perpendicular to this plane and $(90 - \theta')$ is the angle between $\underline{H}$ and $\underline{J}$ then the measured odd transverse voltage is $V_{\mathcal{H}} \cos\delta \cos\theta'$ where $V_{\mathcal{H}}$ is the voltage when $\delta = \theta' = 0$.

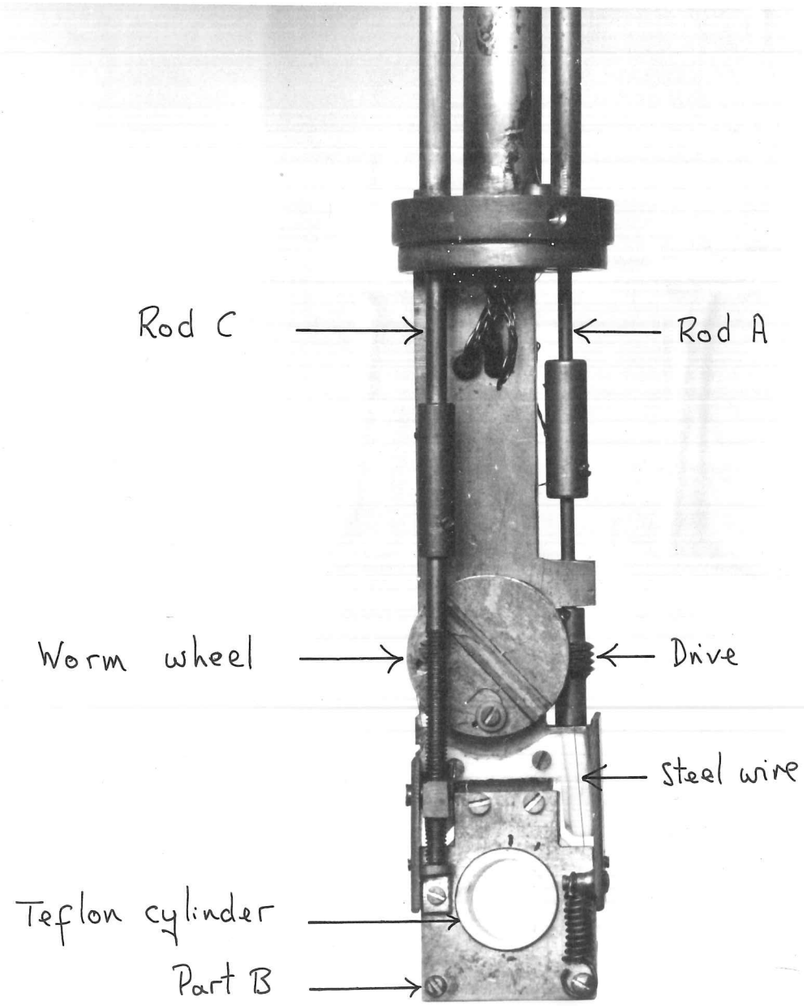

Fig. 2-11. The mechanism for rotating and tipping the specimen.

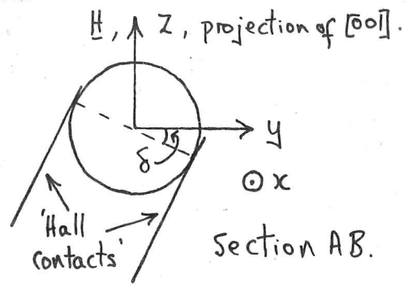

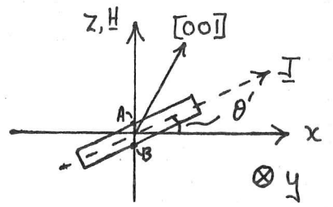

Fig. 2-10.

The value of δ could be estimated at the end of each experiment, after the suspension had been lifted out, by finding the angle through which the crystal had to be rotated to bring the 'Hall contacts' parallel to the suspension axis i.e. parallel to $\underline{H}$.

b) The Mechanism for rotating and tipping the crystal

The mechanism is shown in the photo (fig. 2-11). The teflon cylinder, in which the crystal was placed with its axis parallel to that of the cylinder, was linked to a worm wheel by a steel wire (36 S.W.G.). The wheel was rotated by rod A to which was attached the drive. In this way the crystal could be rotated through 180° about its axis. The part B could be tipped through approximately $\pm 10^{\circ}$ about on axis perpendicular to the suspension axis and the cylinder

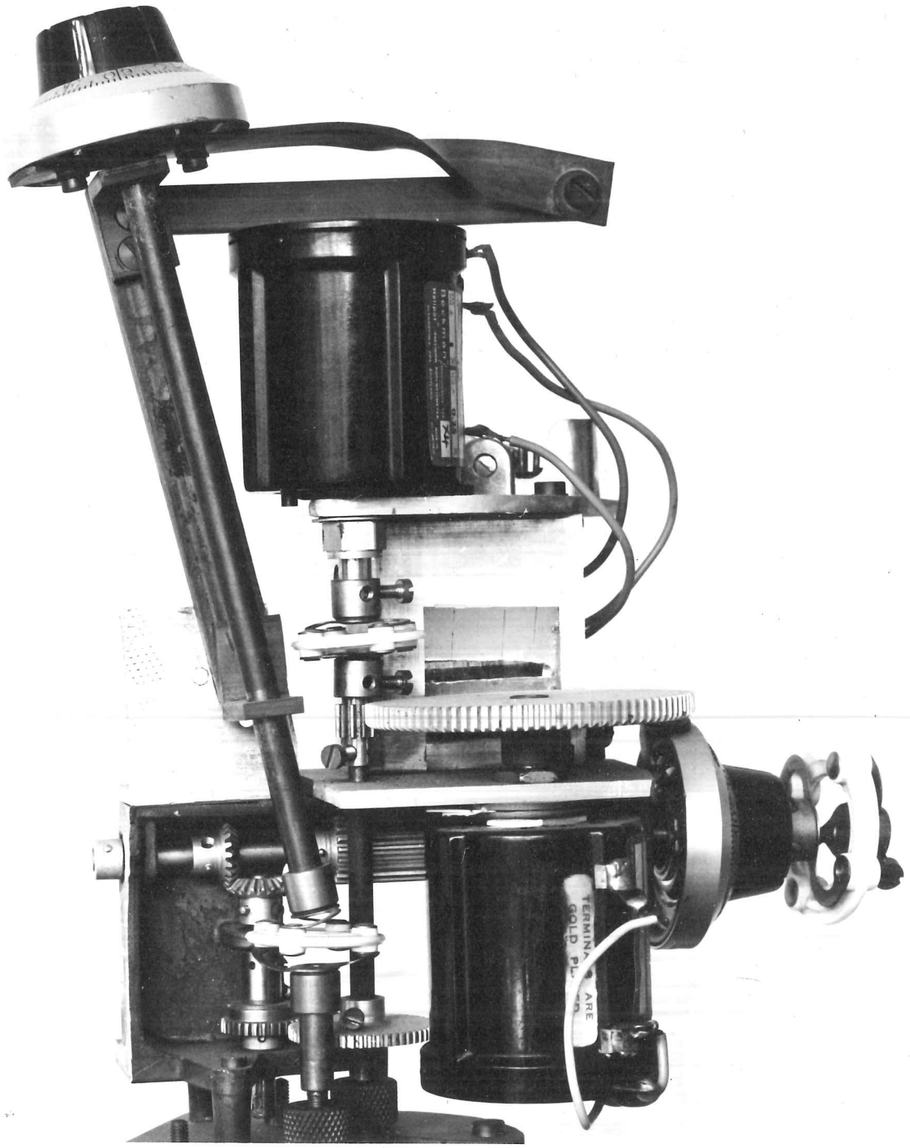

Fig. 2-12. The top of the suspension.

axis by means of rod C. The amount of tip was measured by a turns counter reading to hundredths of a revolution attached to the rod at the top of the suspension. When plotting a rotation diagram i.e. transverse magnetoresistance, ρ_{xx}, against the angle of rotation, the rod A was driven by a motor, the arrangement of gear wheels being as shown in fig. 2 - 12. By connecting a helipot to the rod A , a voltage, proportional to the angle through which the crystal had been rotated, was produced and this was fed to the X-axis of a pen recorder. The transverse magnetoresistance was measured with a Keithley nanovoltmeter whose output was fed to the Y-axis of the recorder. I am indebted to Dr. R. C. Young for the use of his suspension and drive unit.

c) Measurements made at 1.2°K

A temperature of 1.2°K was reached in the standard way by pumping on liquid helium thermally isolated by a vacuum space from the main reservoir containing helium at 4.2°K.

d) Production of the magnetic field

The field was produced by a B.O.C. superconducting solenoid-type magnet with a maximum field of about 50 kg. The dependence of field on magnet current was measured with a fluxmeter and found to be linear to less than 1% over a field range from 0 to 45 kg. One great advantage of this type of magnet for the present experiment was that the field direction could be reversed easily by reversing the direction of the current.

2-6) Establishment of the sign of the Hall coefficient

The Hall coefficient, R_H, is related to the Hall field, $\underline{E}_H$, current density, $\underline{J}$, and magnetic field $\underline{H}$ by the equation

$$\underline{E}_H = R_H \underline{H} \times \underline{I}$$

Thus if $\underline{H}$ is in the direction shown, with end A of the crystal connected to the positive power supply terminal and B to the negative so that $\underline{J}$ is in the direction shown, then if R_H is positive, the Hall contact H_1 will be positive with respect to H_2.

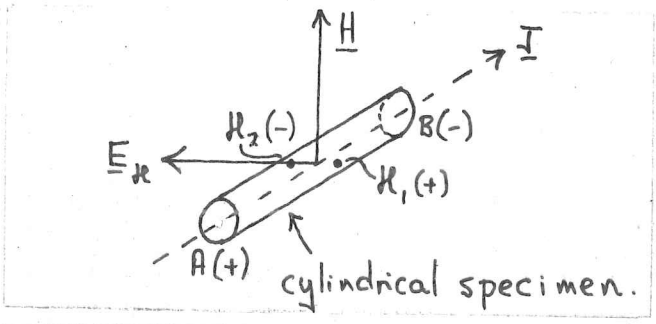

Fig. 2-13

2-7) Calibration of the tip angle setting as measured by the turns counter attached to rod A (see figs 11, 12) in terms of the angle θ from H to [001]

The change in tip angle of the holder for a given change in tip setting was found by noting the deflection of a beam of light reflected from a mirror attached to the holder.

Now, as mentioned before, measurements of the transverse voltage, V_T, were made when H was very close to, or in, the plane defined by J and [001]. Thus a change in the angle of tip of the holder produced the same change in the angle θ and to associate a value of θ to each tip setting all that needed to be known was one fixed point i.e. one tip setting for which the angle θ was known. How this fixed point was chosen for each crystal is indicated when the results are given. One method of checking this allocation of θ values for the Sn^{11}, Sn^{25} and Sn^{37} crystals makes use of their rotation diagrams of transverse magnetoresistance, ρ_{xx}. As mentioned before, as the tip angle i.e. the angle between H and the projection

of [001] on the plane of rotation of $\underline{H}$, increases, then anomalies I, II, III disappear but peaks occur when $\underline{H}$ is exactly perpendicular to ⟨100⟩ and ⟨110⟩, and periodic open orbits can appear. The separation of these peaks depends on the tip angle and increases as this angle increases, as is clear from the stereogram below:-

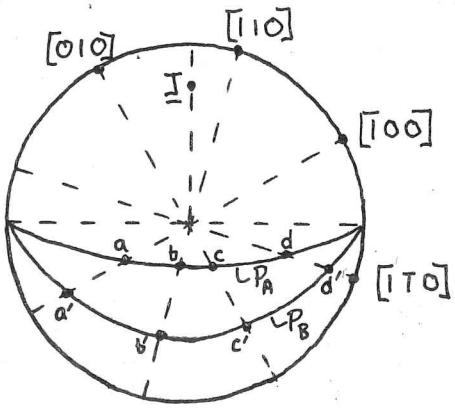

Fig. 2-14.
$\underline{I}$ is parallel to the crystal axis. P_A and P_B are the planes of rotation of the magnetic field about $\underline{I}$; the latter corresponds to the greater tip angle.

It is not clear why four peaks do not always occur corresponding to the field directions a, b, c, d above, but sometimes less (see figs. 5-2, 5-3).

Chapter 3. Crystal Preparation.

3-1) The reason for choosing the Czochralski technique

It was mentioned in chapter one that if the dislocation density was such that a given type of orbit contained a dislocation, then the resultant randomization of the phases of these orbits led to the disappearance of quantum mechanical phase coherence effects for these orbits. Clearly, it was desirable to choose a method of crystal preparation which led to the introduction of as few dislocations as possible. In particular, the area of the δorbit at 40 KG is about $4 \times 10^{-10} cm^2$. Thus a dislocation density less than about $2.5 \times 10^9 cm^{-2}$ is required for oscillations to be observed at 40 KG in the conductivity due to phase coherence round the δ orbit.

Judged by the above criterion, the Czochralski method of crystal pulling is the best. In this method, a seed crystal is dipped into the melt and then slowly withdrawn, pulling the desired crystal behind it. This has the desirable feature that no mould is required for the crystal and hence strains introduced by differential contraction between it and the mould do not arise.

3-2) Dislocations - their sources, and steps taken to reduce their number.

Even using the above method, dislocations can occur in the crystal. The main sources of dislocations and the steps taken to reduce the

number introduced from a given source, are listed below:-

(a) Dislocations propagate into the crystal from the seed.

The number of these was reduced by reducing the number in the seed. This was done by etching the seed in Conc. HCL to remove any surface damage.

(b) Dislocations are produced from the thermal shock given to the seed as it is dipped into the melt.

These were reduced in number by making the seed tip small.

(c) Epitaxial growth produces dislocations.

By ensuring that the seed tip had fully melted before starting to pull, it was hoped to reduce this effect. This precaution was also necessary to ensure that the pulled crystal had the same orientation as the seed.

The number of dislocations present in the pulled crystal can be further reduced as follows:-

A continuous withdrawal of the crystal causes a "quenching-in" of vacancies and if the withdrawal rate is sufficiently fast, a supersaturation of vacancies can occur. Dash (16) points out that this favours climb of dislocations with an edge component and a pure edge dislocation can be driven completely out of the crystal. To provide maximum opportunity for the dislocation to grow out, the diameter needs to be kept small for a distance equal to several times its diameter.

On the other hand, Elbaum (17) points out that a dislocation loop may be expected to nucleate by the collapse of vacancy discs when the free energy associated with the dislocation loop is less than that of the vacancy disc, and that this will occur at a sufficiently high supersaturation of vacancies. Also the elastic energy of a dislocation is much lower in a metal than in Silicon or Germanium which is what Dash was working with. Howe and Elbaum (18) pulled tapered aluminium crystals (69s purity) and found that the dislocation density, ρ_D, increased with increasing growth rate and diameter. They found that ρ_D increased linearly:- $(5\rightarrow10) \times 10^4 cm^{-2}$, as the growth rate increased:- (1→4)mm./min., for a crystal diameter = 0.3mm; also ρ_D increased linearly:- $(5\rightarrow10) \times 10^4 cm^{-2}$ as the diameter increased:- (0.3→0.4)mm. for a growth rate = 2.4mm/min.

The procedure finally adopted in the present experiment was to pull first at a fairly high temperature so that the crystal necked down from about 1mm diameter to 0.3mm. diameter over a length 1cm. and then, at a lower temperature, to pull a uniform crystal, diameter = 1mm. at a withdrawal rate = 3mm./min. If the results for aluminium were any way similar to those for tin, then they would imply that the crystal should have a dislocation density of order $10^6 cm^{-2}$. Results mentioned later indicate that the dislocation density was of order $3 \times 10^7 cm^{-2}$, but some of these were probably introduced in

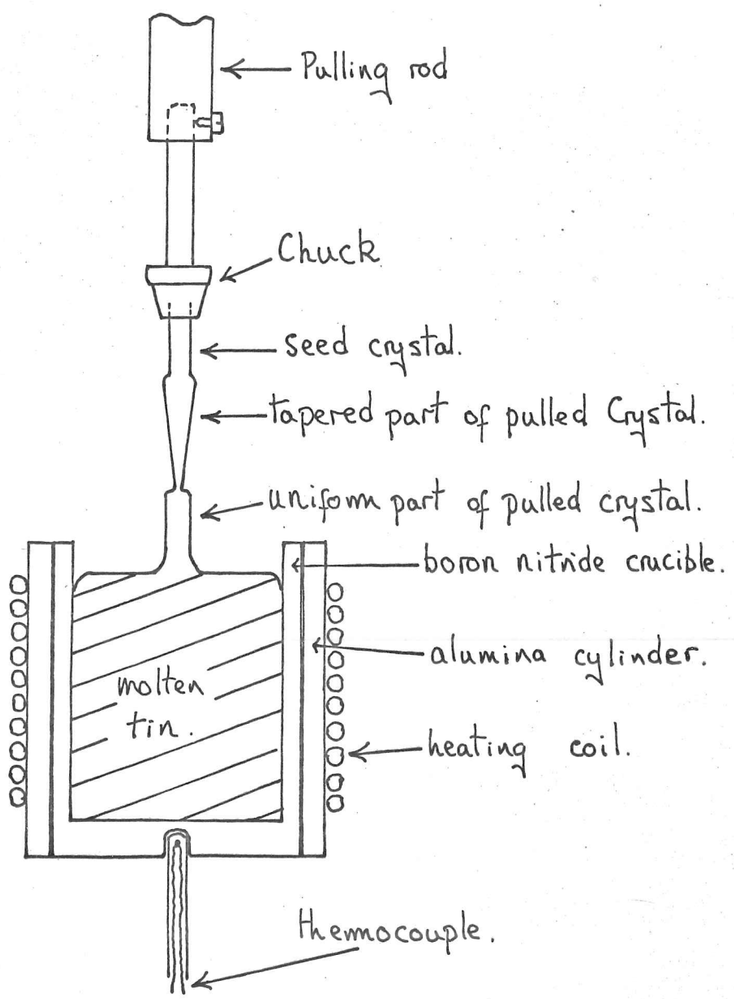

Fig. 3-1. The arrangement for crystal pulling. (schematic)

mounting the crystal in its holder.

3-3) Technique for growing [110] crystals

A [110] crystal, 8mm. x 1mm. x 1mm., for use as a seed was spark cut from a large single crystal of tin kindly grown by H. Davies. (The tin was supplied by 'Cominco' and was the 69 grade in purity.) Before being clamped in a chuck, the crystal was etched in Conc. HCL. The tin, from which the crystal was to be pulled, was contained in a boron nitride crucible. It was heated by a heating coil stuck with alumina cement on to a section of alumina tube which fitted tightly over the crucible. The set-up is illustrated in fig. 3-1.

To ensure that the seed tip melted readily when dipped in the melt, it was necessary to have the surface of the melt clean and this was ensured by only melting the tin under vacuum (pressure about 10^{-4}mm.Hg.) so that no oxide layer was formed.

When the seed had melted at the tip, it was withdrawn at a speed of about 3mm./min. and the pulled crystal was allowed to taper over a distance of about 1 cm. to a diameter of ½mm. or less. During this process, the power input was such that the temperature was increasing at a rate of about 3°c./min.

Technique for pulling a crystal of uniform cross-section.

The crystal diameter was sensitive to changes in melt temperature. To damp down any fluctuations in temperature caused by fluctuations in

power input, the amount of melt was made fairly large - about 60gms. It was thought that if the crystal was pulled fairly fast (about 3mm./min.) then slow fluctuations in melt temperature would have no effect and the crystal would be uniform. However, a crystal pulled at this speed from a melt at temperature equilibrium, tended to taper inwards and the melt temperature started to rise. One method of overcoming this is to pull the crystal very slowly (about 1cm./hr.) so that equilibrium conditions always prevail. This has the disadvantages (a) that any slow fluctuations in temperature would change the diameter and (b) it takes a long time to get the melt to the correct equilibrium temperature. Another method was therefore used. To counterbalance the increase in temperature that occured on pulling, the power input was set such that the temperature was falling when the pulling was started. To pull uniform cylindrical crystals of diameter = 1mm., at a rate = 3mm./min., it was found necessary to have the temperature initially falling at a rate of about 0.5^{o}c./min.

3-4) Growth of Sn^{11}, Sn^{25} and Sn^{37} crystals.

The crystal Sn^{25} was pulled with a seed of the same orientation which had been spark cut from the large single crystal prepared by H. Davies.

Now the numbers 11, 25, 37 are the value for each crystal of the

angle between the normal to the crystal axis and [001], the normal being in the plane containing the crystal axis and [001]. The Sn^{11} and Sn^{37} crystals were thus pulled using the Sn^{25} seed which was dipped into the melt at the appropriate angles to the vertical as shown below:-

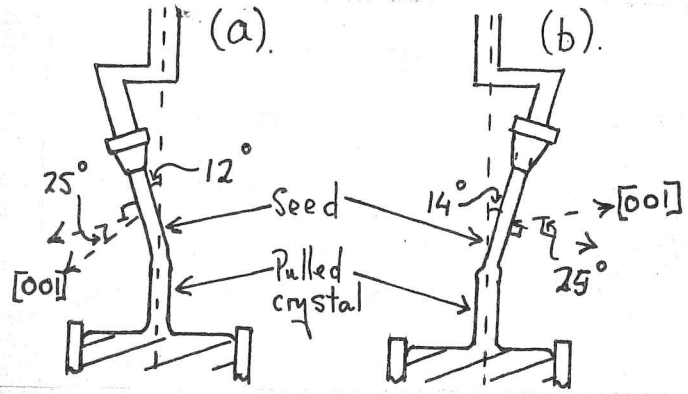

Fig. 3-2.
(a). Growth of Sn^{37} from Sn^{25}.
(b). Growth of Sn^{11} from Sn^{25}.

The Sn^{11} and Sn^{37} crystals pulled out approximately vertically and a check on their orientation by back reflection of X-rays showed that they had grown to within about $\pm 2^{o}$ of the intended orientation.

Method of cutting off the uniform crystal at the neck.

At the end of the pulling operation the whole crystal was of shape shown below (fig. 3-3). The crystal was then immersed up to the neck in molten soft paraffin wax. When the wax had solidified a drop of Conc. HCL was placed round the neck and this ate it away. I am indebted to H. Davies for this idea.

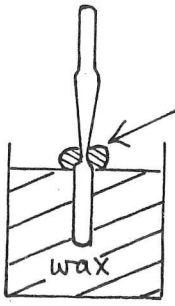

Fig. 3-3.
Illustration of how the crystal is cut at the neck using acid.

Attachment of the leads to the crystal

One current lead was soldered (using tin-indium, low melting-point, solder) to the protruding end of the crystal while it was still in the wax. The crystal was then pulled out with this lead and the wax removed with warm benzene. The other current lead was then soldered to the crystal, care being taken to ensure that the solder spread completely over the end face of the crystal. The 'loop contacts' and 'Hall contacts' of the crystal holder were then sprung open and the crystal lowered into position by a current lead. Thus at no time was the crystal clamped or held in any way until it was placed in the holder.

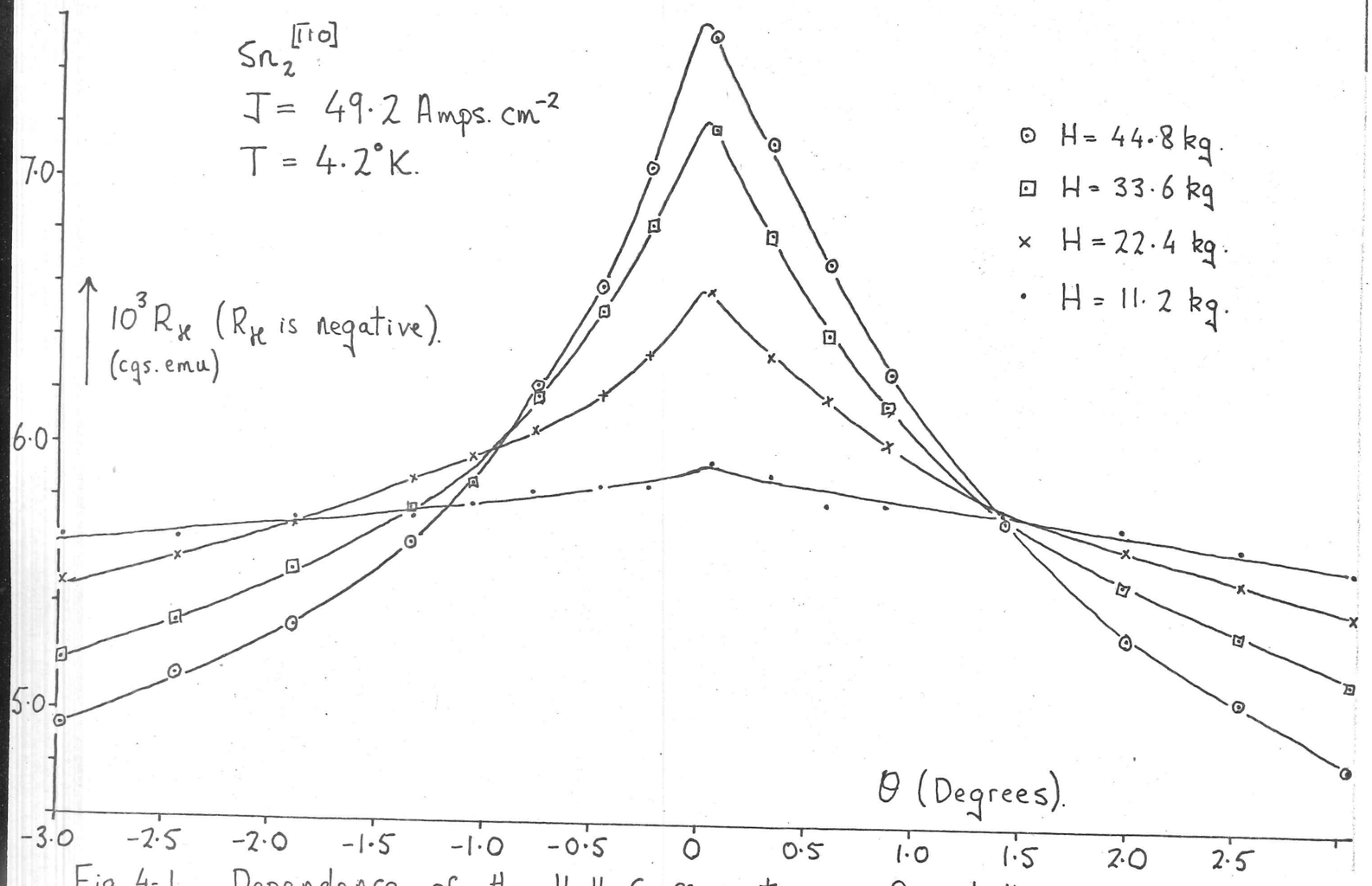

Fig. 4-1. Dependence of the Hall Coefficient on θ and H.

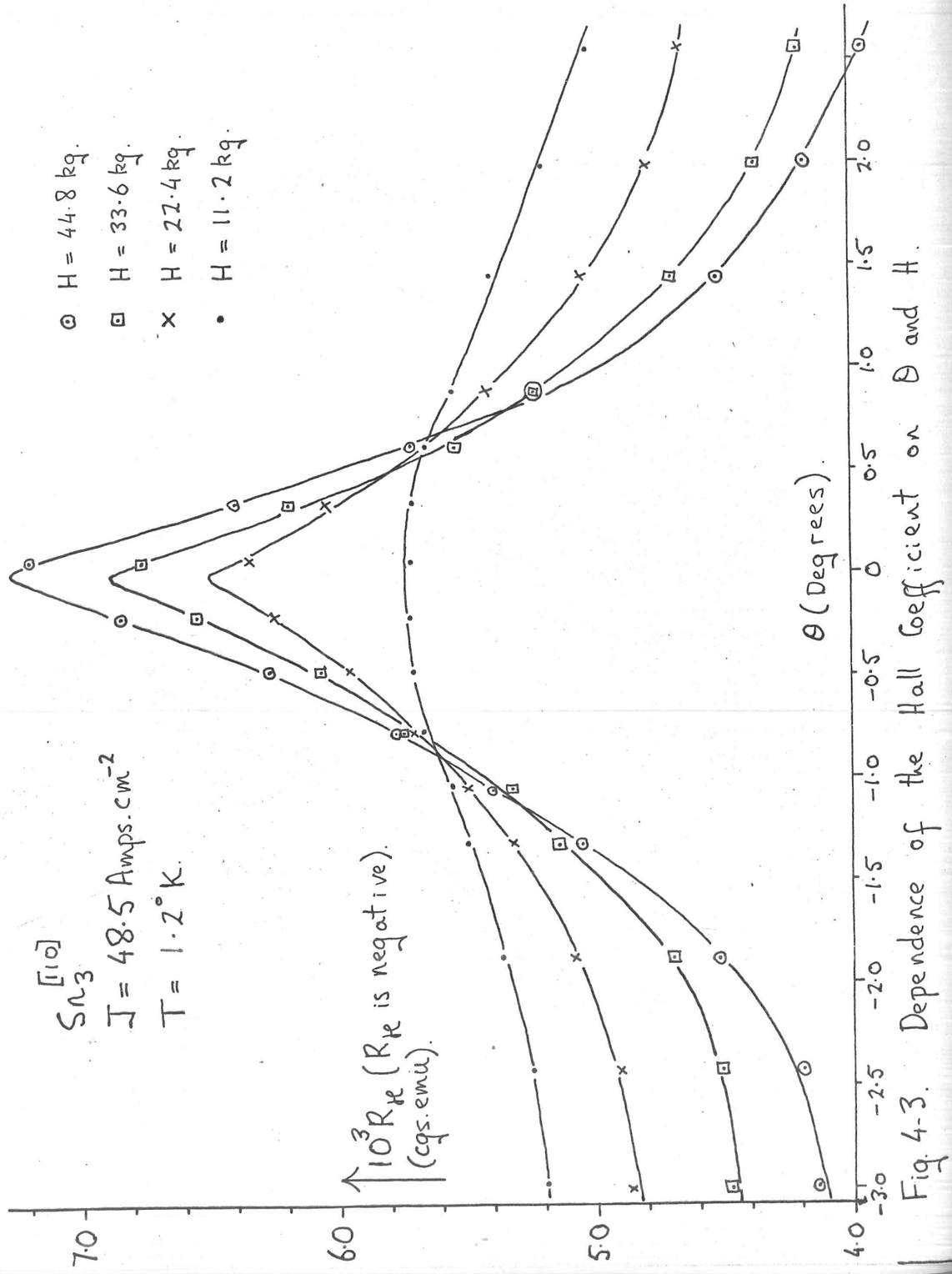

Fig. 4-3.

Chapter 4. The results and their interpretation for the case when the magnetic field direction is within about 5° of [001].

The results were obtained with the five [110] single crystals mentioned earlier and denoted by the symbols Sn_1 [110] to Sn_5 [110]. Each crystal was first orientated such that H was close to [001] and lying in the plane containing the crystal axis and [001], as described previously. Examples of the rotation diagrams of the transverse magnetoresistance, ρ_{xx}, obtained in doing this are shown in fig 2-7. As shown in this figure, anomalies I and II, occur when the field is about 21° and 35° from [001] in agreement with the 22° and 37° observed by Young (4). The position of each anomaly is taken to be the point of greatest slope of fall of resistance associated with the anomaly.

Results. 4-1. Non-oscillatory behaviour of the Hall coefficient, R_H.

A graph showing the variation of R_H with angle θ for various values of the magnetic field, H, for Sn_2 [110] at 4.2°K is shown in fig 4-1. θ is the angle between H and [001], H lying in the plane defined by the crystal axis and [001], so that the transverse even voltage is zero. The stereogram below indicates the plane in which the field was tipped:-

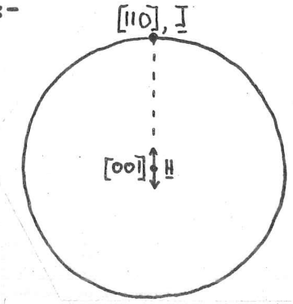

Fig. 4-2. The full line indicates (not to scale) the directions covered by H.

The Hall coefficient was found to be independent of magnetic field strengths, H, up to about 7kg., but as fig. 4-1 shows, within an angular range of about $\pm 1.3^{\circ}$ from $\theta = 0$, R_H becomes more negative as H increases above this value. Outside the above range of θ, R_H becomes less negative as H increases. Similar results were obtained for $Sn_1[110]$ at $4.2^{\circ}K$ and for $Sn_2[110]$ and $Sn_3[110]$ at $1.2^{\circ}K$. The graph of R_H against angle θ for $Sn_3[110]$ at $1.2^{\circ}K$ is shown in fig. 4-3. A summary of the results for $Sn_{1,2,3}[110]$ is given below:-

Table 4-1

Specimen	Temperature ($^{\circ}K$)	'linear' value of $R_H \times 10^3$ (emu.)	Angular Separation of cross-over points (degrees)	The change in R_H at $\theta = 0$ as H changes: $0 \rightarrow 44.8$kg.
$Sn_1[110]$	4.2	$-(5.4 \pm 0.5)$	1.2 ± 0.4	1.8×10^{-3}
$Sn_2[110]$	4.2	$-(5.8 \pm 0.5)$	1.4 ± 0.4	1.9×10^{-3}
$Sn_2[110]$	1.2	$-(6.4 \pm 0.6)$	1.0 ± 0.3	2.2×10^{-3}
$Sn_3[110]$	1.2	$-(5.6 \pm 0.5)$	0.8 ± 0.3	1.7×10^{-3}

Unfortunately, the results for Sn_2 [110] at 4.2°K and 1.2°K were taken on different days so that to attribute the difference in the results solely to a difference in temperature might be misleading.

The linear value of R_H is the value of R_H calculated from the Hall voltage in the region where it depends linearly on the field strength. Kachinskii (19) obtained a value of R_H equal to $(-4.8 \pm 0.2) \times 10^{-3}$ emu for $\underline{H}$ // [001]. Hays and McLean (15) found $R_H = |(5.5 \pm 0.3)| \times 10^{-3}$ emu.

The cross-over points are defined as the angles $\pm \theta_c$ for which, at $|\theta| > |\theta_c|$, R_H becomes less negative as H increases and, at $|\theta| < |\theta_c|$ R_H becomes more negative as H increases. No firm conclusions can be made about temperature dependence of θ_c.

The change in R_H (more negative) at $\theta = 0$ as H increases from zero to 44.8kg. does not appear to depend much on temperature. However, for $|\theta| > |\theta_c|$, the decrease in R_H, ΔR_H say, as $\underline{H}$ increases, for a given value of θ, appears to become greater as the temperature is decreased. This is indicated by the results given in the table below:-

$\Delta\theta$ (degrees)	Mean value of $\Delta R_H \times 10^3$ (emu) at $\pm \Delta\theta$ as H changes from 11.2 to 44.8 kg.			
	T = 4.2°K		T = 1.2°K	
	Sn_1 [110]	Sn_2 [110]	Sn_2 [110]	Sn_3 [110]
0.5	0.30	0.32	0.41	0.59
1.0	0.38	0.52	0.77	0.89
1.5		0.66	1.08	1.03
2.0		0.79	1.38	1.09

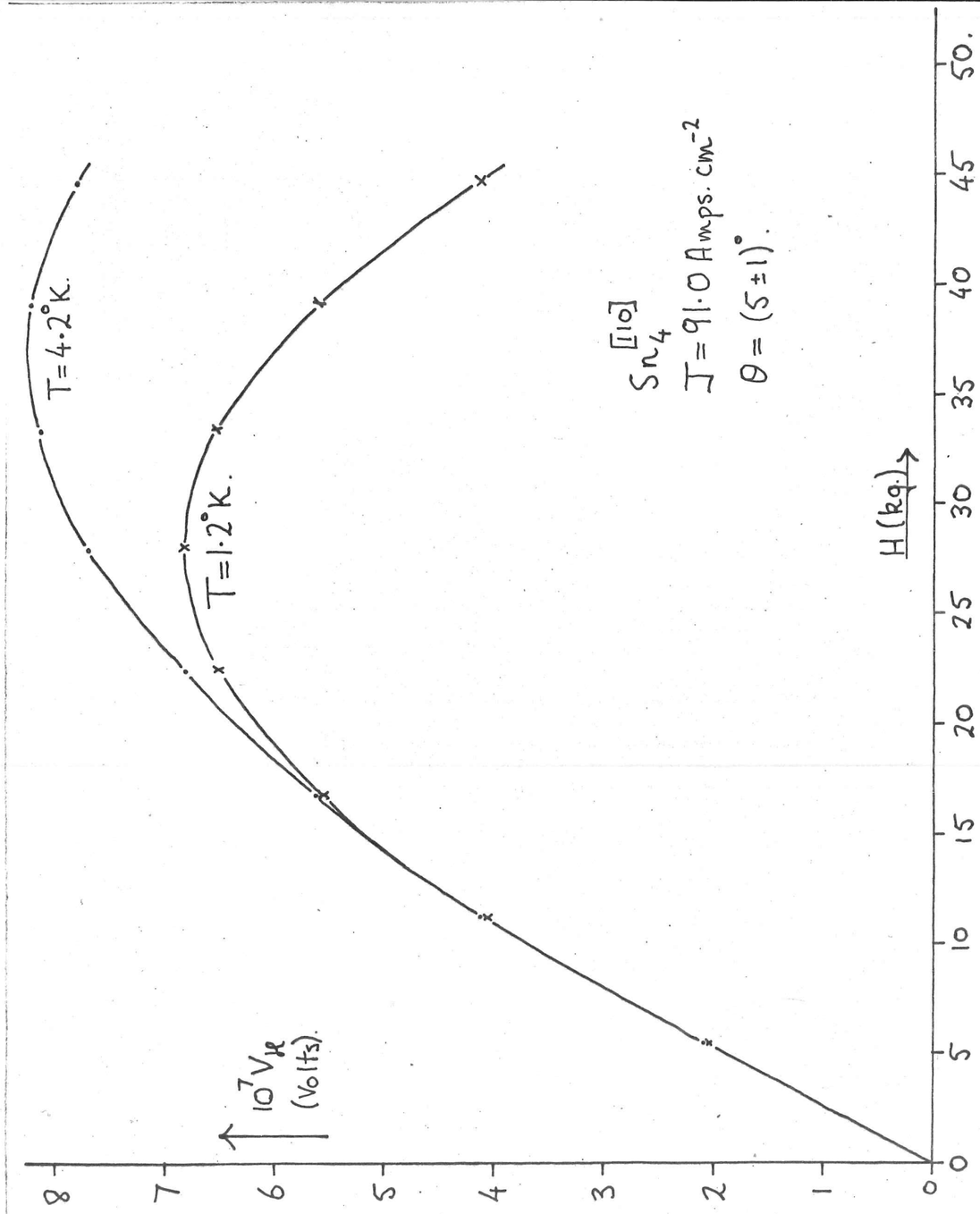

Fig.4-4. Dependence of the Hall voltage on H at T= 4·2°K and 1·2°K. $\theta \doteq 5°$

$\Delta\theta = \theta - \theta_c$, where $\theta(>\theta_c)$ is the position at which R_H was measured.

More convincing evidence for this behaviour was obtained for $Sn_4^{[110]}$ from measurements of the dependence of the Hall voltage, V_H, on the magnetic field strength at T = 1.2°K and 4.2°K. The results are shown in fig 4-4.

To summarize, the results that are clear cut and need to be explained are:-

1) R_H has a value $-(5.8 \pm 0.5) \times 10^{-3}$emu. calculated from the Hall voltage in the region where it depends linearly on the magnetic field strength, and with $\underline{H} \,//\, [001]$; T = 4.2°K.

2) R_H becomes more negative as H increases for H > (8 ± 2)kg., but the change becomes progressively smaller as the angle θ increases from 0 to θ_c ($\theta_c \doteq 1°$).

3) For $|\theta| > |\theta_c|$, R_H becomes less negative as H increases for H > (8 ± 2)kg and this change in R_H becomes greater as the temperature is decreased.

Theory. 4-1a) Why R_H is negative.

When $\underline{H}$ is very close to [001], the number of open orbits is very small and becomes zero for $\underline{H} \,//\, [001]$. Thus equation (2-3) may be written

$$R_H = \frac{1}{(n_- - n_+)e} \qquad (4\text{-}1)$$

Tin has eight electrons per smallest unit cell and these exactly fill four Brillouin zones so that when there are no open orbits, tin is compensated i.e. $n_- = n_+$. However, when H is close to [001], electron orbits ζ can occur on the fourth zone open hole surface and hole orbits λ on the fifth zone open electron surface. This disturbs the balance of the number of carriers so that the compensation is destroyed. Both Kachinskii (19) and Hays and McLean (15) appear to assume that the destruction of compensation is due solely to the orbits ζ, and on this basis Hays and McLean estimate that the thickness, Δk_z, measured parallel to [001], of the region of the hole surface on which the orbits ζ occur is given by $\Delta k_z = (1.10 \pm 0.07) k_o$ where $k_o = \frac{2\pi}{a} = 1.08 \times 10^8 \text{ cm}^{-1}$. This agrees quite well with the value predicted from Weisz' model, namely that Δk_z lies between 0.91 k_o and 1.05 k_o. The value for R_H, -5.8×10^{-3} emu, obtained in the present experiment gives $\Delta k_z = 1.14 k_o$. (In deriving this result, the area in K-space of the ζ orbit is taken as 0.96 k_o^2 - a value deduced from fig. A1-4). It is not clear why such good agreement is achieved between theory and experiment when the effect of having hole orbits λ on the fifth zone surface is ignored.

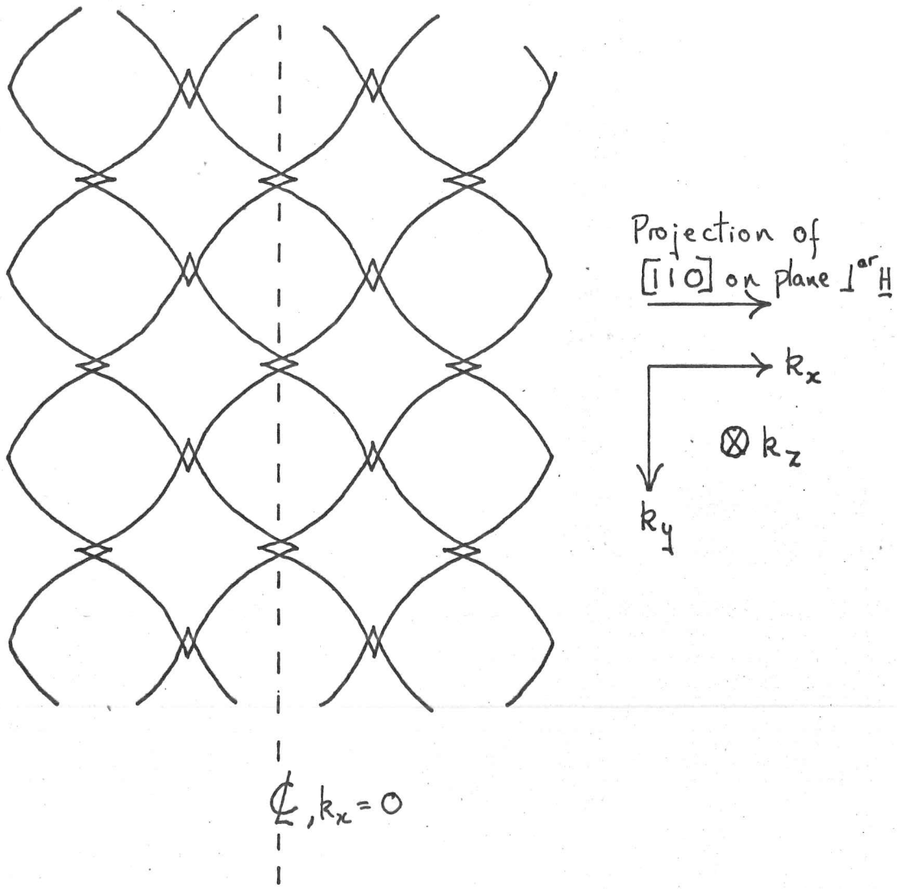

Fig. 4-5 Linear chain formed when $\underline{H}$ is tipped from [001] towards [110].

4-1b) Explanation of the dependence of R_H on H for $\theta < \theta_c$

We have already seen in Chapter 1 that there is considerable evidence for the linking by magnetic breakdown of the orbits ζ and δ to form a two-dimensional network of coupled hole orbits, H, (see fig. 1-11) for a sufficiently high magnetic field along [001]. As the field is increased the probability of breakdown increases and thus the fraction of charge carriers that are on hole orbits increases whereas the fraction on electron orbits, ζ, decreases. Thus equation (4-1) implies that R_H should become more negative, since $(n_- - n_+)$ is decreasing. As shown later, the value of the breakdown field, Ho, at different heights, k_z, above the central (001) plane can be calculated from the variation of R_H with H, for $\underline{H}$ // [001]. Now, as the angle θ is increased from zero, the plane normal to $\underline{H}$ cuts the Fermi surface at varying height above the basal plane. The breakdown field has a definite minimum in the central (001) plane of the Brillouin zone so that in this case, not all orbits are equally coupled. For example, in fig. 4-5, tilting of $\underline{H}$ in the $k_x - k_z$ plane, where in this case k_y is parallel to $[\bar{1}\bar{1}0]$, causes the breakdown field to vary with $|k_x|$ from a small value at $k_x = 0$ and the plane section passes through the centre of the zone to such a high value at large $|k_x|$ that breakdown is very unlikely. Thus the two-dimensional network is broken up into a series of linear chains of finite width, the width decreasing as θ is increased.

This has the effect of decreasing the number of hole orbits, H, so that for a constant field value, one would expect R_H to become less negative as θ is increased, as is observed.

4-1c). The dependence of R_H on H and T for $\theta > \theta_c$.

Since R_H becomes less negative as H increases for $\theta > \theta_c$, the explanation of this behaviour cannot involve magnetic breakdown as this has the opposite effect on R_H. A possible clue to the explanation may be given by the temperature dependence, for we have seen that, as the temperature is decreased, the change in R_H for a given change in H becomes greater. It looks as though small angle scattering by the phonons plays a part. Now when H is tipped away from [001] open orbits can appear on the fourth and fifth zone open surfaces. We may no longer be able to neglect the term in β', the open orbit conductivity, in equation (2-3) and thus we have that

$$R_H = \frac{e(n_- - n_+)}{\beta'(n_- y_- + n_+ y_+) + e^2(n_- - n_+)^2} \qquad (4\text{-}2)$$

Now a particle running along the top of the fourth zone hole surface, say, on an open orbit, may be scattered to a position closer to the central (001) plane where the orbits are closed, thus leading to a decrease in β'. For a given value of H and θ, decreasing the temperature would thus be expected to lead to an increase in β' and

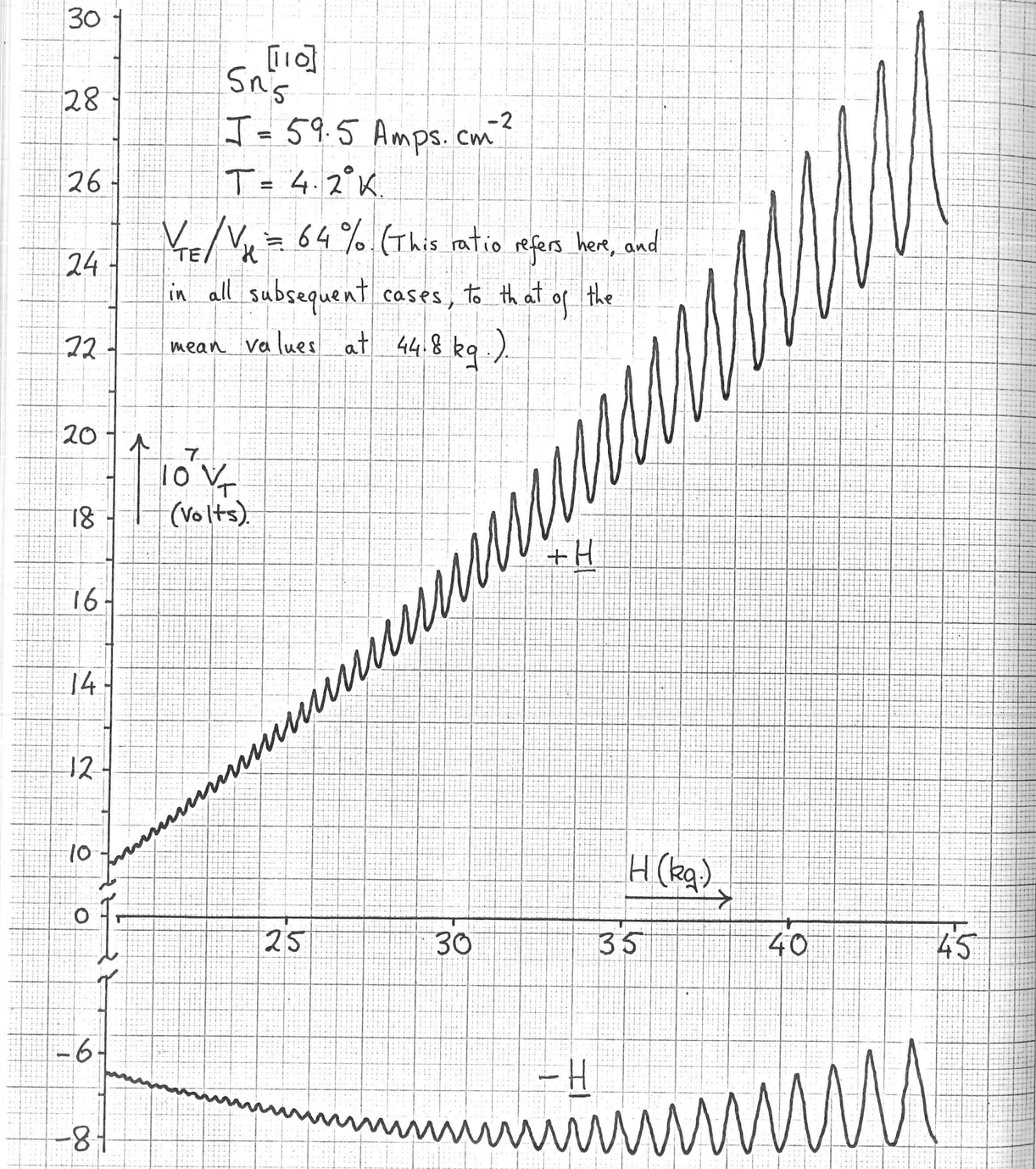

Fig. 4-6. Experimental record of transverse voltage versus magnetic field when $V_{TE} > V_H$.

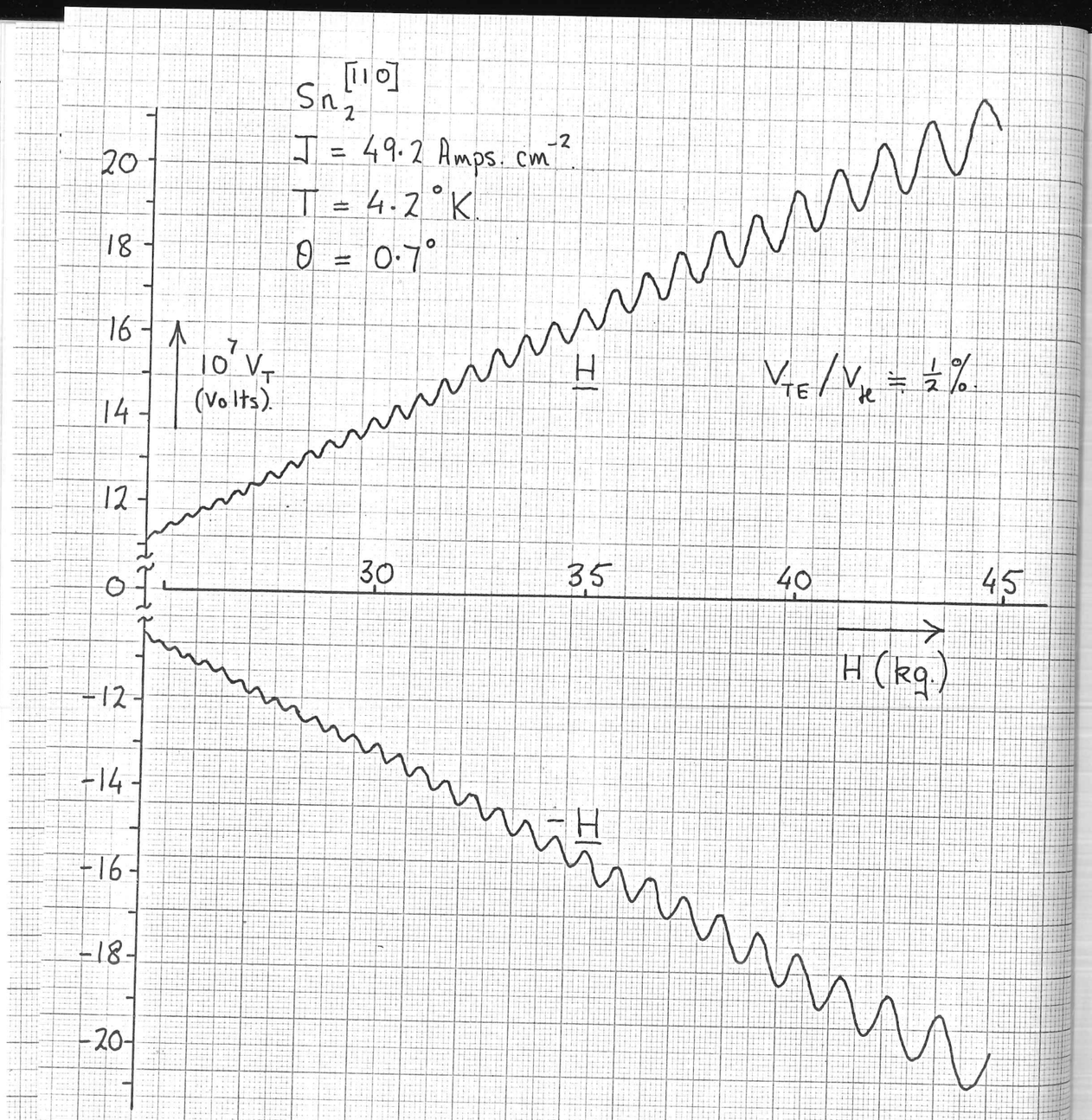

Fig. 4-7. Experimental record of transverse voltage versus magnetic field when $V_{TE} \ll V_H$.

hence a decrease in R_H, as is observed. The reason why R_H becomes less negative as H increases is still not clear and a more detailed study of the field and temperature dependence of R_H needs to be done before any firm conclusions can be made.

Results. 4-2) Oscillatory behaviour of the Hall Voltage and Transverse even voltage.

For field directions close to [001] and for field strengths, H, greater than about 20 kg., oscillations periodic in 1/H were observed in the Hall voltage, V_H, and in the transverse even voltage, V_{TE}. The oscillations in V_H could be distinguished from those in V_{TE} by the fact that the former underwent a phase change of 180° when the magnetic field was reversed whereas the latter remained unchanged. The oscillations in V_{TE} were of the same phase as those in V_H when the transverse even field and the Hall field were in the same direction. Experimental traces of the transverse voltage, V_T, made up of the Hall voltage and transverse even voltage, against the magnetic field strength, showing these oscillations, are given in figs 4-6 and 4-7. In fig. 4-6, $V_{TE} = 0.64\ V_H$ and the oscillations in V_{TE} are of greater amplitude than those in V_H. In fig. 4-7 where $V_{TE} \doteq 0.005\ V_H$, the oscillations are predominately in V_H and can be seen to reverse phase when $\underline{H}$ is reversed in direction. The frequency of these oscillations is $(0.168 \pm 0.003) \times 10^7$ g.

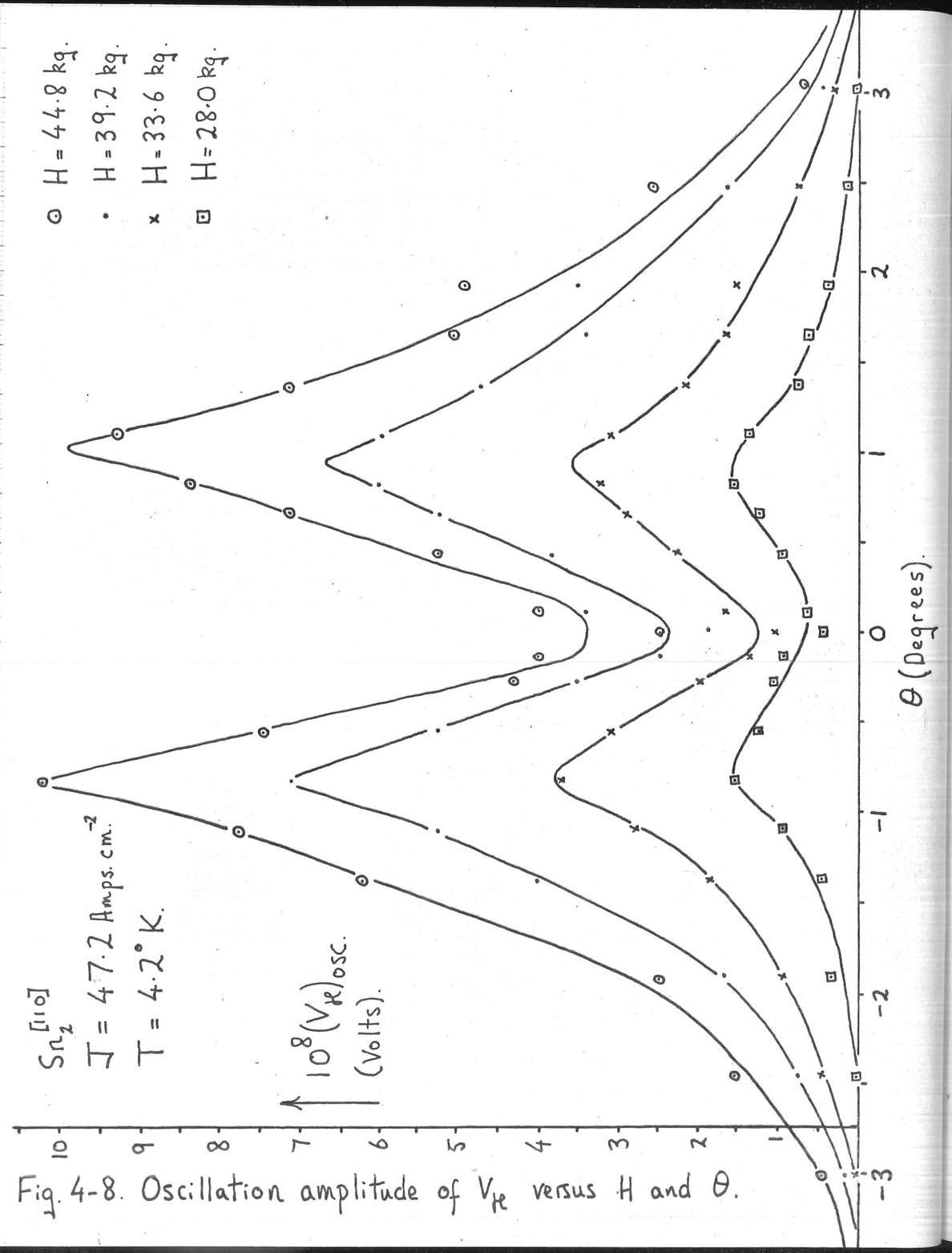

Fig. 4-8. Oscillation amplitude of V_H versus H and θ.

and is in close agreement with the value obtained by Young (20) and Hays and McLean (15) and attributed to phase coherence round the hole orbit δ.

When the field was tipped away from [001] in a plane containing J and [001], so that the transverse even voltage was zero, the amplitude of the oscillations in the Hall voltage was found to vary with angle θ between H and [001] as shown in fig. 4-8. As θ was increased from zero the oscillation amplitude rose to a definite maximum at $\theta \doteqdot \pm 1^\circ$ and then fell away to zero as θ increased beyond this. The positions of the peaks do not appear to change with field strength. Similar results were obtained for Sn_1 [$\bar{1}10$] at 4.2°K and for Sn_2 [$\bar{1}10$] and Sn_3 [$\bar{1}10$] at 1.2°K. Table 4-3 below summarizes the results for these specimens.

Table 4-3 J = 52.2Amps.cm^{-2}
H = 44.8kg.

Specimen	Temperature (°K)	Maximum $(V_H)_{osc.} \times 10^8$ (volts).	Minimum $(V_H)_{osc.} \times 10^8$ (volts).	Peak Separation (degrees)
Sn_1 [$\bar{1}10$]	4.2	10.4 ± 0.6	3.8 ± 0.6	1.6 ± 0.2
Sn_2 [$\bar{1}10$]	4.2	10.5 ± 0.4	2.5 ± 0.6	2.0 ± 0.1
Sn_2 [$\bar{1}10$]	1.2	15.0 ± 0.4	3.8 ± 0.6	2.3 ± 0.2
Sn_3 [$\bar{1}10$]	1.2	13.6 ± 0.6	6.2 ± 0.6	1.5 ± 0.2

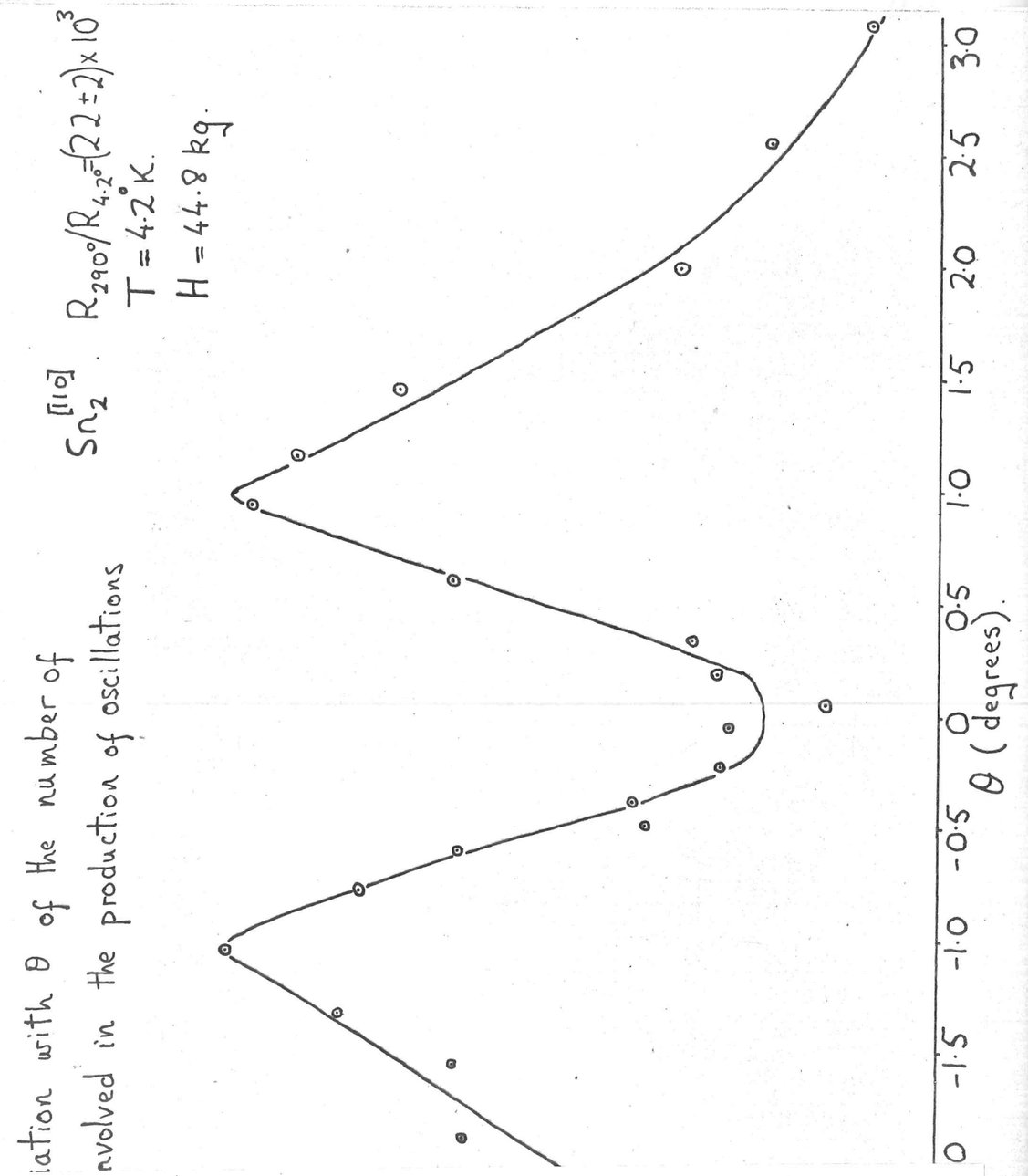

ation with θ of the number of
nvolved in the production of oscillations

(V_H) osc. is half the peak to peak value of the oscillations in the Hall voltage.

The results for $Sn_2^{[110]}$ at 4.2°K and 1.2°K were taken on different days so to attribute the difference in results solely to the difference in temperature might be misleading. Nevertheless, it appears that the oscillation amplitude increases as the temperature is decreased. The results do not allow any firm conclusions to be made about the dependence on temperature of the angular separation of the peaks.

From the results for $Sn_2^{[110]}$ at 4.2°K a graph of $N_{osc.}$ against angle θ is plotted (see fig. 4-9), where $N_{osc.}$ is the number of electrons per cm^3 involved in the production of the oscillations in V_H. Its relation to the amplitude of the oscillations in V_H is deduced below:-

When $\underline{H}$ is close to parallel to [001] we have seen that the Hall coefficient R_H is given by

$$R_H = \frac{1}{Ne}$$

where N = net number of electrons per unit volume.

$$\therefore \quad \frac{1}{Ne} = \frac{E_H}{HJ} = \frac{1}{HJ}\left(E_{H,m} + E_{H,osc.}\right)$$

where $E_{H,m}$ is the mean value of the Hall field and $E_{H,osc.}$ is the oscillatory value.

Also, suppose $N = N_m + N_{osc.}$

where N_m = number of electrons per unit volume not involved in breakdown.

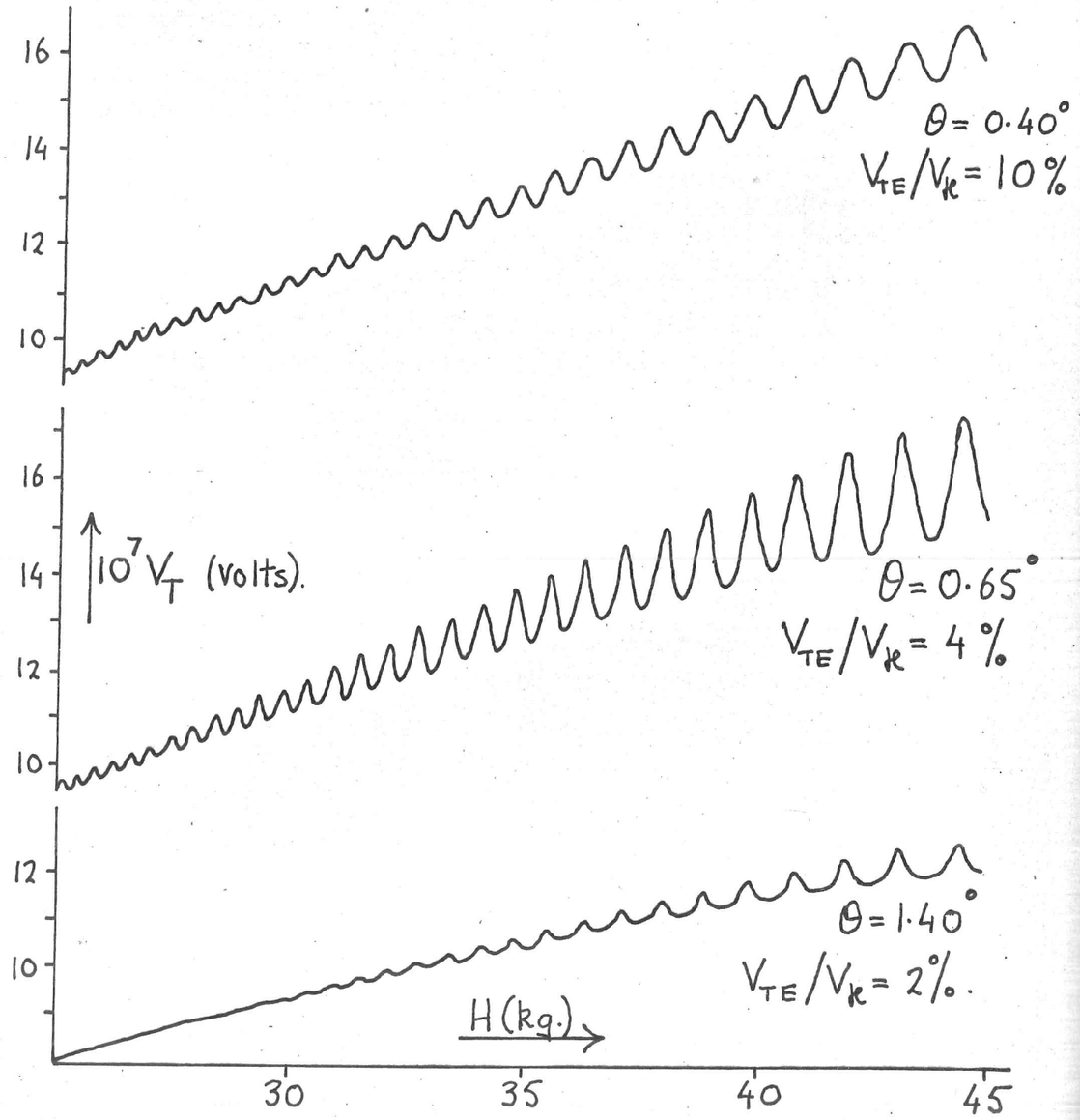

Fig. 4-10. Dependence of the oscillation shape on θ.

then $N_m + N_{osc.} = \frac{HJ}{e}\left(E_{H,m} + E_{H,osc.}\right)^{-1}$

$$\doteq \frac{HJ}{e}\left(\frac{1}{E_{H,m}} - \frac{E_{H,osc.}}{(E_{H,m})^2}\right)$$

since $E_{H,osc} \leq 0.1\ E_{H,m}$

$$\therefore \quad N_{osc.} = \left|\frac{HJ}{e} \cdot \frac{E_{H,osc.}}{(E_{H,m})^2}\right|$$

or $$N_{osc.} = \left|\frac{4HI_s}{\pi d e} \cdot \frac{V_{H,osc.}}{(V_{H,m})^2}\right| \qquad (4\text{-}3)$$

where d = specimen diameter,

I_s = specimen current.

The values of N_{osc} in fig. 4-9 may be compared to the value of the total net number, N, of electrons per unit volume, when H is parallel to [001], obtained from the low field (<8kg) value of R_H for Sn_2 [$\bar{1}$10] at 4.2°K: $|R_H| = 5.8 \times 10^{-3}$ emu., so that the equation $R_H = 1/Ne$ implies that $N = 1.1 \times 10^{22}$ electrons per unit volume.

At T = 4.2°K, the oscillations are sinusoidal for all values of θ, but when the temperature is decreased to 1.2°K, the character of the oscillations varies with θ as shown in fig. 4-10. At θ = 0 they are still sinusoidal, but as θ is increased they become less so and by θ = 1.4° they are clearly non-sinusoidal.

At fields $\gtrsim$ 40KG and at T = 1.2°K, fast oscillations, also periodic in 1/H, were observed in the transverse voltage, V_T. The measurements were made on Sn_2 [110]. Before looking for the fast oscillations, the field was tipped away from [001] in the plane containing [001] and $\underline{J}$, so that $V_{TE} = 0$, until the amplitude of the slow oscillations in the Hall voltage was a maximum. To increase the amplitude of the oscillations still further, the field was rotated about 0.2° out of the plane containing $\underline{J}$ and [001] so that $V_{TE} \neq 0$ and slow oscillations in V_{TE} also occured, reinforcing those in V_H. The stereogram below (not to scale) indicates the final direction of the magnetic field relative to [001] and $\underline{J}$ (which is within $\pm 1°$ of [110])

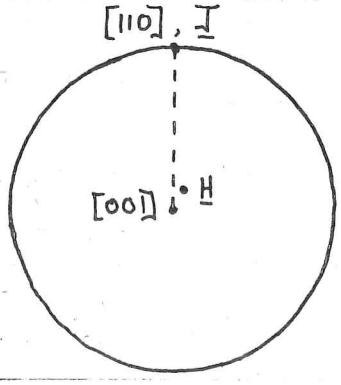

Fig. 4-11. An illustration (not to scale) of the direction of $\underline{H}$ when fast oscillations were observed.

The direction of $\underline{H}$ was such that, at 40KG, the amplitude of the slow oscillations in V_{TE} was 1.78 times that of the oscillations in V_H, and the mean value of V_{TE} was 0.58 times that of V_H. When the sensitivity

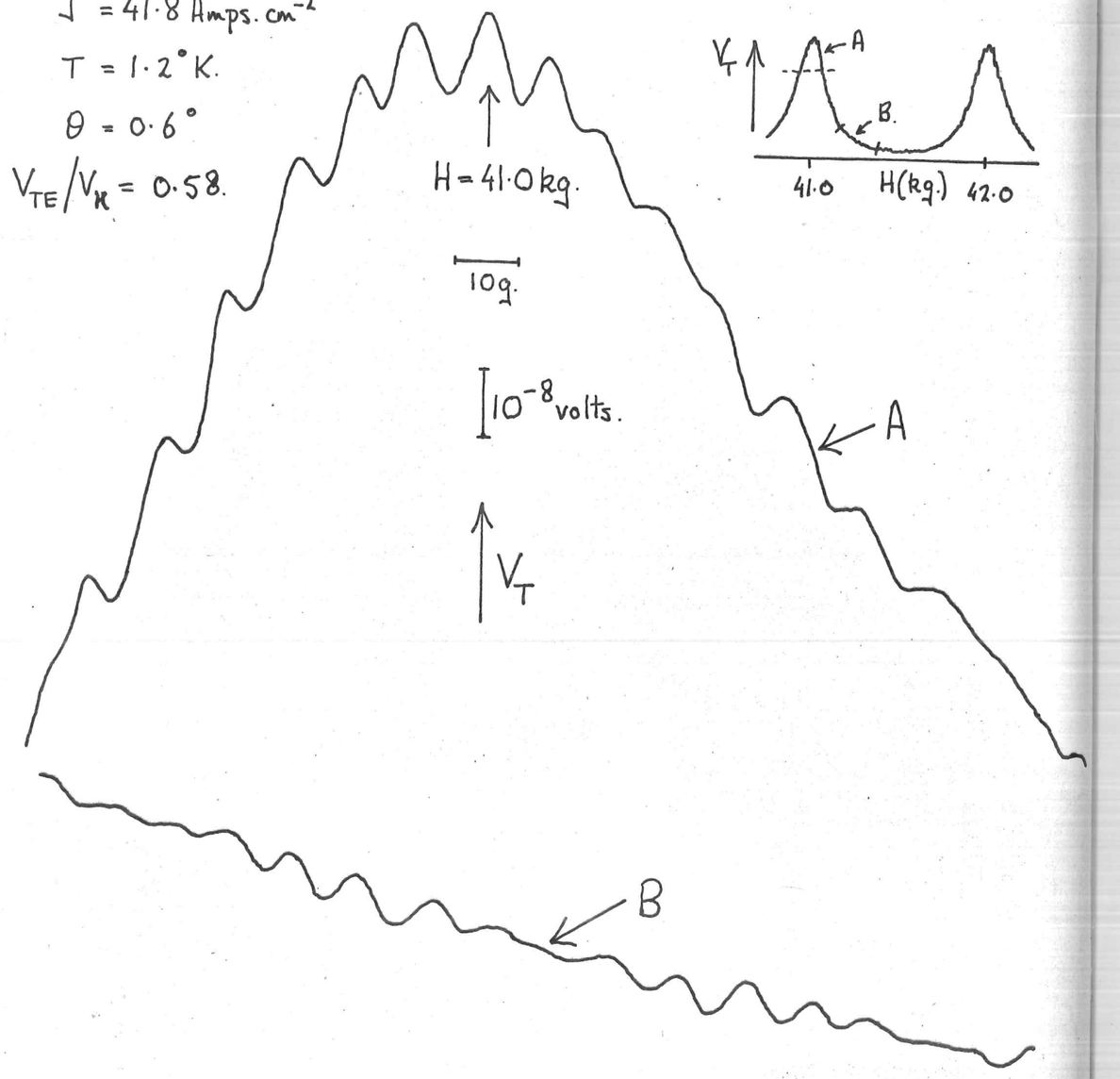

Fig. 4-12. Two sections of the experimental record of transverse voltage versus H showing fast oscillations.

of the detector was increased, the slow oscillations were seen to be non-sinusoidal as sketched in the inset in fig. 4-12. Superimposed on these slow oscillations (frequency = $[0.168 \pm 0.003] \times 10^7$g)' were fast oscillations (frequency = $[1.3 \pm 0.1] \times 10^8$g.) whose amplitude was greatest at the peak of the slow oscillations. Unfortunately, measurements were made for only one direction of field so it is not possible to say whether the fast oscillations were occuring in V_{TE} or V_H or both. Two sections of the pen recorder trace of the transverse voltage against field strength are shown in fig.4-12. Some beating was also seen. Similar results were obtained by Young(14) in measurements of the transverse magnetoresistance, .

To summarize, the results that need to be explained are:-

1) the occurence of slow oscillations in the Hall voltage; their amplitude dependence on angle θ and on field strength, H, and temperature; the dependence of the shape of the oscillations on θ at T = 1.2°K.

2) the occurence of slow oscillations of the same period in the transverse even voltage.

3) the occurence of fast oscillations in the transverse voltage.

Theory. 4-2a) An oscillatory Hall voltage. H // [001].

Consider first the case when the field is parallel to the c-axis. The central (001) section of the Fermi surface is believed to be as

shown in fig. 1-9. In weak fields large and small orbits are independent but in stronger fields breakdown couples them into a two dimensional network. The quantization of the levels of the small orbits causes the coupling between the large orbits to vary in an oscillatory manner with the periodicity of the de Haas-van Alphen effect of the small orbits. Thus the trajectory of an electron varies periodically and hence also the current density in accordance with the expression

$$\underline{J} = \frac{e^2}{4\pi^3 \hbar} \int \underline{L} \left(\underline{E} \cdot d\underline{S} \right) \qquad (4\text{-}4)$$

where $\underline{L}$ is the effective path of electrons created by the displacement of the element $d\underline{s}$ of the Fermi surface. (a derivation of this expression is given in appendix 2).

It is thought that the (001) section of the δ orbit varies with height above the central (001) plane and has an extremal area at $k_z = 0$ i.e. in the central plane. Thus the oscillatory properties are not the same at all k_z and we assume that the simplification applicable to the de Haas-van Alphen effect applies here also - namely, that there is an effective zone in which oscillations occur and outside of which they can be ignored. The effective zone is much thinner than the breakdown zone.

It is convenient to reduce the orbit network of fig. 1-9 to the square pattern of fig. 4-13 in which the sole function of the small

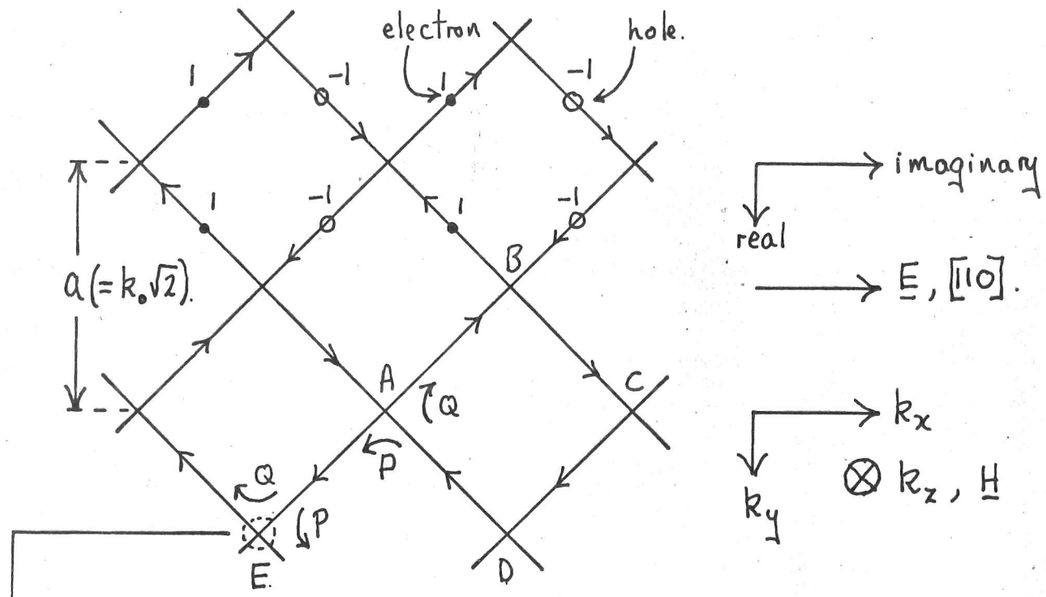

Fig. 4-13. The 2-dimensional network in k-space. The network in real space is got by rotating the one above 90° anticlockwise about k_z and scaling linear dimensions by a factor $\hbar/(eH)$.

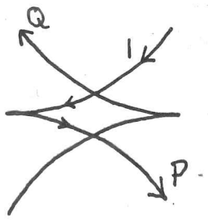

Fig. 4-14. The meaning of P and Q.

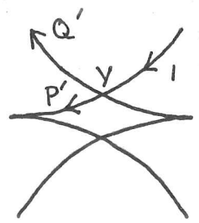

Fig. 4-15. The meaning of P' and Q'.

P' = Probability of free electron path being taken.
Q' = Probability of Bragg diffracted path being taken at junction Y.

orbit is to determine the probabilities that an electron arriving at a junction will go left (p) or right (Q) where, clearly, P + Q = 1. The meaning of P and Q is shown in fig 4-14.

Now if an electric field $\underline{E}$ is applied parallel to [110], in the real space network equal numbers of electrons are created on every arm of the network going from right to left and equal numbers of holes on all the rest; hence, in k-space, the electrons and holes, represented by the numbers +1 and -1, are generated on the arms as shown in fig. 4-13. We may evaluate the integral (4-4) round orbit ABCD in k-space. If α is the thickness of the effective de Haas-van Alphen zone, then the contribution of each arm to ds equals $\pm\frac{1}{2}a\alpha$, the sign being the same as in fig. 4-13. If collisions are infrequent compared to the cyclotron period $\frac{2\pi}{\omega_c}$, all electrons generated on a given arm will have the same history after they have passed the first junction point. Thus we can treat all electrons starting on one arm as though they started at its middle, which is therefore the mean starting point for electrons on the arm. Also, the mean terminal point for a given arm can be defined as the centroid, after a long time, of the particles created on that arm. The distance from mean starting point to mean terminal point is the effective path, $\underline{L}$, for that arm. The effective path relative to O for electrons created on DA B, $\underline{L}_{DAB}$ say, is equal to the sum of the effective paths for the arms DA and AB, each being weighted in

proportion to their extension along DB. Clearly, by symmetry

$$\underline{L}_{DAB} = -\underline{L}_{BCD}$$

Therefore equation (4-4) becomes

$$\underline{J} = \frac{e^2 E a \alpha}{2\pi^3 \hbar} \cdot \underline{L}_{DAB} \qquad (4\text{-}5)$$

Now, by Onsager's theorem, a path L_{DAB} in real space is equivalent to a path $\Lambda_{DAB} = \frac{eH}{\hbar} L_{DAB}$ in $\underline{k}$-space, the two being mutually perpendicular.

$$\therefore \quad \underline{J} = \frac{e E a \alpha}{2\pi^3 H} \cdot \underline{\Lambda}_{DAB} \qquad (4\text{-}6)$$

We now calculate $\underline{\Lambda}_{DAB}$.

Suppose that a particle generated on AD has a mean terminal point, relative to O, represented by the complex number X. Then, by -symmetry, the mean terminal point for a particle generated on AB is -ix and for one generated on AE it is i(X-a). Consider a particle starting on AD, having a probability P of moving onto AE and having a mean terminal point i(X-a), and a probability Q of moving on to AB and having a mean terminal point -ix, then

$$X = iP(X-a) - iQX$$

hence

$$X = \frac{-aPi - aP(1-2P)}{1 + (1-2P)^2} \qquad (4\text{-}7)$$

Now, the mean terminal point for DAB is $\frac{1}{2}$ (x-ix), and the mean starting point for DAB is $-\frac{ai}{4}$. Thus

$$\Lambda_{DAB} = \frac{1}{2}\left(X - iX + \frac{ai}{2}\right) \tag{4-8}$$

We are concerned with calculating the Hall conductivity and hence in real space we want the effective path normal to $\underline{E}$ and thus the effective path in k-space parallel to $\underline{E}$. Thus we want to calculate the imaginary component of Λ_{DAB} as given by equation (4-8). Substituting the value of X from equation (4-7) gives

$$(\Lambda_{DAB})_{imaginary} = \frac{a}{2}\left\{\frac{1-2P}{1+(2P-1)^2}\right\} \tag{4-9}$$

$\therefore$ (4-6) $\Rightarrow$

$$\sigma_{yx} = \frac{ea^2\alpha}{4\pi^3 H}\left\{\frac{1-2P}{1+(2P-1)^2}\right\} \tag{4-10}$$

where x is parallel to the crystal axis.

Up until now we have not taken into account the fact that phase coherence exists around the small orbits δ. When this is done (11) the probabilities P and Q of the electron making its exit by two alternative routes (see fig. 4-14) are given by

$$Q = \frac{2Q'(1-\cos\phi)}{1+Q'^2-2Q'\cos\phi}\ , \quad P = \frac{P'^2}{1+Q'^2-2Q'\cos\phi} = 1-Q. \tag{4-11}$$

The meaning of P' and Q' is indicated in fig. 4-15. ϕ ($= A_k\hbar/(eH)$ where A_K is the area of the δ orbit in k-space) is the phase length round the δ orbit which changes with H causing P and Q to oscillate with

the de Haas-van Alphen frequency of the δ orbit.

Now $P' = 1-Q' = \exp.(-H_o/H)$, and as shown later the value of H_o in the central (001) plane is estimated to be about 9kg.; thus, at H = 44.8kg., P' = 0.82.

From (4-11) we see that as Cos ϕ goes from +1 to -1, P goes from $P'^2/(1-Q')^2$ to $P'^2/(1+Q')^2$. Thus we find that the change in $(1-2P)/[1+(2P-1)^2]$ is 0.54. If we define $H\sigma_{xy}/e$ as the electron density, N, then the fluctuation, ΔN, in the electron density is given by

$$\Delta N = \frac{0.54\, a^2 \alpha}{4\pi^3} \qquad (4\text{-}12)$$

From fig. 4-9 we have that $\Delta N \doteq 1.5 \times 10^{20}\,cm^{-3}$.; also $a = \sqrt{2}.k_o$ and writing α as $2\beta k_o$, (4-12) gives $\beta = 0.007$. Thus the effective de Haas-van Alphen zone extends a height of about $0.007k_o$ above the central (001) plane, at 44.8 kg.

Now $$\rho_{yx} = \frac{\sigma_{xy}}{\sigma_{xx}\sigma_{yy} - \sigma_{yx}\sigma_{xy}}$$

and we have seen that when $\underline{H}$ is parallel to $[001]$, $\sigma_{yx}\sigma_{xy} \gg \sigma_{xx}\sigma_{yy}$ and thus

$$\rho_{yx} = -\frac{1}{\sigma_{yx}} \qquad (4\text{-}13)$$

where σ_{yx} is given by (4±10). The expression (4-10) shows that σ_{yx} is odd in $\underline{H}$ and thus one expects the oscillations to reverse phase when the field is reversed asis observed. Thus, to summarize, we have

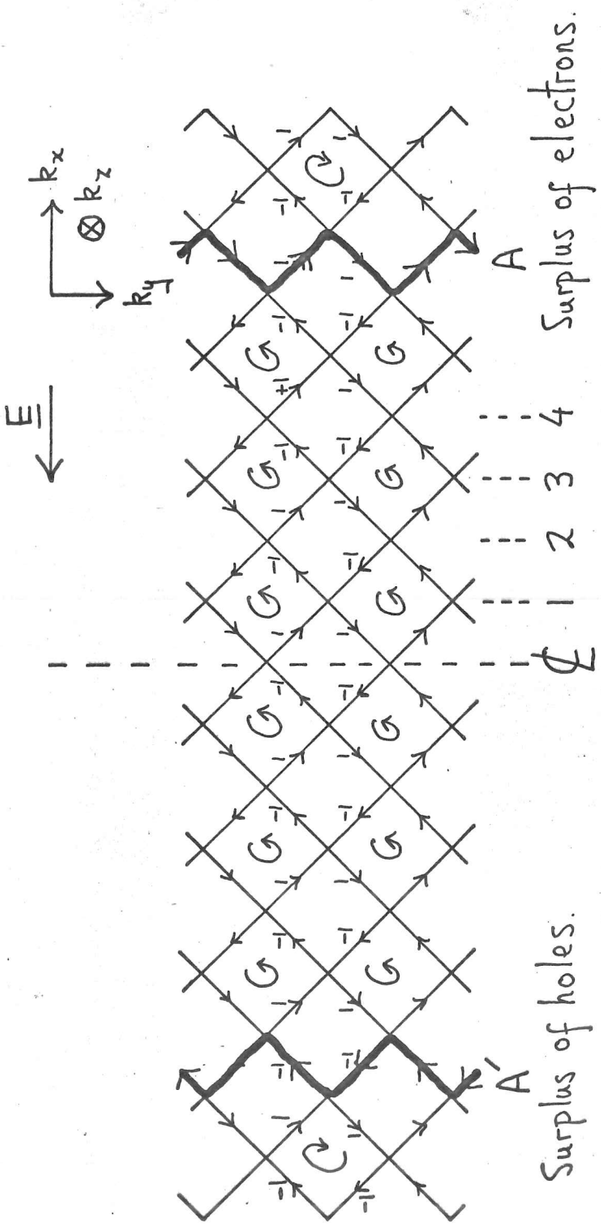

Fig. 4-16. Chain of finite width formed when H is tipped from [001] towards [110].

seen why oscillations occur in ρ_{yx} for H // [001], why they reverse phase when H is reversed, and we have also obtained an estimate for the thickness of the effective de Haas-van Alphen zone.

4-2b) Oscillations in the Hall voltage when H is close to but not parallel to [001].

Let us now consider what happens when the field is tilted away from [001]. Suppose H is tilted in the k_x - k_z plane, as shown in fig. 4-16. One consequence of this we have already noted - namely, the increase in the breakdown field from a small value when $k_x = 0$ to such a high value at large $|k_x|$ that breakdown is very unlikely. In the present experiments H was much higher than the central breakdown field so that for small $|k_x|$ the orbits are anti-clockwise and weakly coupled whereas for large $|k_x|$ they are clockwise and weakly coupled. In between, where H is of the same order as the breakdown field, H_o, the orbits are strongly coupled and an electron here can pursue an irregular path. A second consequence of the tilting is that the size of the small orbits varies with k_x having a minimum at $k_x = 0$. Thus the oscillatory properties vary with K_x. We thus make the same simplifying assumption if as we made in the case H // [001] - namely, that there is an effective zone in which oscillations occur and outside which they can be ignored. This effective de Haas-van Alphen zone is much thinner than the breakdown

zone and we shall assume that only the orbit junctions lying on the line $k_x = 0$ are subject to de Haas-van Alphen oscillations.

The process of calculating the conductivity by the effective path method involves starting electrons from every element $d\underline{S}$ of the Fermi surface in number proportional to $\underline{E}.d\underline{S}$. Thus with $\underline{E}$ parallel to k_x, the initial distribution of electrons and holes is as shown in fig. 4-16 by the numbers ± 1. As pointed out before, to determine the Hall conductivity we need to find their effective path parallel to $\underline{E}$ i.e. in the $-k_x$ direction. (11, 23)

The Physical situation is not falsified by the assumption that P and Q do not vary smoothly with k_x but that out to a certain distance, Q is small, and then changes abruptly to unity. If Q were actually zero in the central strip then electrons and holes created on the arms at the start of the calculation would perform closed orbits as shown in fig. 4-16 and there would be a sinuous path for electrons around A and for holes around A'. As Q is not quite zero, the particles wander from orbit to orbit and eventually, if there are no collisions, they spread evenly over the central strip, no matter how small Q may be. Thus the effective paths in k-space in the direction parallel to $\underline{E}$ for the particles on all the arms of the network will be independent of P and Q, and thus there should be no oscillations in the Hall conductivity. However, when $Q \ll 1$, a very large number of cyclotron periods are

required for this spreading process so that a very small amount of scattering may prevent its being completed. In this case, particles starting on the right half, where electrons outnumber holes, do not move right across to mix with those on the left half where there is an excess of holes. The shortened X-components of the effective paths of both types of particles lead to a modified value of the Hall conductivity. Also, the ability of the particles to cross the centre line is determined by Q and hence oscillates at the de Haas-van Alphen frequency causing the Hall conductivity to also oscillate. Thus we see that a long but finite relaxation time for the electrons is an essential condition for the explanation of the effect. This is very unusual as one expects the Hall constant to be independent of the existence of scattering when $\omega_c \tau \gg 1$.

Detailed Calculation.

The following theory is due to Pippard.

As was the case when $\underline{H}$ // [001] we may write

$$\sigma_{yx} = \frac{e a \alpha}{8\pi^3 H} \sum \left(\pm \Lambda_x \right) \qquad (4\text{-}14)$$

where α is the thickness of the effective de Haas-van Alphen zone and Λ_x the effective path in the k_x direction in k-space, the signs being the same as in fig. 4-16. If the k_x coordinate of the centre of a typical arm is $\frac{1}{2}aX_o$ and the centroid of all particles starting on this arm is finally located at $\frac{1}{2}aX_\infty$, then $\Lambda_x = \frac{1}{2}a(X_\infty - X_o)$.

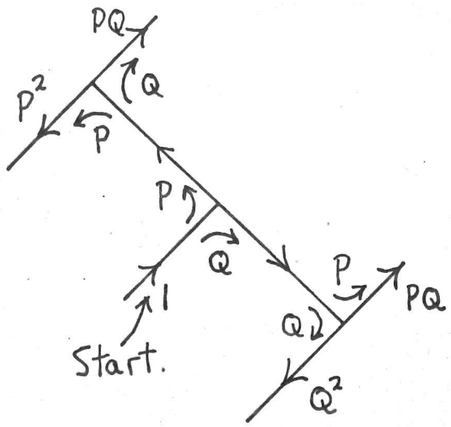

Fig. 4-17.

Rules for evolution of the distribution when Q is constant.

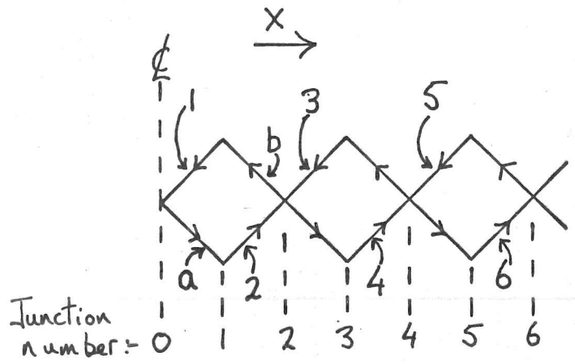

Fig. 4-18.

An element of the network of fig. 4-16.

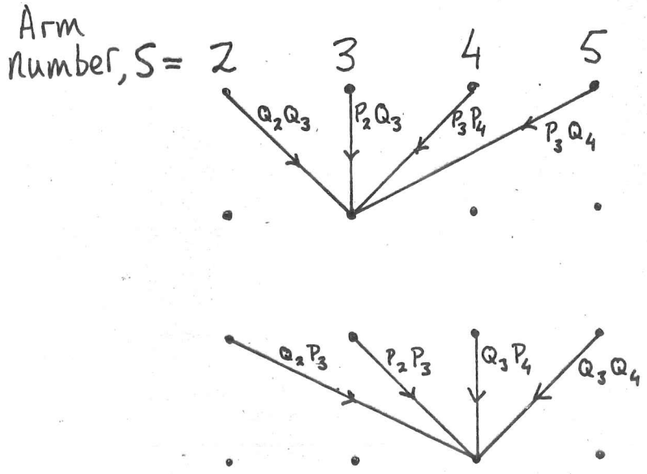

Fig. 4-19.

Rules for evolution of the distribution when Q varies.

We are only concerned with the oscillatory part of β_{yx} resulting from variations of X_∞ and so we may ignore X_o and write for the variations of β_{yx}

$$\Delta\beta_{yx} = \frac{e a^2 \alpha}{16\pi^3 H} \sum(\pm \Delta X_\infty) = \frac{e a^2 \alpha}{16\pi^3 H} \Delta M \qquad (4\text{-}15)$$

To find the total moment M, of the particles about the central line and its variations with H we need to follow the evolution of the particles on the network until their centroid has reached its final position. Since, however, $\omega_c \tau \gg 1$, it is sufficient and convenient to only look at the distribution twice in each cyclotron period when all the particles on one arm have moved onto neighbouring arms in accordance with the scheme shown in fig. 4-17. Suppose now that there is no scattering. The pattern has translational symmetry in the y-direction so we need only describe the population of particles on the arms of an element such as is shown in fig. 4-18. Suppose we label a set of parallel arms as shown in fig 4-18. If $n_{r,s}$ is the population of the arm whose serial number is S at a time $r\left(\frac{\pi}{\omega_c}\right)$ after the initial ± 1 distribution was set up, then by reference to fig. 4-17, we have

$$\left.\begin{aligned} \text{for S odd}, \quad & n_{r+1,s} = P^2 n_{r,s+1} + PQ(n_{r,s} + n_{r,s+2}) + Q^2 n_{r,s-1} \\ \text{S even}, \quad & n_{r+1,s} = Q^2 n_{r,s+1} + PQ(n_{r,s} + n_{r,s-2}) + P^2 n_{r,s-1} \end{aligned}\right\} \qquad (4\text{-}16)$$

Also $n_{o,s} = +1$ for S odd, -1 for S even.

We now show how, for an extended network, this evolution may be described approximately as a diffusion process. Let us consider the evolution of some special distributions:-

1) The same initial population on all arms: $n_{r,s} = C$. From (4-16) we see that since $P + Q = 1$, $n_{r+1,S} = C$ and the population remains unchanged.

2) Alternating population: $n_{r,s}$ is alternately $\pm C$; then $n_{r+1,s}$ is alternately $\mp(1-2Q)^2 C$ and unless Q is very small the distribution decays in about 1/4Q steps. Thus a distribution alternating between N and M soon reaches a steady distribution of $\frac{1}{2}$ (N + M) on each arm which remains unchanged.

3) A generalized gradient: for S odd, $n_{r,s} = sA + B$

for S even, $n_{r,s} = sC + D$.

This distribution may be dissected into a part which persists unchanged and a part which decays at the same rate as in case (2).

For the long-term evolution of the pattern we are concerned only with the persistent part and Pippard has shown its structure to be:

$$\left.\begin{aligned} \text{for S odd,} \quad & n_{r,s} = \tfrac{1}{2}(A+C)(s+\alpha) + \tfrac{1}{2}(B+D) + \tfrac{1}{2}(A-C)\beta \\ \text{for S even,} \quad & n_{r,s} = \tfrac{1}{2}(A+C)(s-\alpha) + \tfrac{1}{2}(B+D) + \tfrac{1}{2}(A-C)\beta \end{aligned}\right\} \qquad (4\text{-}17)$$

where

$$\alpha = \left(\tfrac{1}{2} - Q^2\right) \Big/ \left(P^2 + Q^2\right),$$

$$\beta = \left(P^2 - \tfrac{1}{2}\right) \Big/ \left(P^2 + Q^2\right).$$

Hidden within this stationary state is a flux of particles across the network of $\frac{2PQ}{P^2+Q^2} \times \frac{1}{2}(A+C)$. $\frac{1}{2}$ (A + C) is the mean gradient of the population, if we average the populations of the arms in pairs, so that we may regard the evolution as proceeding according to a one-dimensional diffusion equation:-

$$\frac{\partial n}{\partial r} = D \frac{\partial^2 n}{\partial x^2} \qquad (4\text{-}18)$$

where r is time measured in units of $\frac{\pi}{\omega_c}$, X is distance in units of $\frac{1}{2}a$, and $D = \frac{2PQ}{P^2+Q^2}$.

Let us consider now the effect of collisions. In real space an isotropic collision prevents the electron concerned from making any further contribution, on average, to the motion of the centroid of all electrons; it can therefore be regarded as being stopped dead by collision. Similarly, in $\underline{k}$ space, as the distribution evolves the electrons that suffer collisions are deposited on the network until ultimately all electrons are at rest. It is their centroid which determines X_∞. When collisions exist, a small fraction $\varepsilon \left(= \frac{\pi}{\omega_c \tau}\right)$ of the electrons are brought to rest in each time interval. If M_r is the moment in the r^{th} time interval in the absence of collisions, then when collisions are present the moment actually left in evolution is $M_r e^{-r\varepsilon}$ and the moment of the electrons brought to rest in this time interval is $\varepsilon M_r e^{-r\varepsilon}$. Thus the value of M, with its variations M to be inserted in (4-15) is $\varepsilon \sum_r M_r e^{-r\varepsilon}$, with M_r calculated for the collision -

free case. This is only the contribution of the electrons on the numbered arms in fig. 4-18. Clearly, by symmetry, the contributions to M of the regions on the left of the centre line are the same as those on the right. Also, we may suppose that the particles deposited from the S^{th} arm are deposited at its centre and thus the centroid of the particles deposited from a pair of arms such as 1 and 2 will have an X-coordinate equal to 1. The X-coordinate of the centroid of particles deposited from arms a and b will also be X = 1. Thus the unnumbered arms will make the same contribution to M as the numbered arms and we can write from (4-15)

$$\Delta \beta_{yx} = \frac{e a^2 \alpha}{4\pi^3 H} \varepsilon \sum_r \Delta M_r e^{-r\varepsilon}$$

This may be expressed as fluctuations of the electron density N defined as $H\beta_{yx}/e$:-

$$\Delta N = \frac{a^2 \alpha}{4\pi^3} \varepsilon \sum_r \Delta M_r e^{-r\varepsilon} \qquad (4\text{-}19)$$

We have seen that for an extended network, the evolution may be treated as a diffusion process. We now need to consider what the initial distribution looks like. Consider the case where Q varies with X so that the rules for evolution become those shown in fig. 4-19. $n_{0,s}$ = 1 for S odd and -1 for S even, and after one time interval the distribution has changed to

for S odd : $n_{1,s} = Q_s (P_{s-1} - Q_{s-1}) - P_s (P_{s+1} - Q_{s+1})$

for S odd : $n_{1,s+1} = -Q_s (P_{s+1} - Q_{s+1}) + P_s (P_{s-1} - Q_{s-1})$

Thus the sum of the occupations for two neighbouring arms does not vanish, but has the values $2(Q_{s+1} - Q_{s-1})$. As Q varies from its central value, Q_o, to unity far out, the smoothed distribution (i.e. the average of pairs of arms) contains $2P_o$ particles congregating around that part of the network where Q varies most rapidly.

The diffusion of $2P_o$ particles on a network with varying P and hence varying diffusion constant presents a large computational problem. To simplify matters therefore, we suppose that Q takes a constant small value up to a certain number, w, of junctions from the centre line and then rises abrupt to unity; w defines the effective half-width of the breakdown strip. The initial distribution is thus $2P_o\,\delta(X-w)$, and P_o of the particles diffuse in the strip, the other P_o being stuck in closed orbits just outside. There is a similar source of opposite sign on the other side, $-2P_o\,\delta(X-w)$. The inability of the particles to diffuse out of the strip can be simulated by imaging the distribution in the boundaries $\pm w$, without change of sign. Thus we need to solve the problem of the diffusion on an infinite line of the initial distribution $\sum_{-\infty}^{\infty}{}' (-1)^n 2P_o\,\delta[X-(2n+1)w]$.

We are primarily interested in the effect of changing the value of Q at the centre line. One special case that can readily be solved is that for Q = 0, so that no particles can cross the centre line. This situation can be simulated by giving all the images positive signs so that the

initial distribution is $\sum_{-\infty}^{\infty} 2P_0\,\delta[x-(2n+1)w]$ and the net flux of particles across the centre line is zero. This will only give the correct evolution in the strip $0<X<w$ but this is all we need to know.

The difference in M(r) between these two cases turns out to be given by

$$\Delta M_r = (M_r)_{Q=0} - (M_r)_{Q=Q_0} = \frac{4P_0 w\beta}{\sqrt{\pi}} \sum_{n\,\text{odd}}^{\infty} e^{-4n^2\beta^2} \qquad (4\text{-}20)$$

where $\beta = w/(4Dr)^{\frac{1}{2}}$.

Thus (4-16) implies that the difference in electron density determining the Hall constant in the two situations is given by

$$\Delta N = \frac{a^2\alpha P_0 w^2 \varepsilon}{2\pi^{7/2} D^{1/2}} \sum_{n\,\text{odd}}^{\infty} \sum_{r}^{\infty} r^{-1/2} \exp.\left(-4n^2\beta^2 - r\varepsilon\right)$$

$$\doteqdot \frac{a^2\alpha P_0 w^2}{2\pi^3} \left(\frac{\varepsilon}{D}\right)^{\frac{1}{2}} \sum_{n\,\text{odd}}^{\infty} \exp.\left[-2nw\,(\varepsilon/D)^{\frac{1}{2}}\right].$$

$$\therefore \quad \Delta N = \frac{a^2\alpha P_0 w^2}{4\pi^3} \left(\frac{\varepsilon}{D}\right)^{\frac{1}{2}} \operatorname{Cosech}\left[2w\,(\varepsilon/D)^{\frac{1}{2}}\right]. \qquad (4\text{-}21)$$

This expression may be taken as a measure of the amplitude of the Hall effect oscillations.

If we take the breakdown zone in k-space to be the region of k_z within which the breakdown field, H_0, is less than the applied field,

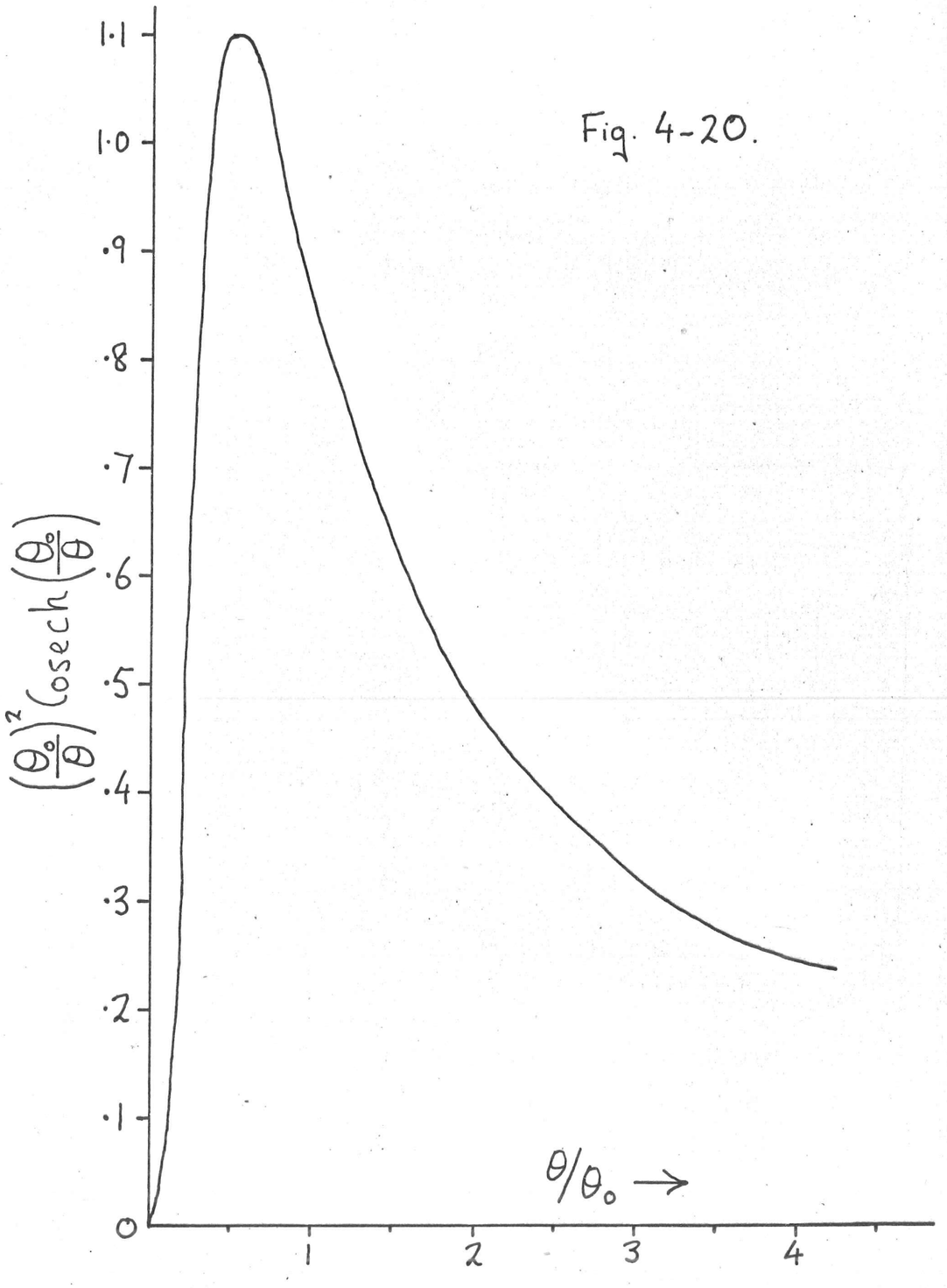

Fig. 4-20.

then $w = h/(a\theta)$ where h is the height of the breakdown zone. Also, from (4-11), the mean value of Q_0 (averaged over one oscillation period) is given by

$$Q_0 \doteq \frac{2H_{00}}{H} \qquad \text{if} \quad H_{00} \ll H$$

H_{00} is the breakdown field in the central plane of the zone. Thus $D \doteq 4H_{00}/H$ and since $\varepsilon = \pi/(\omega_c\tau)$, (4-21) may be written as

$$\Delta N = \tfrac{1}{2} N_0 \left(\frac{\omega_0\tau}{\pi}\right)^{1/2} \left(\frac{\theta_0}{\theta}\right)^2 \operatorname{Cosech}\left(\frac{\theta_0}{\theta}\right) \qquad (4\text{-}22)$$

in which $N_0 = a^2\alpha/4\pi^3$, the number of electrons in the de Haas-van Alphen band of the Brillouin zone, ω_0 is the cyclotron frequency at H_{00} and $\theta_0 = \frac{h}{a}\left(\frac{\pi}{\omega_0\tau}\right)$.

Comparison with results.

A graph of $\left(\frac{\theta_0}{\theta}\right)^2 \operatorname{Cosech}\left(\frac{\theta_0}{\theta}\right)$ against $\frac{\theta}{\theta_0}$ is shown in fig. 4-20. From equation (4-22) we see that this gives the angular dependence of ΔN and it is clearly similar to that observed experimentally. To see whether the parameters are reasonable we choose θ_0 to be 1.0° so that experimental and theoretical curves coincide about half way down from the peak on the outside. For the sample measured, the resistance ratio was about 20,000 which gives $\omega_c\tau$ a value of about H/300, where H is in kilogauss. H_{00}, as shown later, is estimated to be about 9 kg. so that $\omega_0\tau$ has a value of 30. Thus we deduce that the breakdown zone has a height of about

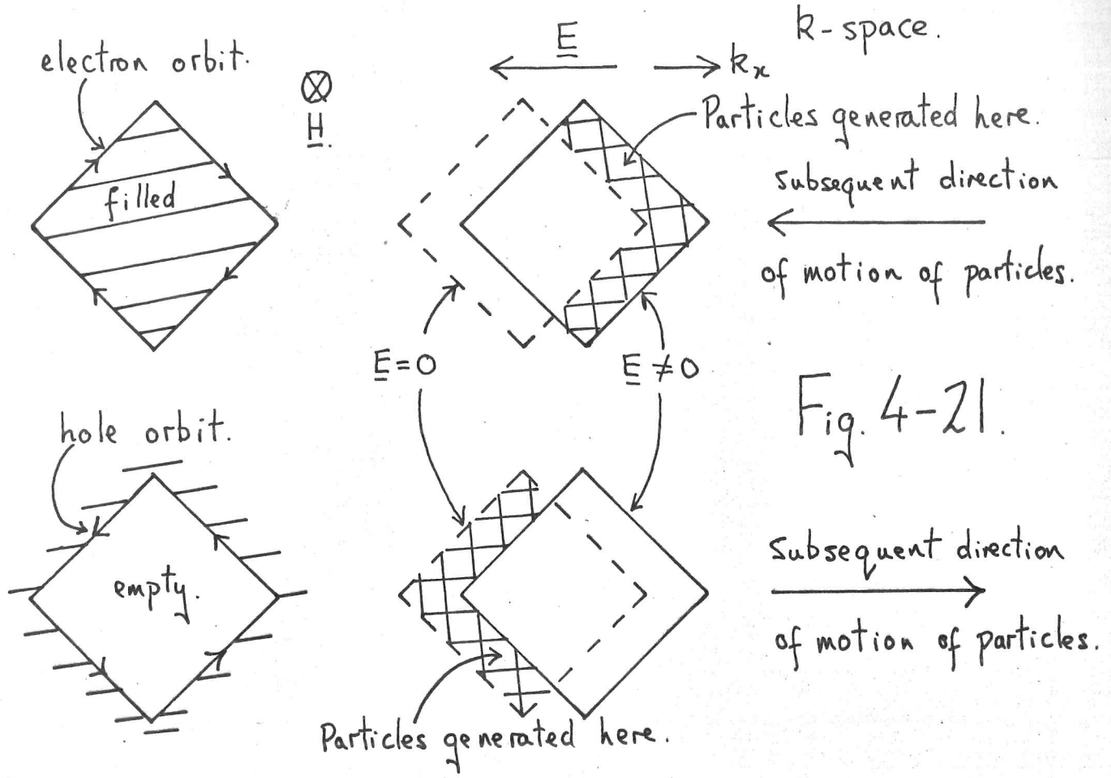

Fig. 4-21.

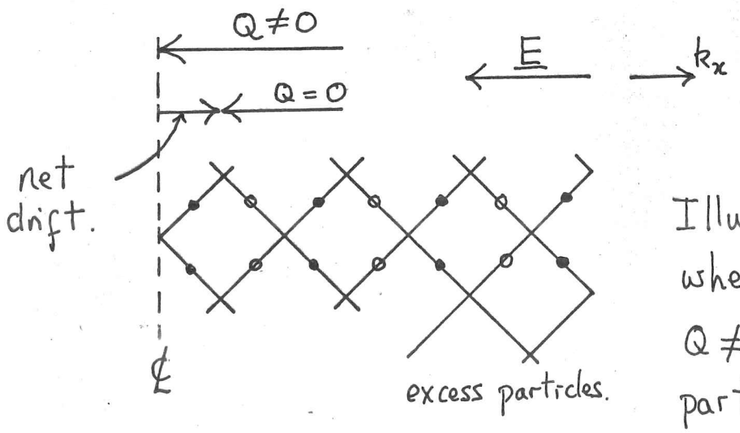

Fig. 4-22.

Illustration of how, when Q changes from $Q \neq 0$ to $Q=0$, the particles effectively drift in a direction opposite to $\underline{E}$, which is characteristic of hole-like behaviour.

0.08 k_o at 45 kg. ($k_o = 1.08 \times 10^8 cm^{-1}$). Also from the value of ΔN at the point half way down from the peak on the outside, we estimate that the height of the de Haas-van Alphen zone above the central (001) plane is about 0.01 k_o; this agrees fairly well with the value of 0.007 k_o obtained previously.

4-2C) The dependence of the shape of the oscillations on angle θ.

We have seen in fig. 4-10 how, as the angle θ between $\underline{H}$ and [001] is increased from zero, the shape of the oscillations changes from sinusoidal, becoming more and more spiky. The spikes correspond to R_H becoming more negative which we have seen corresponds to an effective increase in the number of holes present. Thus we may describe the spikes as 'hole-like'.

The following explanation for the occurence of these hole-like spikes is due to Pippard.

Consider an electron orbit - fig. 4-21 - enclosing filled states. Application of an electric field $\underline{E}$ in the $-\underline{k}_x$ direction generates particles and a deficiency of particles as shown, so that the subsequent motion of the particles tending to restore the uniform distribution is in the direction of $-\underline{k}_x$. In the case of hole orbits, the motion is in the opposite direction. Consider now a section of the network (of finite length in the k_x direction) as shown in fig. 4-22. The application of

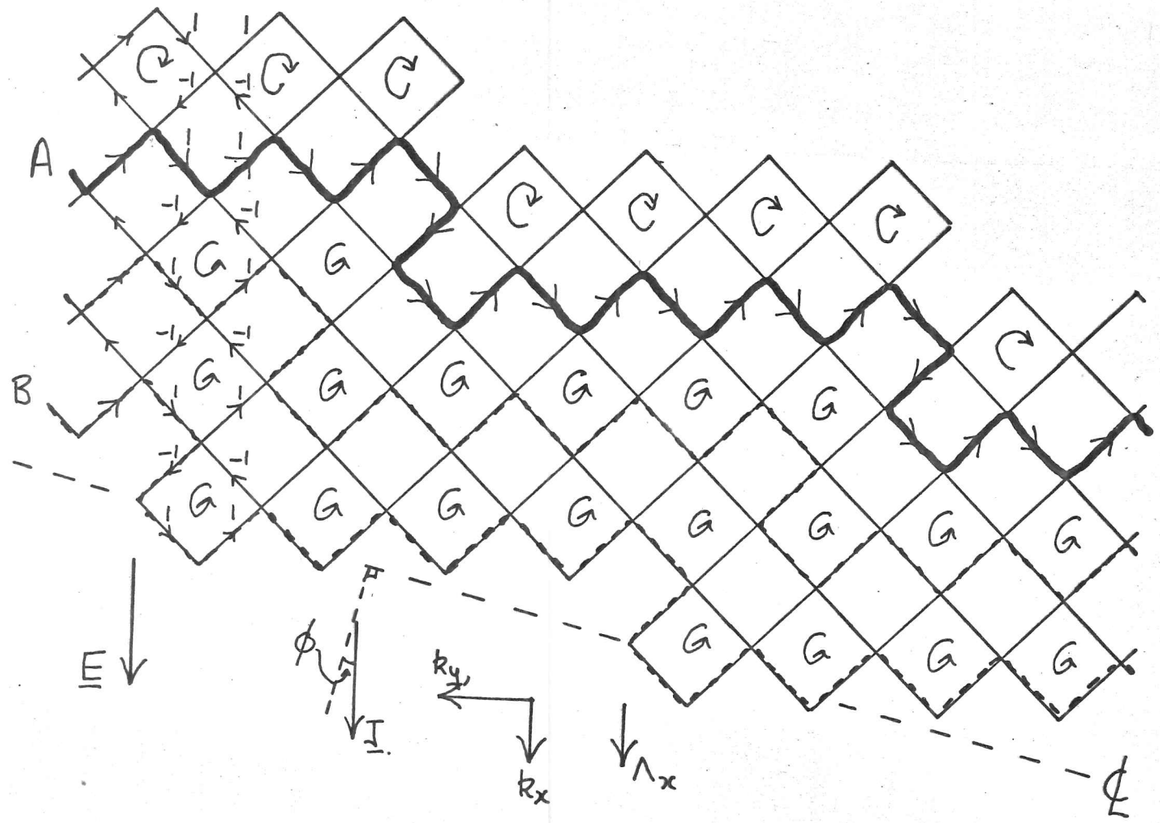

Fig. 4-23. An element of the network, in k-space, of coupled orbits formed when $\underline{H}$ lies just outside the plane defined by [001] and $\underline{I}$, where $\underline{I} \parallel [110]$. The network is similar to that of Fig. 4-16, except that the open orbit at A is aperiodic. (The effective path Λ_x determines δ_{yx}.)

$\underline{E}$ creates an excess of electrons for this section of the network (there is an excess of holes on the other side of the centre line) and they drift from right to left. Now as θ is increased, the strip becomes narrower and the diffusion process is fast enough to spread the particles evenly over the strip. However when Q = 0 the particles are unable to cross the centre line so that when Q = 0 it is as though there was an effective drift of the particles from left to right as illustrated in fig. 4-22. We have seen that this is characteristic of behaviour of 'hole-orbits'. Thus we expect that, as θ is increased, the oscillations in V_H begin to look like hole-like spikes, which occur whenever Q = 0, as is observed.

4-2d) Oscillations in the transverse voltage when $\underline{H}$ does not lie in the plane, P, defined by $\underline{J}$ and $\overline{[001]}$.

Let us consider the case where $\underline{H}$ lies close to $\overline{[001]}$ but just outside the plane, P. The network of coupled orbits forms a strip of finite width as before but in this case its axis makes an angle (90 - ϕ), say, with $\underline{J}$ (for the specimen studied, $\underline{J} \parallel \overline{[110]}$). This is illustrated in fig. 4-23. Suppose we make the same simplifying assumption as before, namely that out to a certain distance from the centre line Q is small and then changes abruptly to unity. In the present case the orbits performed by the particles are similar to those

performed when H lay in the plane defined by J and [001], except that now the open orbit traversed by electrons at A is aperiodic rather than periodic. With the electric field, E, applied as shown there is an excess of electrons on one side of the strip (fig. 4-23); these will diffuse towards the centre line and we expect to see an oscillatory Hall voltage as before. In the present case, however, magnetic breakdown does not occur over the same range of k_z values at each of the junctions which lie closest to the centre line, so that the number of orbits which undergo breakdown in the de Haas-van Alphen zone is reduced. Thus a reduction in the amplitude of the oscillations in the Hall voltage is expected when the field is moved out of the plane defined by J and [001].

Let us now consider how oscillations in the transverse even voltage arise. We have that

$$(\rho_{yx})_{even} = \frac{\sigma' H^2 \sin\phi \cos\phi}{\sigma'(n_- \gamma_- + n_+ \gamma_+) + (n_- - n_+)^2 e^2}$$

where $(90 - \phi)$ is the angle between the open orbit direction in $k_\pm$ space and the projection of J on the plane perpendicular to H. The open orbit conductivity, σ', is made up of two components. One due to the aperiodic open orbits which run along the top and bottom of the fourth and fifth zone open surfaces, and take no part in the breakdown process. The second component comes from aperiodic open orbits such as that at A (fig. 4-23) which arise due to the linking of the orbits by

breakdown. Since Q is not quite zero even for the junctions near the centre line, it is possible for similar open orbits to occur on the rest of the network as indicated by the dotted lines in fig. 4-23. Suppose Λ_o is the effective path in k-space measured parallel to the mean direction of the open orbit, for a particle generated on one of the arms of the open orbit. It is clear that this has a component $\Lambda_o \sin\phi$ in the direction of E, and hence the open orbits formed by breakdown contribute to the conductivity term σ_{yx}. To get some estimate for Λ_o we consider the case where H lies in the plane defined by J and [001] so that the open orbits are periodic.

Young (14) has derived an expression for Λ_o for the case where orbits γ and δ are coupled into a linear chain along [110] as shown in fig. 1-12. Taking into account phase coherence effects on both γ and δ orbits he found that Λ_o was given by

$$\Lambda_o = \frac{a}{2|b|^2} \qquad (4\text{-}23)$$

where $$|b|^2 = \frac{1+\cos(\omega-\alpha+\beta)}{Q\{1+\cos(\omega+\alpha+\beta)\}}$$

2α and 2β are the phase shifts around orbits γ and δ, and are related to their areas in k-space (at the Fermi surface) by $2\alpha = \hbar A_\gamma/(eH)$, $2\beta = \hbar A_\delta/(eH)$. Exp.$(i\omega)$ is the phase factor by which the wave function is multiplied upon translation through one repeat spacing, a,

of the network. Using expression (4-23) for Λ_0, Young found that the transverse magnetoresistance exhibited very large slow oscillations with a period in 1/H corresponding to phase coherence around the δ orbit; smaller amplitude, higher frequency ($f = 1.2 \times 10^8$ g.) oscillations were observed due to the orbit γ. The amplitude of the latter oscillations was found to be a maximum at the peak of the slow oscillations. Thus, even if ϕ is small, we expect to see slow oscillations in the even component of ρ_{yx} due to the oscillatory component of the open orbit conductivity. Smaller amplitude, faster oscillations are also expected. However, of the possible open orbits shown in fig. 4-23, only those which pass through the effective de Haas-van Alphen zone will contribute to the oscillations.

The occurence of slow oscillations in the Hall voltage and transverse even voltage, and fast oscillations in the transverse voltage, when H lies close to [001] but just outside the plane P is thus accounted for. It is worth noting that the occurence of fast oscillations due to the orbit γ at about 40kg. implies that the dislocation density of the specimen, Sn_2[110], is about $3 \times 10^7 cm^{-2}$. This is because at 40kg., the area of the γ orbit is about $3.5 \times 10^{-8} cm^2$ and no oscillations are expected if the dislocation density is such that the γ orbit contains a dislocation (11).

4-3) Dependence of the breakdown field, H_o, on height, k_z, above the central (001) plane

From the change in the value of $R_{//}$ as the field, parallel to [001], is increased we can calculate the net decrease, ΔN, in the number of electrons per unit volume caused by the conversion of electron orbits ζ, into hole orbits, H, by magnetic breakdown. Assuming a relation between H_o and k_z of the form $H_o = B(k_z^2 + A^2)$ where A, B are constants, we then proceed to obtain values for A and B by the method of curve fitting.

Detailed calculation

Consider the cross section (in the central (001) plane) of the fourth zone hole surface as shown below:-

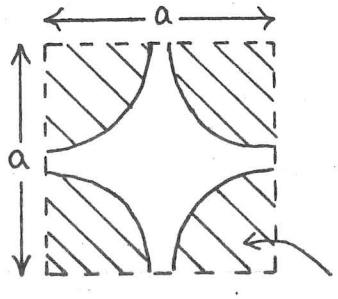

Fig. 4-24. Cross section in the central (001) plane of the fourth zone hole surface.

$a = \sqrt{2}.\, k_o$, $k_o = 1.08 \times 10^8\ cm^{-1}$.

The shaded regions are those enclosed by the electron orbit ζ and contain filled states. The unshaded region is the empty region enclosed by the hole orbit, H, when breakdown occurs. If we suppose that, for a given field along [001], breakdown is completely up to a height βk_o above the central (001) plane and is zero beyond this height, then the net decrease, ΔN, in the number of electron states per unit volume caused by the conversion of orbit ζ into orbit H is given by

$$\Delta N = \frac{1}{4\pi^3} \cdot 2k_o^2 \cdot 2\beta k_o \qquad (4\text{-}24)$$

From the variation of $R_{\mathscr{H}}$ (= $\frac{1}{Ne}$ where N is the net number of electrons per unit volume) with $\underline{H}$, for $\underline{H} \parallel [001]$, the variation of ΔN, and hence of β, with $\underline{H}$ may be determined. The results are tabulated below:-

Table 4-3

H (kg)	$R_H \times 10^3$ (emu)			
	Sn_1[110] (4.2°K)	Sn_2[110] (4.2°K)	Sn_2[110] (1.2°K)	Sn_3[110] (1.2°K)
0-5	5.40	5.78	6.40	5.60
11.2	5.56	5.94	6.66	5.76
22.4	6.12	6.60	7.26	6.50
33.6	6.70	7.24	7.90	6.90
44.8	7.20	7.64	8.60	7.28

Table 4-4

H (kg)	$\Delta N \times 10^{22}$ (cm^{-3})					$\beta \times 10^2$
	Sn_1	Sn_2	Sn_2	Sn_3	mean	
0-5	0	0	0	0	0	0
11.2	0.04	0.03	0.06	0.06	0.05 ± 0.01	1.2 ± 0.2
22.4	0.14	0.13	0.13	0.20	0.15 ± 0.02	3.7 ± 0.4
33.6	0.23	0.22	0.20	0.21	$0.21_5 \pm 0.01$	5.3 ± 0.3
44.8	0.29	0.26	0.26	0.26	0.27 ± 0.01	$6.6_5 \pm 0.2$

We now derive an expression for ΔN in terms of H_o.

The energy gap, $\mathcal{E}$, relevant to breakdown from the γ orbit to the δ orbit varies approximately linearly with the height, k_z, above the central (001) plane, for large k_z, and has a non-zero value at $k_z = 0$ due to the spin-orbit splitting. Thus we assume a dependence of $\mathcal{E}$ on k_z of the form

$$\mathcal{E} = f\left(k_z^2 + g^2\right)^{\frac{1}{2}}.$$

where f, g are constants.

Also, from equation (1-2) we have that

$$H_o \propto \mathcal{E}^2$$

$$\therefore \quad H_o = A\left(k_z^2 + B^2\right) \qquad (4\text{-}25)$$

where A, B are constants and $A B^2 = H_{oo}$, the breakdown field in the central (001) plane.

Suppose that in a thin (001) section of thickness Δk_z, a fraction, F, of the electron orbits are converted to hole orbits by magnetic breakdown. Then the total net decrease, ΔN, in the number of electron states per unit volume is given by

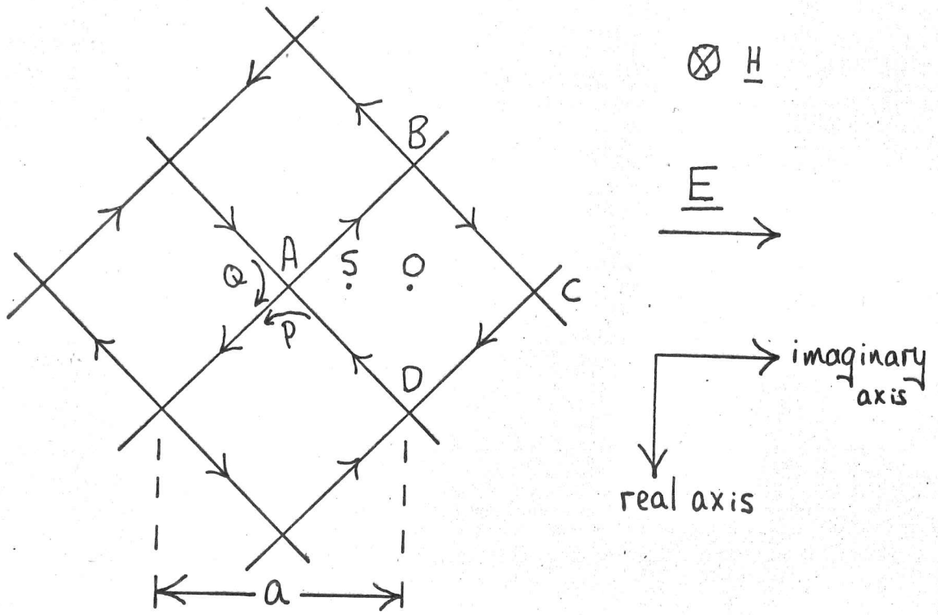

Fig. 4-25. An element of the two dimensional network. S is the mean starting point of particles generated on arms DA, AB; its coordinates relative to O are $(-\frac{ai}{4}, 0)$.

$$\Delta N = \frac{1}{4\pi^3} \cdot 2k_0^2 \int_{-\infty}^{\infty} F\,dk_z \qquad (4\text{-}26)$$

Also $$\Delta N = \frac{k_0^2}{\pi^3} \cdot \beta k_0$$

$$\therefore \quad \beta k_0 = \frac{1}{2} \int_{-\infty}^{\infty} F\,dk_z \qquad (4\text{-}27)$$

The next problem is to find an expression for F in terms of H_o. To do this consider an element of the two dimensional network as shown in fig. 4-25. We have seen that the application of an electric field E, as shown, generates particles on the arms DA, AB, and deficiencies of particles, or holes, on the arms BC, CD. Also we have previously shown that the effective path in the imaginary direction for particles generated on the arm DAB is

$$\left(\wedge_{DAB}\right)_{\text{imaginary}} = \frac{a}{2}\left(\frac{1-2P}{1+\{2P-1\}^2}\right)$$

so that when P = 0 the centroid of the particles moves from S, the mean starting point, to O, and the behaviour of the particles is entirely electron-like. When P = 1, the centroid

P = 1 , the centroid moves from S to A and the behaviour is entirely hole-like. Thus we can take the fraction of electrons that are converted into holes to be the ratio of lengths (YO)/(AO), where Y is the imaginary component of the mean terminal point of particles generated on DAB.

$$\therefore \quad F = \left[\frac{a}{2}\left(\frac{1-2P}{1+\{2P-1\}^2}\right) - \frac{a}{4}\right] \Big/ \frac{a}{2}$$

$$\therefore \quad F = \frac{P^2}{1-2P+2P^2} \qquad (4\text{-}28)$$

Also $P = \exp.\left(-H_o/H\right)$

and $H_o = A\left(k_z^2 + B^2\right)$

$\therefore$ (4-27) becomes

$$\beta k_o = \int_0^\infty \frac{e^{-\frac{2A}{H}\left(k_z^2+B^2\right)}}{1-2e^{-\frac{A}{H}\left(k_z^2+B^2\right)}+2e^{-\frac{2A}{H}\left(k_z^2+B^2\right)}}\, dk_z$$

or $$\beta k_o = B\int_0^\infty \frac{e^{-2(1+x^2)/\gamma}}{1-2e^{-(1+x^2)/\gamma}+2e^{-2(1+x^2)/\gamma}}\, dx \qquad (4\text{-}29)$$

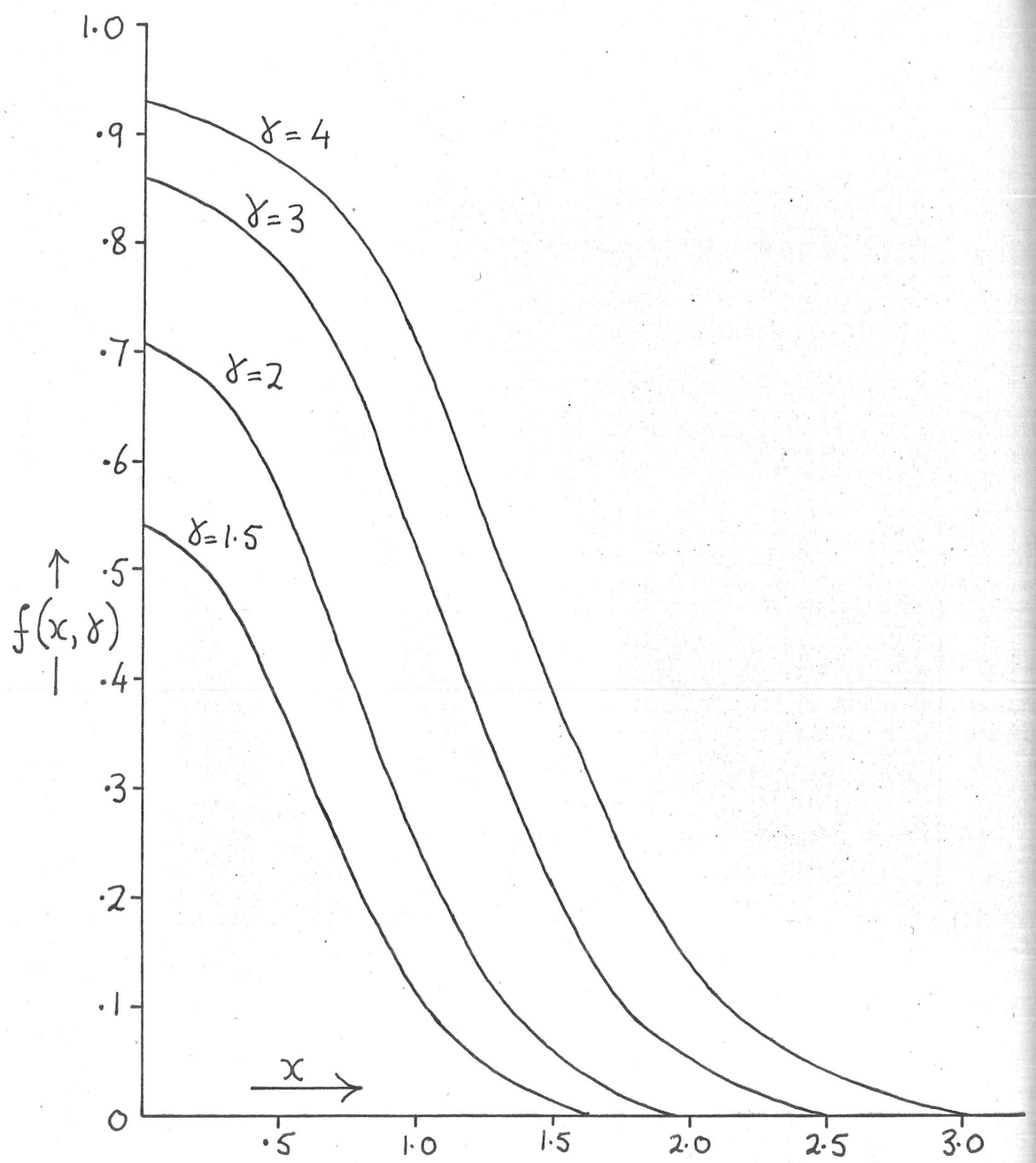

Fig. 4-26. Variation of $f(x, \gamma)$ with x for various values of γ.

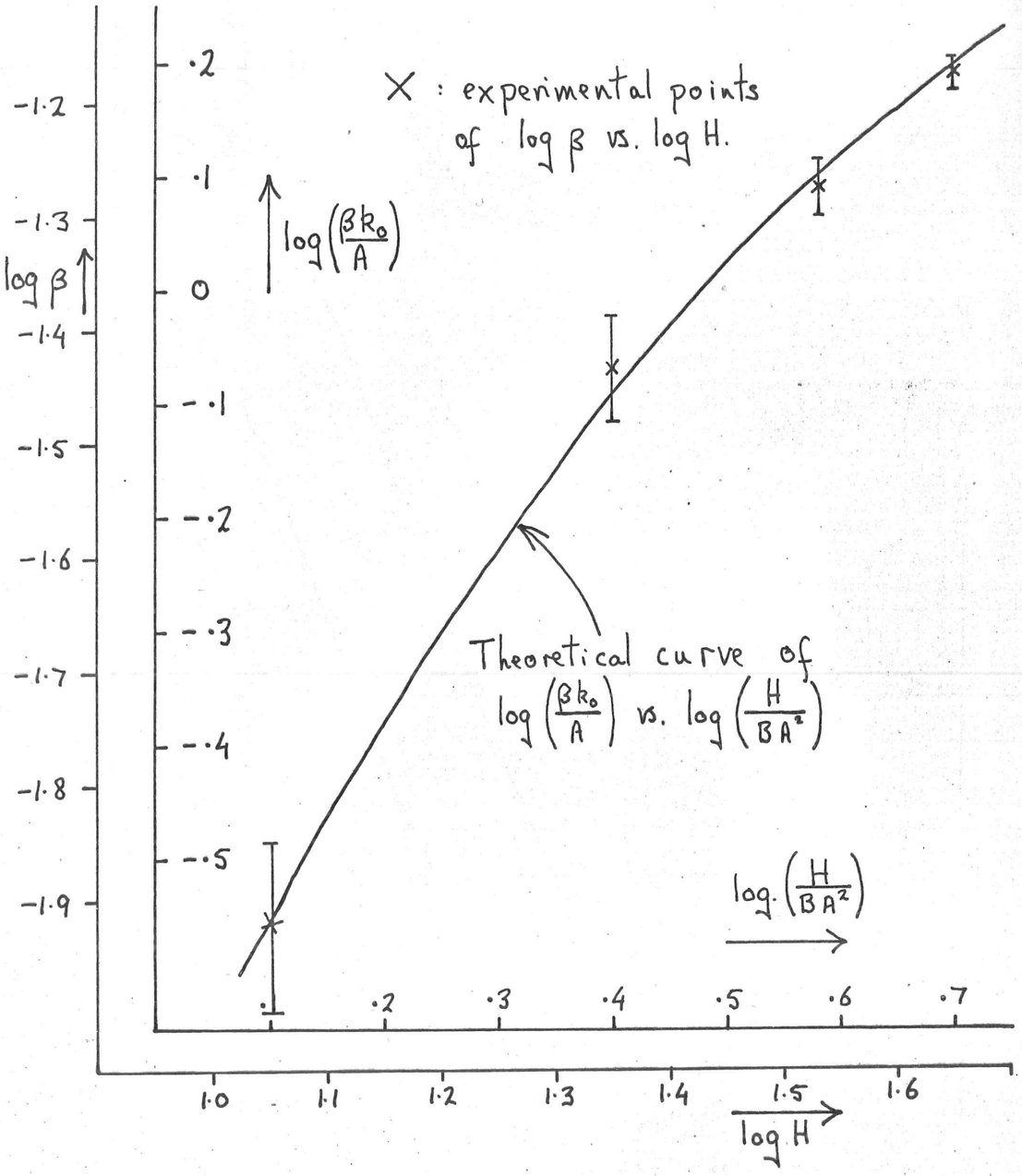

Fig. 4-27. Curve fitting.

where $x = \frac{k_z}{B}$ and $\gamma = \frac{H}{AB^2} = \frac{H}{H_{oo}}$

or $$\frac{\beta k_o}{B} = \int_0^\infty f(x, \gamma)\, dx$$

This integral is evaluated for various values of γ by plotting the curve of $f(x, \gamma)$ against x (fig. 4-26) and measuring the area enclosed by it and the x-axes. Hence the dependence of $\frac{\beta k_o}{B}$ on γ is found. By plotting the curve of $\log\left(\frac{\beta k_o}{B}\right)$ against $\log\left(\frac{H}{H_{oo}}\right)$ and fitting it to the experimental curve of $\log(\beta)$ against $\log(H)$, the values of H_{oo} and B may be estimated. The fitted curves are shown in fig. 4-27.

The values of AB^2 and B at the limits of fitting and at the approximate best fit, as shown in fig 4-27, are:-

	AB^2 (= H_{oo}) (kG)	B	$\therefore$ A
at one limit :	7.9	4.3×10^6	4.25×10^{-10}
at best fit :	8.9	4.7×10^6	4.02×10^{-10}
at other limit :	10.4	5.3×10^6	3.70×10^{-10}

Thus $H_o = (4.0 \pm 0.3) \times 10^{-10} k_z^2 + (9.0 \pm 1.0) \times 10^3$ gauss (4-30)

Table 4-5 below gives the values of H_o for various values of k_z deduced from the above expression and compares them with the values of H_o obtained by Strøm-Olsen (12).

Table 4-5

k_z	H_o(kG)	H_o(kG) (Strøm-Olsen)
0	9.0 ± 1.0	7.7 ± 0.9
$0.02\ k_o$	10.9 ± 1.1	9.8 ± 1.5
$0.03\ k_o$	13.2 ± 1.3	12.0 ± 1.7
$0.04\ k_o$	16.5 ± 1.5	15.6 ± 1.9
$0.05\ k_o$	20.7 ± 1.9	19.5 ± 2.2
$0.06\ k_o$	25.8 ± 2.3	27.6 ± 2.4
$0.17\ k_o$	147 ± 11	-

Thus the results agree within experimental error. The above table shows that at $k_z = 0.17\ k_o$, where $k_o = 1.08 \times 10^8$ cm^{-1}, $H_o \simeq 150$ kg, but evidence given in the next chapter suggests that magnetic breakdown effects at this value of k_z begin to be seen in

fields as low as about 20 kg., when breakdown effects should still be negligible. This casts doubt on the validity of expression (4-30) for the larger values of k_z .

A further piece of information that may be obtained from fig. 4-26 is that at 40kg., the height of the breakdown zone is given by $k_z/B = 3.0$ and hence $k_z = 0.14\ k_o$. This is in fair agreement with the estimate of $0.08\ k_o$ for the height at 45 kg deduced previously.

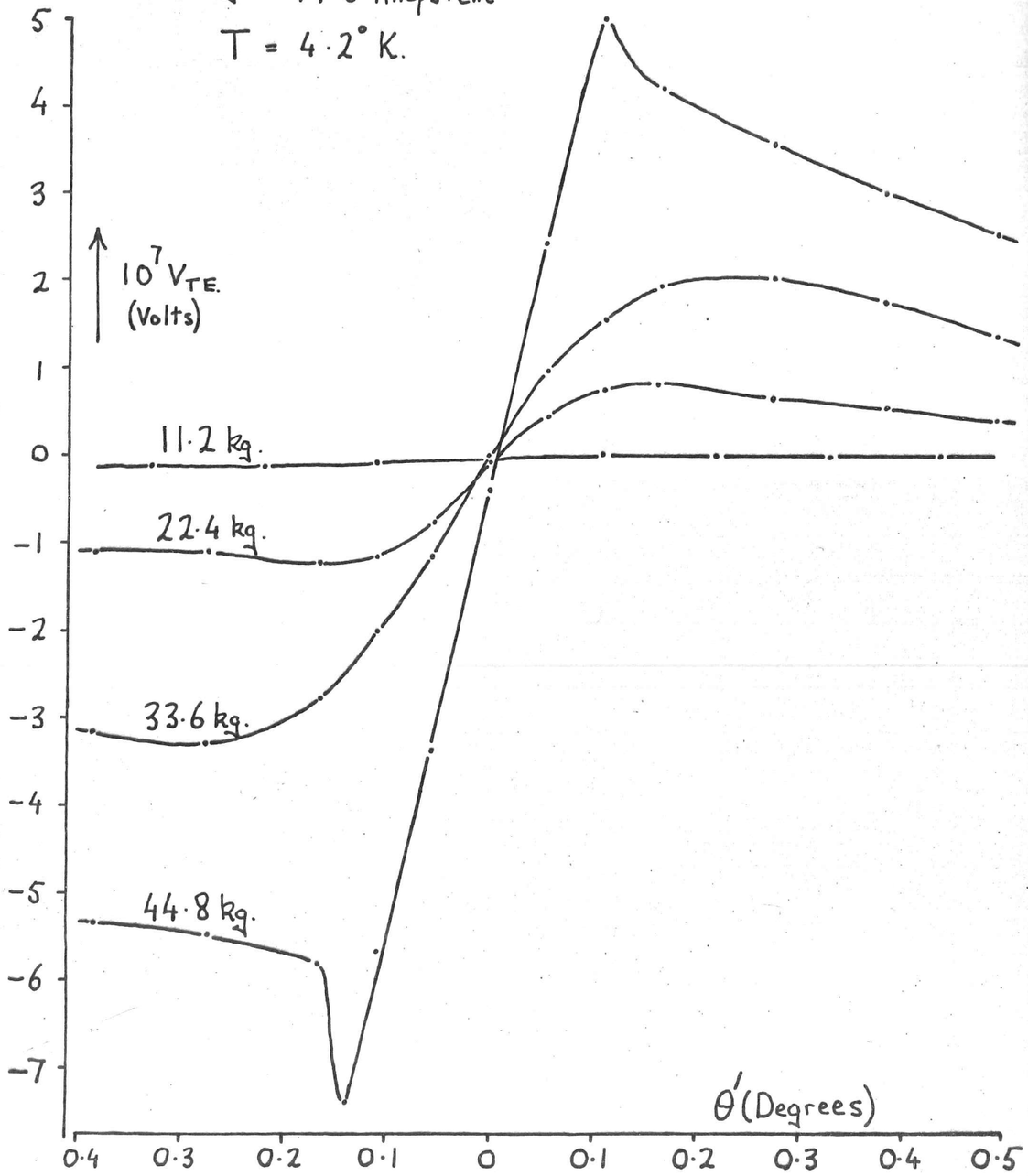

Fig.4-28. Dependence of the Transverse even voltage on θ′and H.

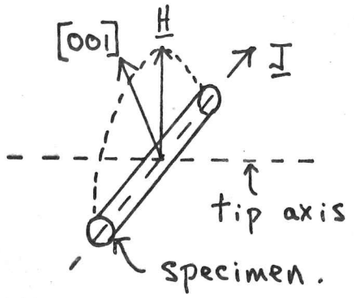

Fig. 4-29a. An illustration of the plane in which H was tipped.

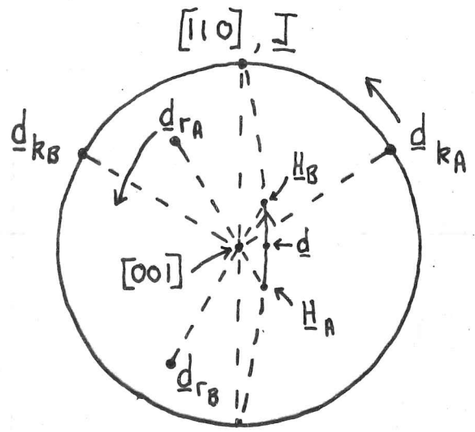

Fig. 4-29b. The effect of changing H in direction from H_A to H_B. The open orbit direction in k-space moves from d_{kA} to d_{kB}. d_{rA} and d_{rB} are the corresponding directions in real space.

Non-oscillatory behaviour of the transverse even voltage when H is close to [001]

4-4) Results

The crystal was first oriented such that H was close to, but not exactly in, the plane defined by J and [001] (J ∥ [110]). The crystal was then tipped about an axis approximately perpendicular to H and J as shown in fig 4-29a, and the dependence of the transverse voltage, V_T, on the angle θ' was determined. θ' is the angle between H and the projection of [001] on the plane in which H was tipped. The angle of closest approach of H to [001] was very small - probably less than 0.1°. A second set of measurements was taken with the field reversed in direction, the transverse **even** voltage being given by

$$V_{TE} = \frac{1}{2}\left(V_{T+} + V_{T-} \right)$$

where V_{T+}, V_{T-} are the values of the transverse voltage for the two opposite directions of field. The dependence of V_{TE} on θ' for several values of magnetic field is shown in fig. 4-28.

The main features are

1) the strong (approximately H^2) dependence of V_{TE} on H.

2) the strong dependence of V_{TE} on θ' especially near $\theta' = 0$, with a reversal in sign of V_{TE} at $\theta' = 0$.

3) The development of the broad maxima on either side of $\theta' = 0$ into sharp peaks as $\underline{H}$ is increased above about 40 kg.

4-4a) Discussion

From equation (2-2) we have that the transverse-even component of ρ_{yx} is given by

$$(\rho_{yx})_{even} = \frac{\delta' H^2 \sin\phi \cos\phi}{\delta'(n_- Y_- + n_+ Y_+) + e^2 (n_- - n_+)^2} \qquad (4\text{-}31)$$

where ϕ is the angle between the open orbit direction in real space and the projection of $\underline{J}$ on the plane perpendicular to $\underline{H}$. Also for $\underline{H}$ very close to [001] we have seen that

$$\delta'(n_- Y_- + n_+ Y_+) \ll e^2 (n_- - n_+)^2$$

$$\therefore (\rho_{yx})_{even} = \frac{\delta' H^2 \sin\phi \cos\phi}{e^2 (n_- - n_+)^2} \qquad (4\text{-}32)$$

The strong dependence of V_{TE} on H obviously follows from (4-32) since this shows that (ρ_{yx}) is proportional to H^2.

$(\rho_{yx})_{even}$ will reverse sign if Cos Ø Sin Ø reverses sign. Consider the stereogram in fig. 4-29b which illustrates the plane in which $\underline{H}$ is tipped. It is clear that as $\underline{H}$ is changed in direction from $\underline{H}_A$ to $\underline{H}_B$, Ø increases from some initial value of about 20° say, becoming 90° when $\underline{H}$ is in the direction $\underline{d}$, where $\underline{d}$ is perpendicular to $\underline{J}$, and increases to some final value of 160° say. Cos Ø Sin Ø reverses sign when $\emptyset = 90^\circ$, which coincides with $\theta' = 0$. The shape of the curve of ρ_{yx} against θ' is similar to that of Cos Ø Sin Ø against Ø as is expected. Since the angle of closest approach of $\underline{H}$ to [001] is very small, it is clear that small changes in angle θ' produce very large changes in Ø, the change in Ø for a given change in θ' becoming greater as θ' approaches zero, and hence ρ_{yx} changes very rapidly with θ' in this region.

No explanation has been found for the development of the broad maxima in ρ_{yx} into sharp spikes as the field is increased above about 40 kg.

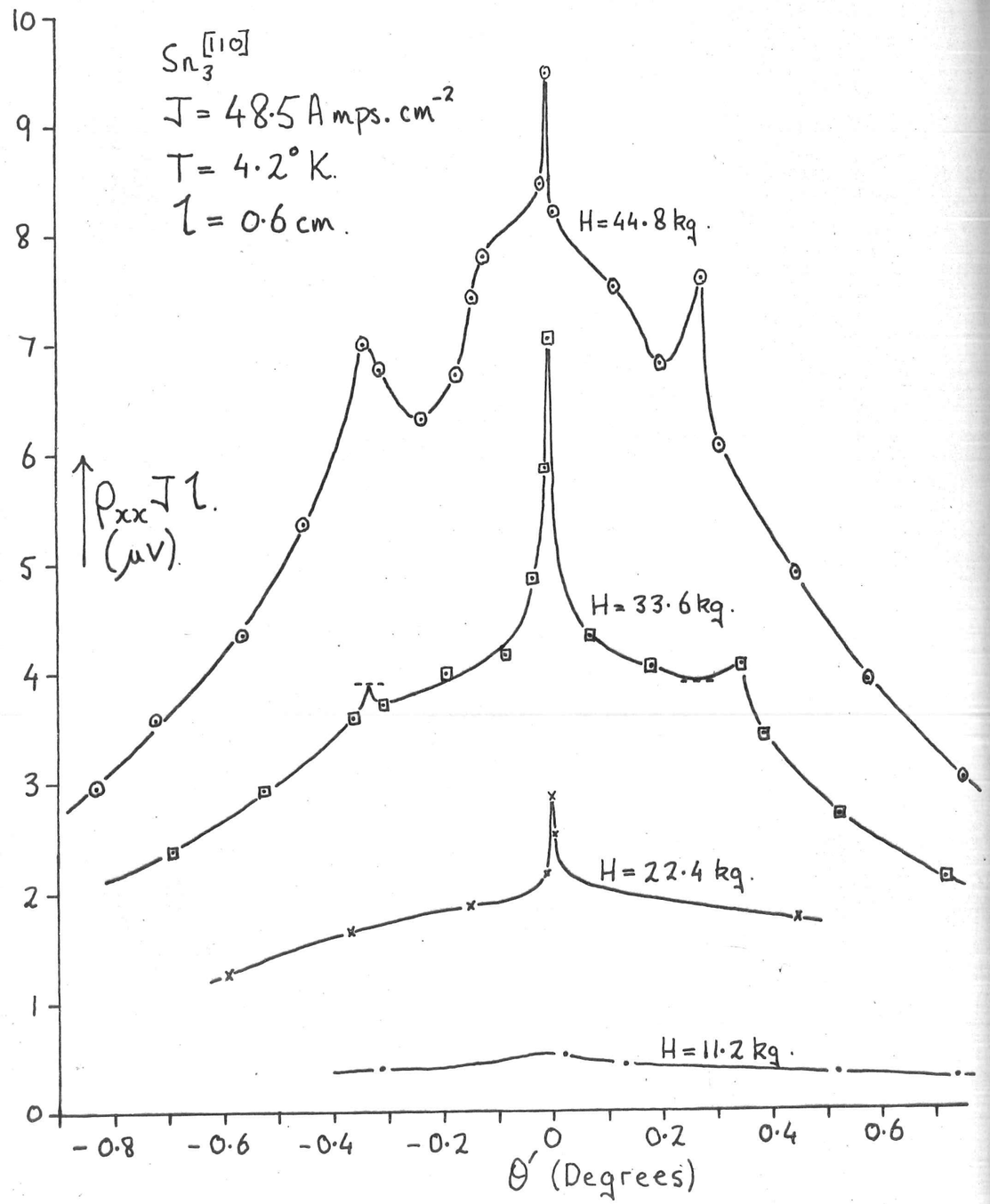

Fig. 4-30. Dependence of transverse magnetoresistance, ρ_{xx}, on θ' and H. The angle of closest approach of H to [001] $\doteqdot$ 0.1°.

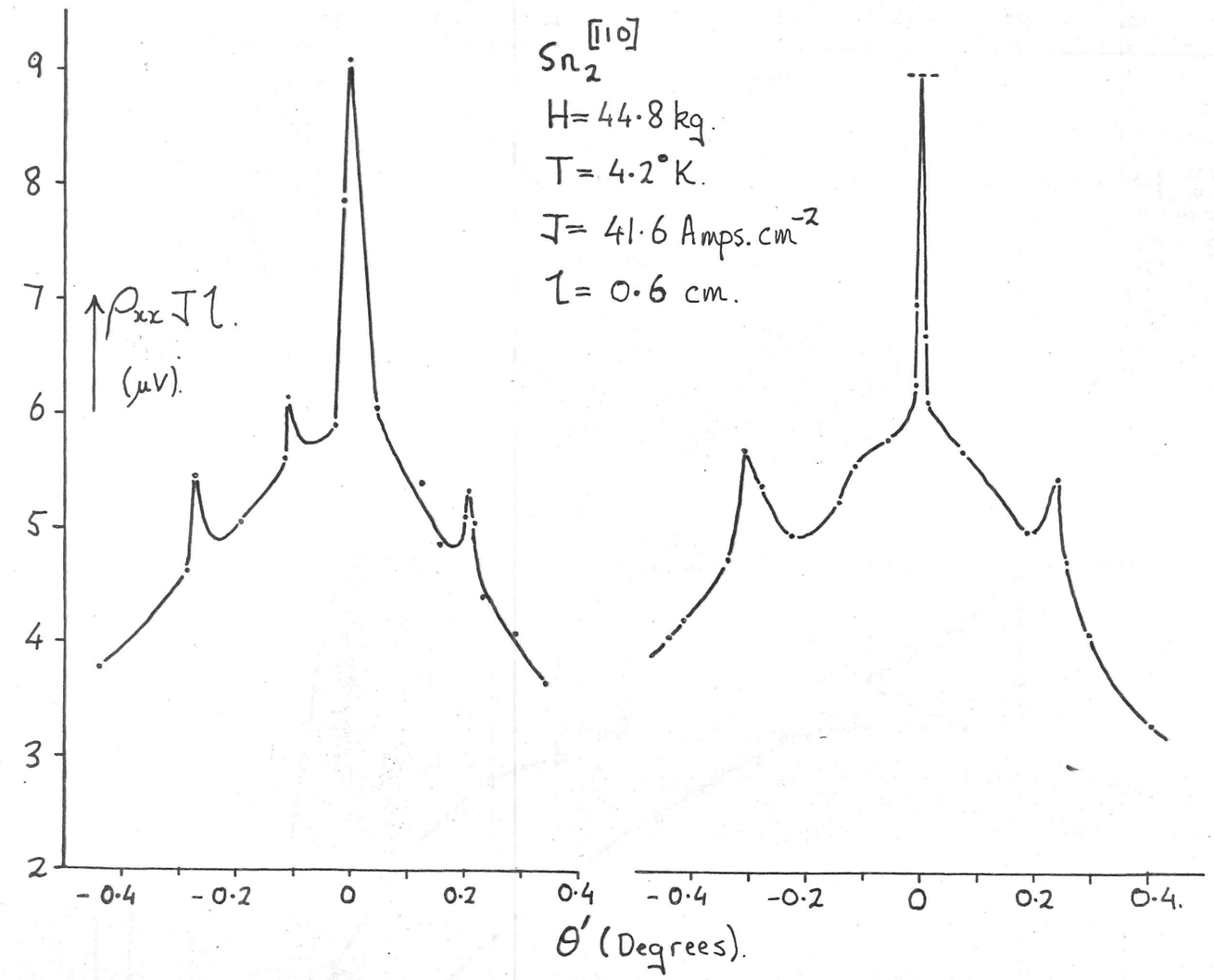

Fig. 4-31. Dependence of Transverse magnetoresistance on θ′. The angle of closest approach of H to [001] ≒ 0.1°.

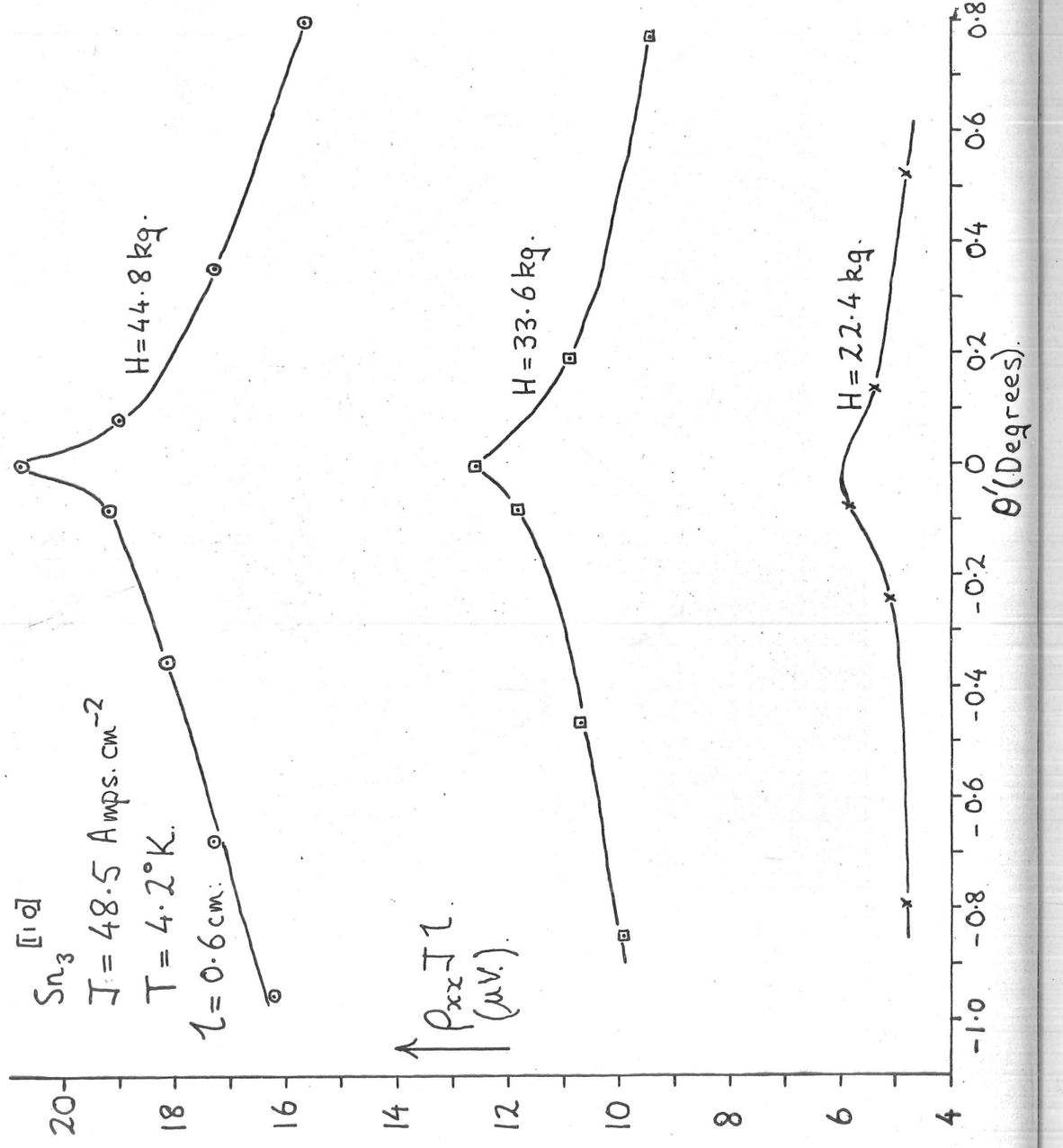

Fig. 4-32. Dependence of transverse magnetoresistance on θ' and H. The angle of closest approach of H to [001] ≒ 1°.

Non-oscillatory behaviour of the transverse magnetoresistance, ρ_{xx}, when H is close to [001]

4-5) Results

The procedure for taking measurements was exactly the same as for the transverse even voltage except that in this case measurements were made for one direction of magnetic field only. The dependence of transverse magnetoresistance on the angle θ' for various values of H is shown in fig. 4-30. Similar results were obtained for Sn_2 [110], the dependence of ρ_{xx} on θ' at 44.8 kg. being as shown in fig 4-31. In both cases the plane in which H was tipped was such that the angle of closest approach, T say, of H to [001] was less then about 0.1°. When T was increased to about 1°, then the dependence of ρ_{xx} on θ' was as shown in fig. 4-32. A stereogram illustrating the new plane in which H was tipped is shown in fig. 4-33 below:-

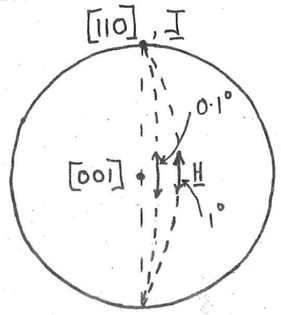

Fig. 4-33. An illustration (not to scale) of the planes in which H was tipped when measuring ρ_{xx}. The angles refer to the closest approach of H to [001].

From fig. 4-32 it can be seen that:-

1) The spike at $\theta' = 0$ has become smaller and less sharp, and ρ_{xx} decreases with increasing θ' less rapidly than before.

2) The value of ρ_{xx} for given values of $\underline{H}$, $\underline{J}$ and θ' has increased; for example, at $\theta' = 0$, $H = 44.8$ kg., ρ_{xx} has approximately doubled in value.

3) As before, there is no sign of saturation at $\theta' = 0$.

4) The subsidiary maxima at $\theta' = (0.25^{o} \pm 0.05^{o})$ have disappeared.

Young (4) has made measurements of ρ_{xx} when the field direction was within $\pm 0.05^{o}$ of [001] and also found that there was no saturation, and that the increase in ρ_{xx} was much faster than H.

4-5a) Discussion

Now, from (1-4) we have that

$$\rho_{xx} = \frac{(n_- \gamma_- + n_+ \gamma_+) + \beta' H^2 \sin^2 \phi}{\beta'(n_- \gamma_- + n_+ \gamma_+) + e^2 (n_- - n_+)^2}$$

and we have seen that for $\underline{H}$ close to [001], $\beta'(n_- \gamma_- + n_+ \gamma_+) \ll e^2 (n_- - n_+)^2$ since when $\underline{H}$ is close to [001] the number of particles on open orbits is very small, though β' should only become zero when $\underline{H} \parallel$ [001].

Thus $$\rho_{xx} \doteq \frac{(n_- \gamma_- + n_+ \gamma_+) + \beta' H^2 \sin^2 \phi}{e^2 (n_- - n_+)^2} \qquad (4\text{-}33)$$

We have seen how a small change in θ' produces a large change in ϕ, the change in ϕ for a given change in θ' becoming greater as θ' approaches zero. Also when $\theta' = 0$, then $\phi = 90^\circ$, and so from equation (4-33) one expects to see ρ_{xx} increasing as θ' is decreased, with a maximum in ρ_{xx} at $\theta' = 0$; this is what is observed. Also, as the angle, T, of closest approach of $\underline{H}$ to [001] is increased, ϕ will change less rapidly with

θ', for small values of θ', and hence ρ_{xx} will not depend so strongly on θ', as is observed.

The increase in ρ_{xx} for given values of $\underline{H}$, $\underline{J}$ and θ' as angle T is increased can be explained in terms of the increase of open orbit conductivity, σ'. Increasing the angle between $\underline{H}$ and [001] allows more open orbits to occur on the fourth and fifth zone open surfaces.

When the field is exactly parallel to [001] the resistance is expected to saturate since σ' becomes zero. The absence of any signs of saturation presumably indicates that even when $\underline{H}$ is very close to [001], $H^2 \sin^2 \phi \gg (n_- y_- + n_+ y_+)$, certainly for $\underline{H} > 10$ kg.

The appearance of subsidiary maxima at $\theta' = (0.25^\circ \pm 0.05^\circ)$ for fields greater than about 30 kg when the angle T was less than about 0.1°, and their non-appearance at fields up to 45 kg when the angle T was about 1°, has not been explained.

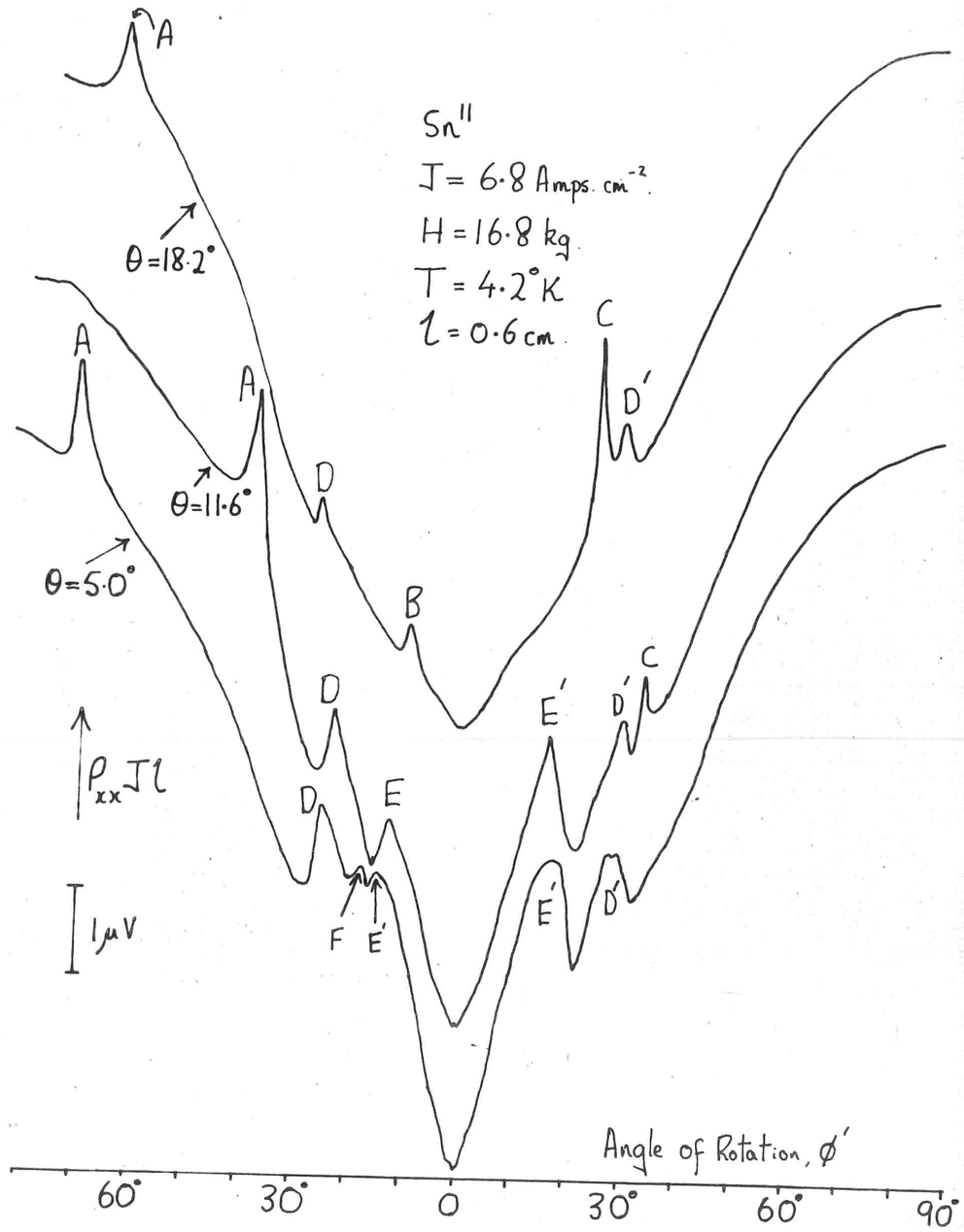

Fig 5-1. Rotation diagram of Transverse Magnetoresistance.

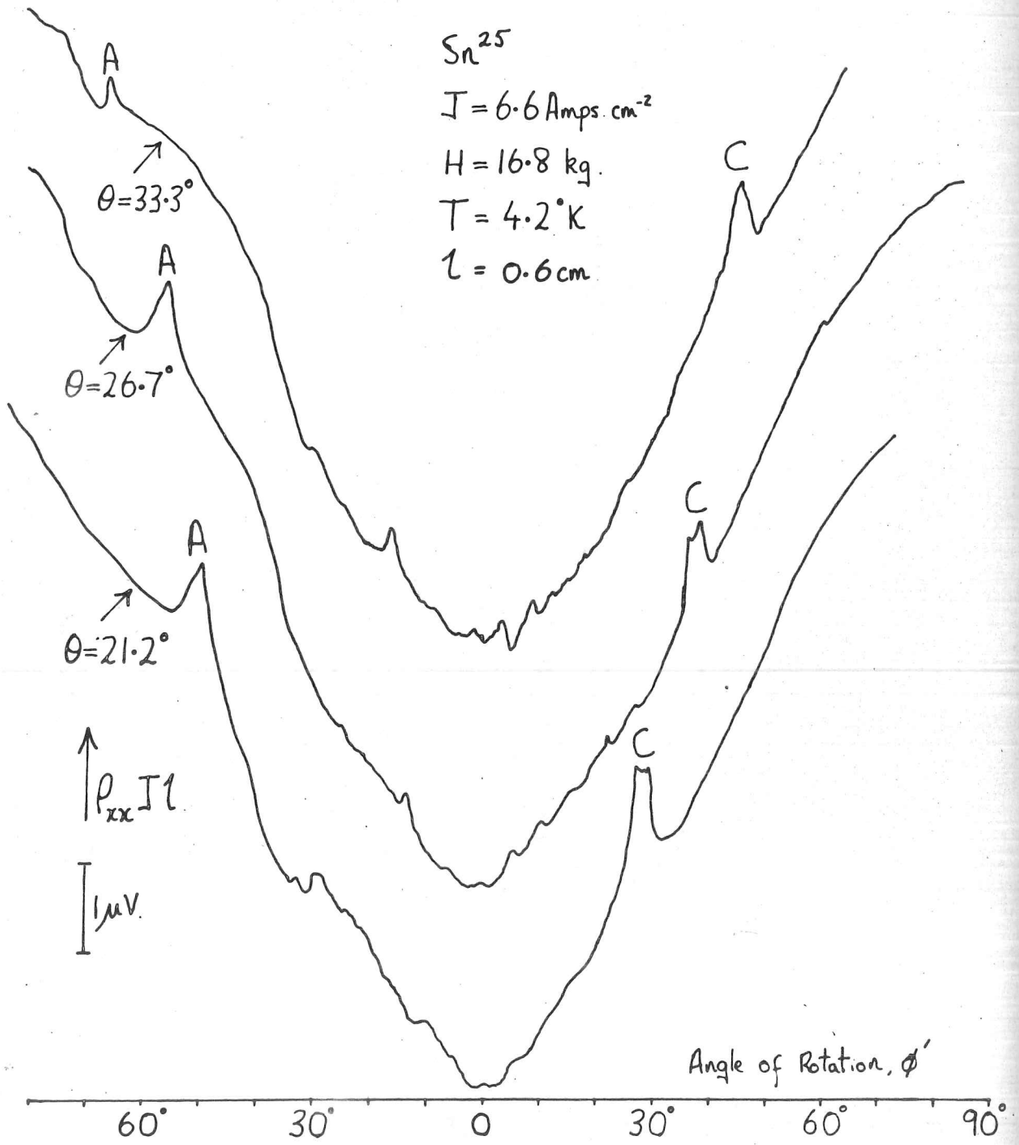

Fig. 5·2 . Rotation diagram of the Transverse Magnetoresistance

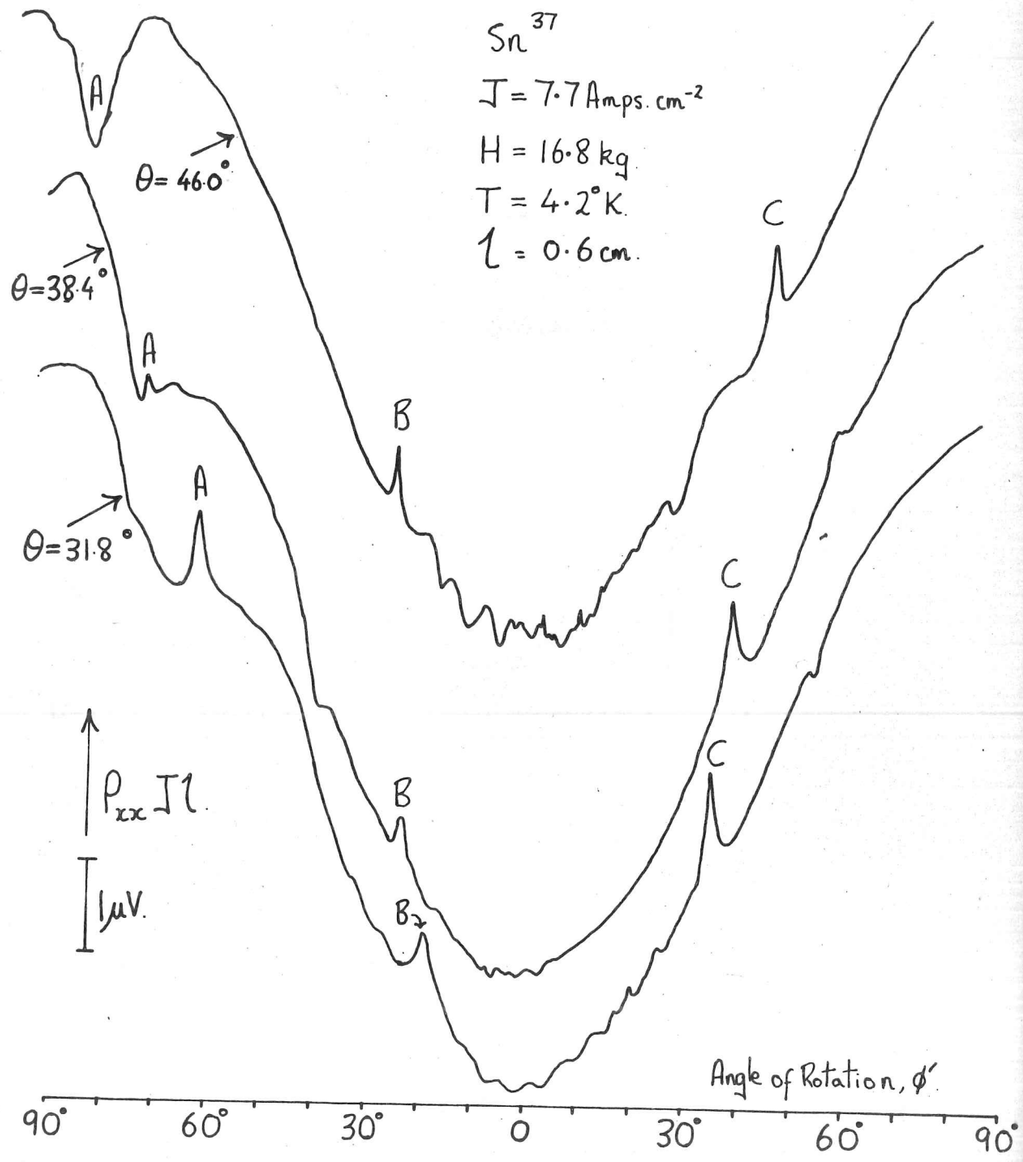

Fig. 5-3. Rotation diagram of the Transverse Magnetoresistance, ρ_{xx}

Chapter 5. The results and their interpretation when H lies between about 5° and 50° from [001].

5-1) Dependence of the transverse magnetoresistance on the angle of rotation of H

The results were obtained using the three crystals Sn^{11}, Sn^{25} and Sn^{37}. Before measuring the transverse voltage, V_T, the crystals were rotated about their axes, which were approximately perpendicular to H, until the transverse magnetoresistance was a minimum. This occured when H, J and [001] all lay in the same plane and thus $V_{TE} = 0$. Some experimental traces showing the variation of transverse magnetoresistance, ρ_{xx}, with angle of rotation are shown in figs. 5-1, 5-2, 5-3. The angle of rotation, ϕ', is the angle between H and the projection of [001] on the plane of rotation of H. The angle θ is the angle between H and [001] when H lies in the plane defined by H, J and [001], i.e. when $\phi' = 0$. The anomaly A occurs at $H \perp^{ar} [110]$ and anomalies B and C occur at $H \perp^{ar} [100]$ and $H \perp^{ar} [010]$. Similar anomalies were seen by Young (4) and Kachinskii (19). As described in chapter two, the correctness of the θ values may be checked by comparing the observed positions of these anomalies with those predicted from the values of θ, and the direction of J. The tables below list the predicted and experimentally determined values of the rotation angles, ϕ', at which H is perpendicular to [110], [100], and [010].

(i) Sn^{25}

Θ (degrees)	Anomaly	ϕ' (predicted) (degrees)	ϕ' (observed) (degrees)
21.2	A ($\underline{H} \perp^{ar} [110]$)	54	52 ± 3
	C ($\underline{H} \perp^{ar} [010]$)	32	29 ± 2
26.7	A	60	61 ± 5
	C	39	38 ± 5
33.3	A	64	71 ± 4
	C	44	46 ± 3

(ii) $\underline{Sn}^{37}$

θ (degrees)	Anomaly	ϕ'(predicted) (degrees)	ϕ'(observed) (degrees)
31.8	A: $\underline{H} \perp^{ar} [110]$	68	63 ± 3
	B: $\underline{H} \perp^{ar} [100]$	19	19 ± 2
	C: $\underline{H} \perp^{ar} [010]$	40	41 ± 2
38.4	A	71	74 ± 3
	B	22	23 ± 2
	C	44	38 ± 3
46.0	A	74	85 ± 4
	B	25	26 ± 2
	C	48	46 ± 3

An interesting feature of the rotation diagrams for Sn^{37} is that as θ is increased from 38.4° to 46°, anomaly A changes from a spike to a minimum. The corresponding change in the angle between H and [001] is an increase from about 75° to 85°. Similar results were obtained by Young (4). According to Weisz' model the broad band of periodic open orbits along [110] on the fourth zone surface cannot exist when H is further than 72° from [001] although a narrow band of open orbits on the fifth zone surface can still be found. Young (4) interprets the change in character of the anomaly in terms of this.

iii) Sn^{11}.

The rotation diagrams for Sn^{11} are difficult to interpret as additional anomalies - probably I and II - have made their appearance. The anomalies I and II are expected to occur when the angle, Y, between H and [001] is about 37° and 22° respectively. The tables below list the predicted positions of anomalies A, B, C, I, II, the positions of the observed anomalies and their possible interpretation.

i) $\theta = 18.2°$

Predicted positions of anomalies:-

Anomaly I : Y = 37°

Anomaly II : Y = 22°

A ($H \perp^{ar} [110]$) : $\phi' = 60°$

B ($H \perp^{ar} [100]$) : $\phi' = 12°$

C ($H \perp^{ar} [010]$) : $\phi' = 25°$

Observed positions:-

Anomaly	ϕ' (degrees)	Y(degrees).	Interpretation
A	64 ± 2		$\underline{H} \perp^{ar} [110]$
B	10 ± 1	20 ± 1	$\underline{H} \perp^{ar} [100]$; II?
C	24 ± 2		$\underline{H} \perp^{ar} [010]$
D	28 ± 2	33 ± 2	I?
D'	28 ± 2	33 ± 2	I?

ii) $\theta = 11.6^{o}$

Predicted positions of anomalies:-

I and II as above.

$\underline{H} \perp^{ar} [110]$: $\phi' = 40^{o}$

$\underline{H} \perp^{ar} [010]$: $\phi' = 17^{o}$

$\underline{H} \perp^{ar} [100]$: $\phi' = 7^{o}$

Observed positions:-

Anomaly	ϕ' (degrees)	Y(degrees)	Interpretation
A	39 ± 3		$\underline{H} \perp^{ar} [110]$
C	33 ± 3	35 ± 3	I?
D	25 ± 2	27 ± 2	
D'	31 ± 3	33 ± 2	I?
E	14 ± 1	18 ± 1	II?
E'	18 ± 2	22 ± 2	$\underline{H} \perp^{ar} [010]$, II

Observed positions:-

Anomaly	ϕ' (degrees)	Y(degrees).	Interpretation
A	64 ± 2		$\underline{H} \perp^{ar} [1\bar{1}0]$
B	10 ± 1	20 ± 1	$\underline{H} \perp^{ar} [100]$; II?
C	24 ± 2		$\underline{H} \perp^{ar} [0\bar{1}0]$
D	28 ± 2	33 ± 2	I?
D'	28 ± 2	33 ± 2	I?

ii) $\theta = 11.6^{o}$

Predicted positions of anomalies:-

I and II as above.

$\underline{H} \perp^{ar} [1\bar{1}0]$: $\phi' = 40^{o}$

$\underline{H} \perp^{ar} [0\bar{1}0]$: $\phi' = 17^{o}$

$\underline{H} \perp^{ar} [100]$: $\phi' = 7^{o}$

Observed positions:-

Anomaly	ϕ' (degrees)	Y(degrees)	Interpretation
A	39 ± 3		$\underline{H} \perp^{ar} [1\bar{1}0]$
C	33 ± 3	35 ± 3	I?
D	25 ± 2	27 ± 2	
D'	31 ± 3	33 ± 2	I?
E	14 ± 1	18 ± 1	II?
E'	18 ± 2	22 ± 2	$\underline{H} \perp^{ar} [0\bar{1}0]$, II

Observed positions:-

Anomaly	ϕ' (degrees)	Y(degrees).	Interpretation
A	64 ± 2		$\underline{H} \perp^{ar} [110]$
B	10 ± 1	20 ± 1	$\underline{H} \perp^{ar} [100]$; II?
C	24 ± 2		$\underline{H} \perp^{ar} [010]$
D	28 ± 2	33 ± 2	I?
D'	28 ± 2	33 ± 2	I?

ii) $\theta = 11.6^{\circ}$

Predicted positions of anomalies:-

I and II as above.

$\underline{H} \perp^{ar} [110]$: $\phi' = 40^{\circ}$

$\underline{H} \perp^{ar} [010]$: $\phi' = 17^{\circ}$

$\underline{H} \perp^{ar} [100]$: $\phi' = 7^{\circ}$

Observed positions:-

Anomaly	ϕ' (degrees)	Y(degrees)	Interpretation
A	39 ± 3		$\underline{H} \perp^{ar} [110]$
C	33 ± 3	35 ± 3	I?
D	25 ± 2	27 ± 2	
D'	31 ± 3	33 ± 2	I?
E	14 ± 1	18 ± 1	II?
E'	18 ± 2	22 ± 2	$\underline{H} \perp^{ar} [010]$, II

Fig.5-4. Variation of Hall coefficient with $\angle\theta$ between H and [001]. T=4.2°K.

I : Sn^{11} A : H = 11.2 kg.
II : Sn^{25} B : H = 22.4 kg.
III : Sn^{37} C : H = 44.8 kg.

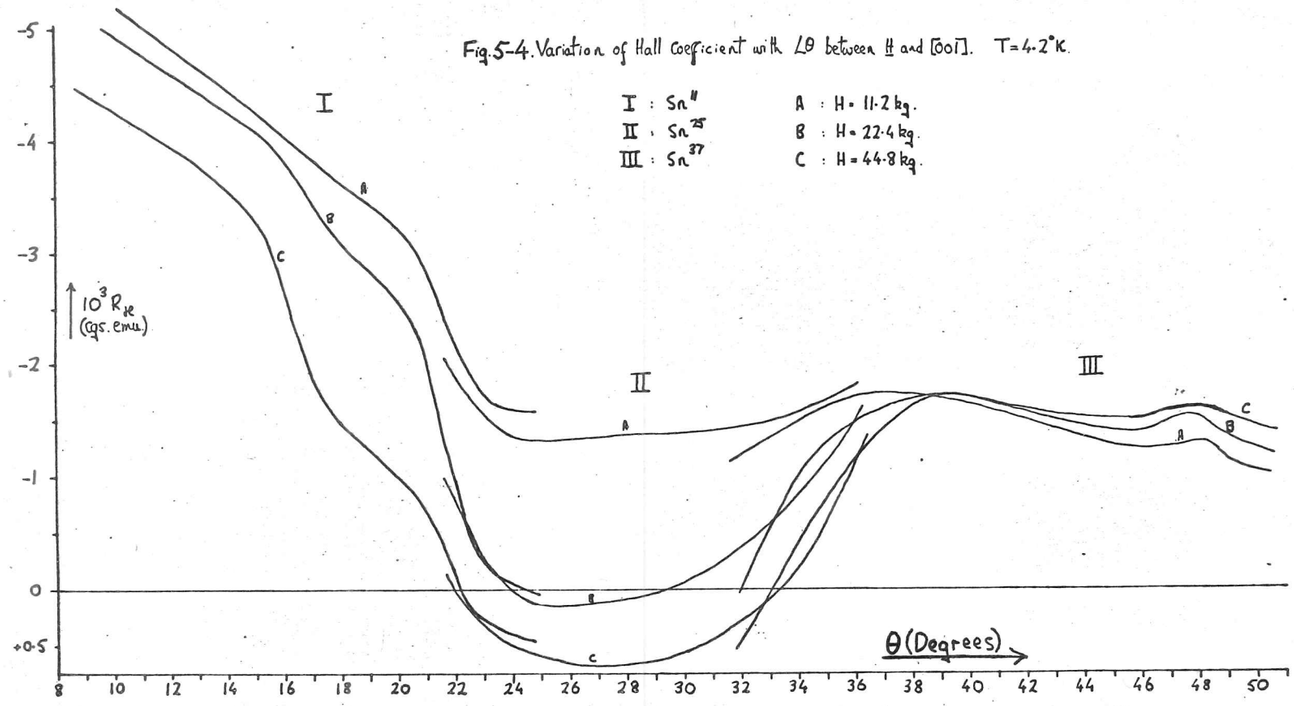

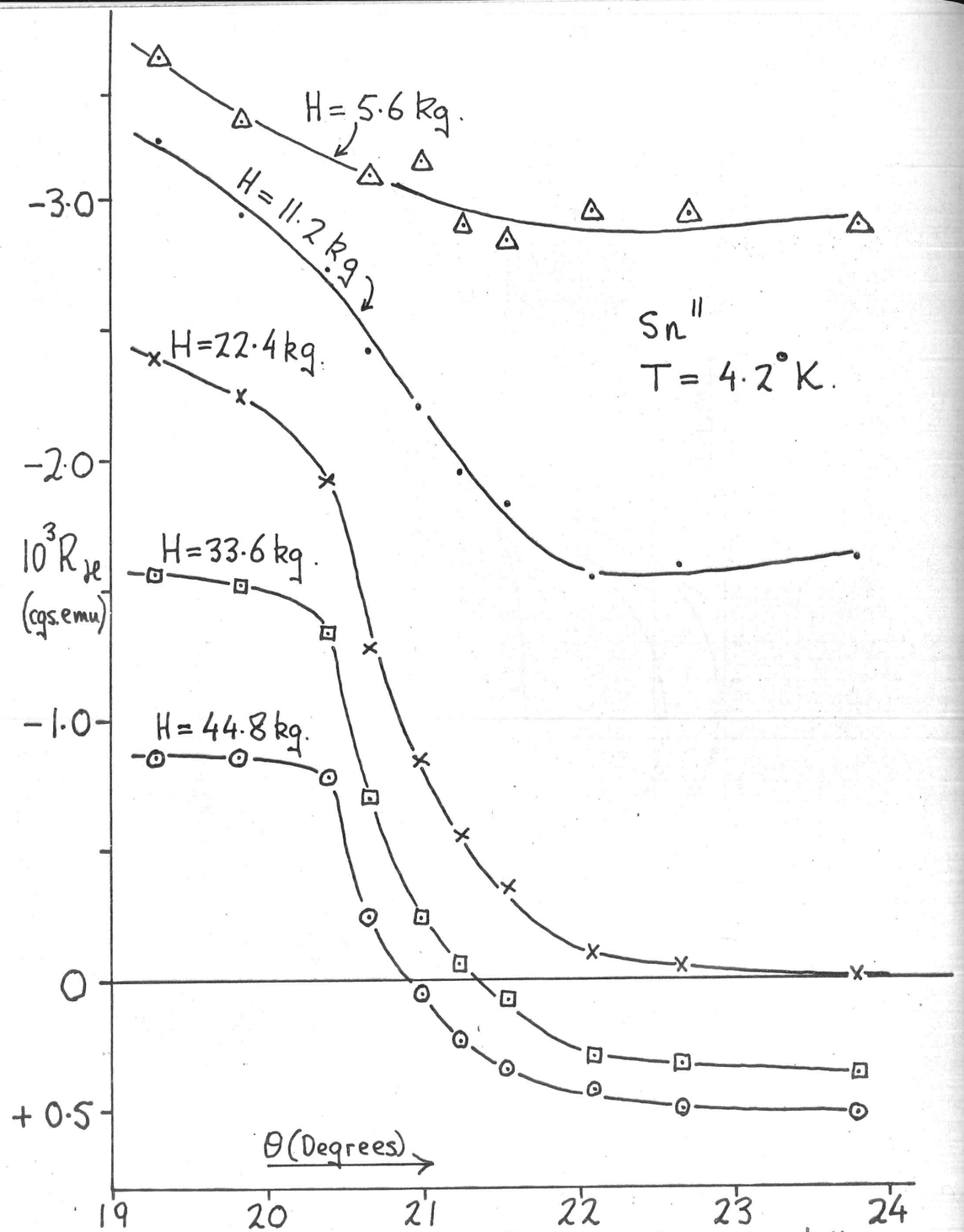

Fig. 5-5. Dependence of the Hall coefficient on θ and H.

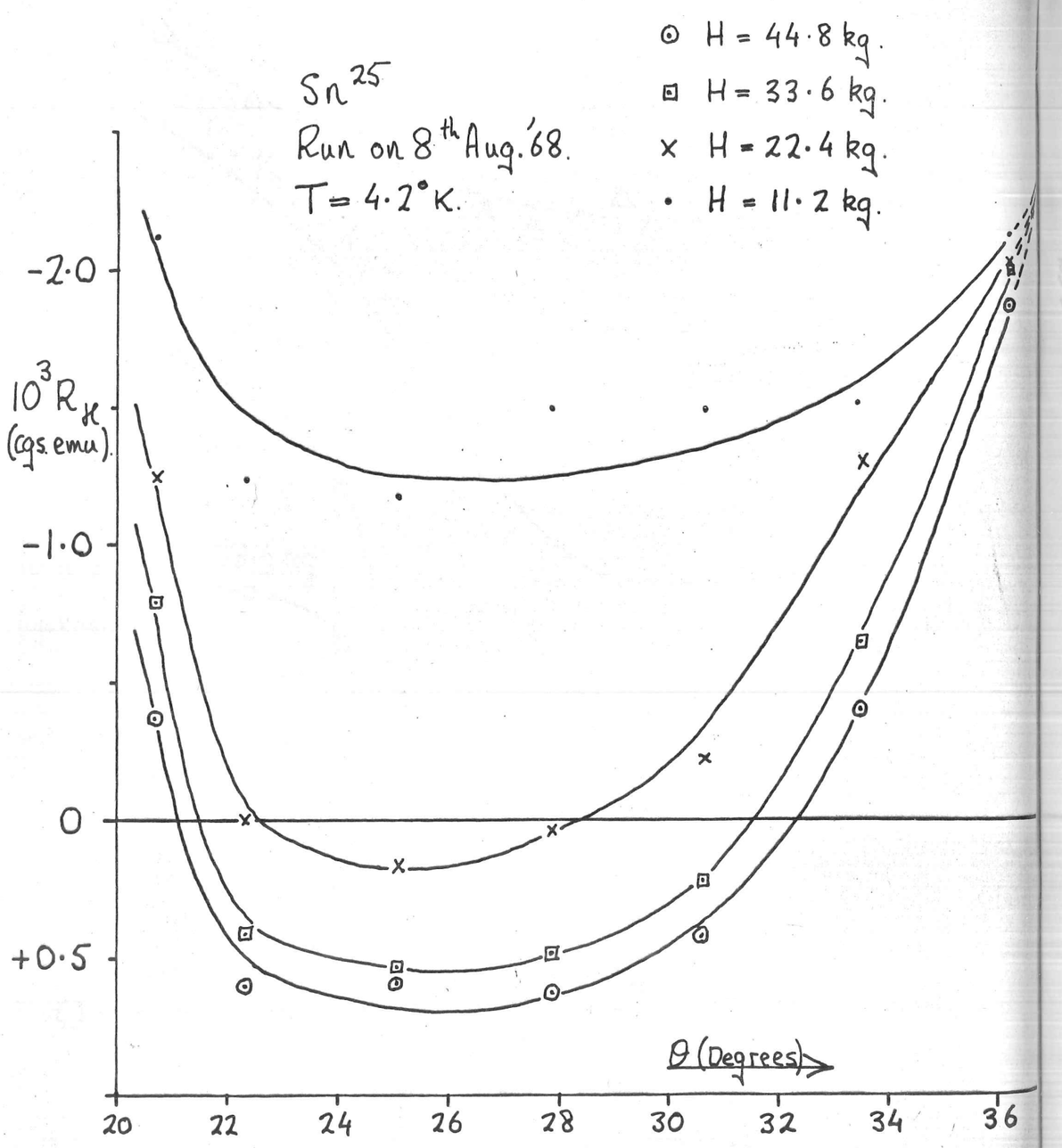

Fig. 5-6. Dependence of Hall coefficient on θ and H.

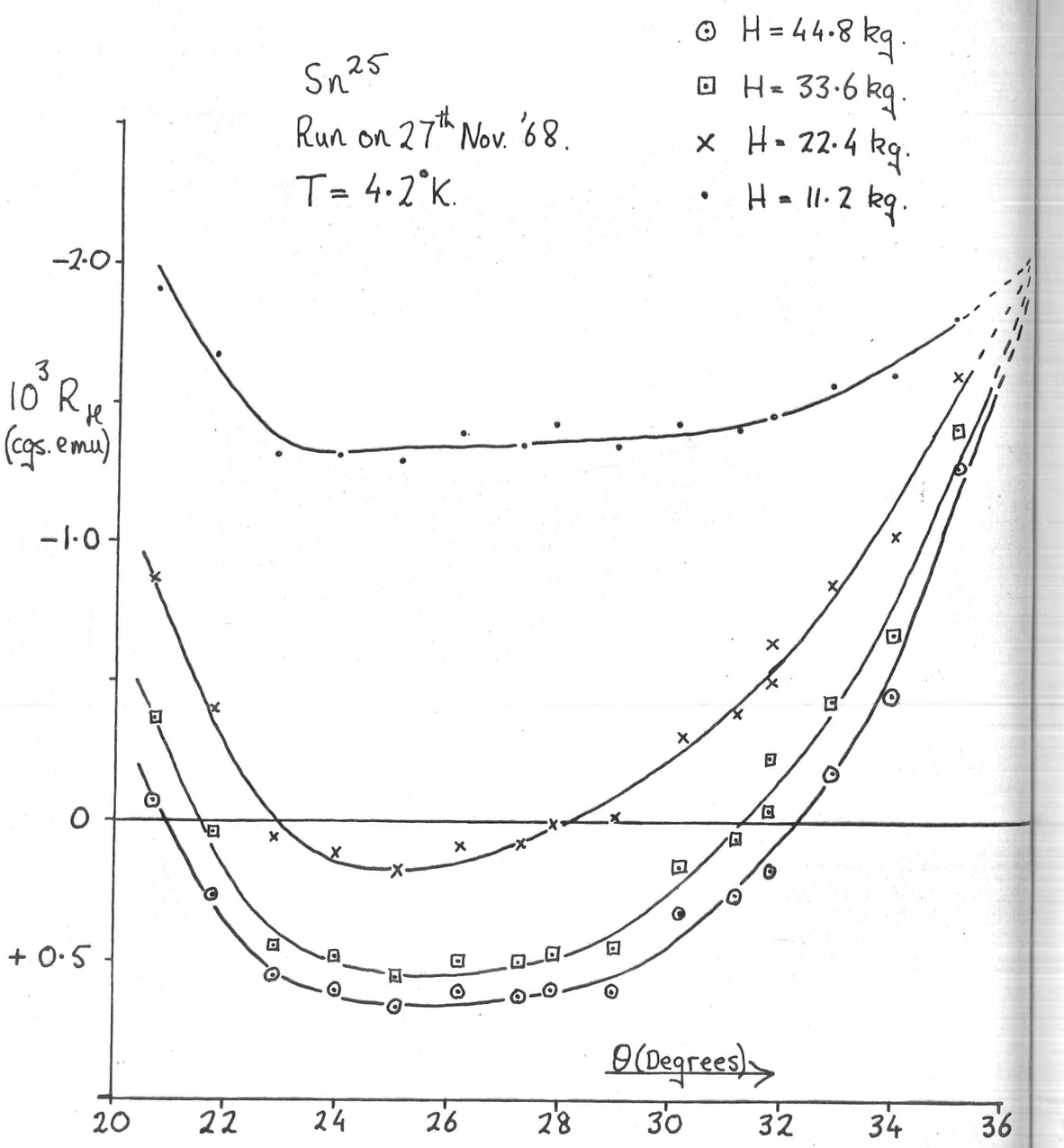

Fig. 5-7. Dependence of the Hall coefficient on θ and H.

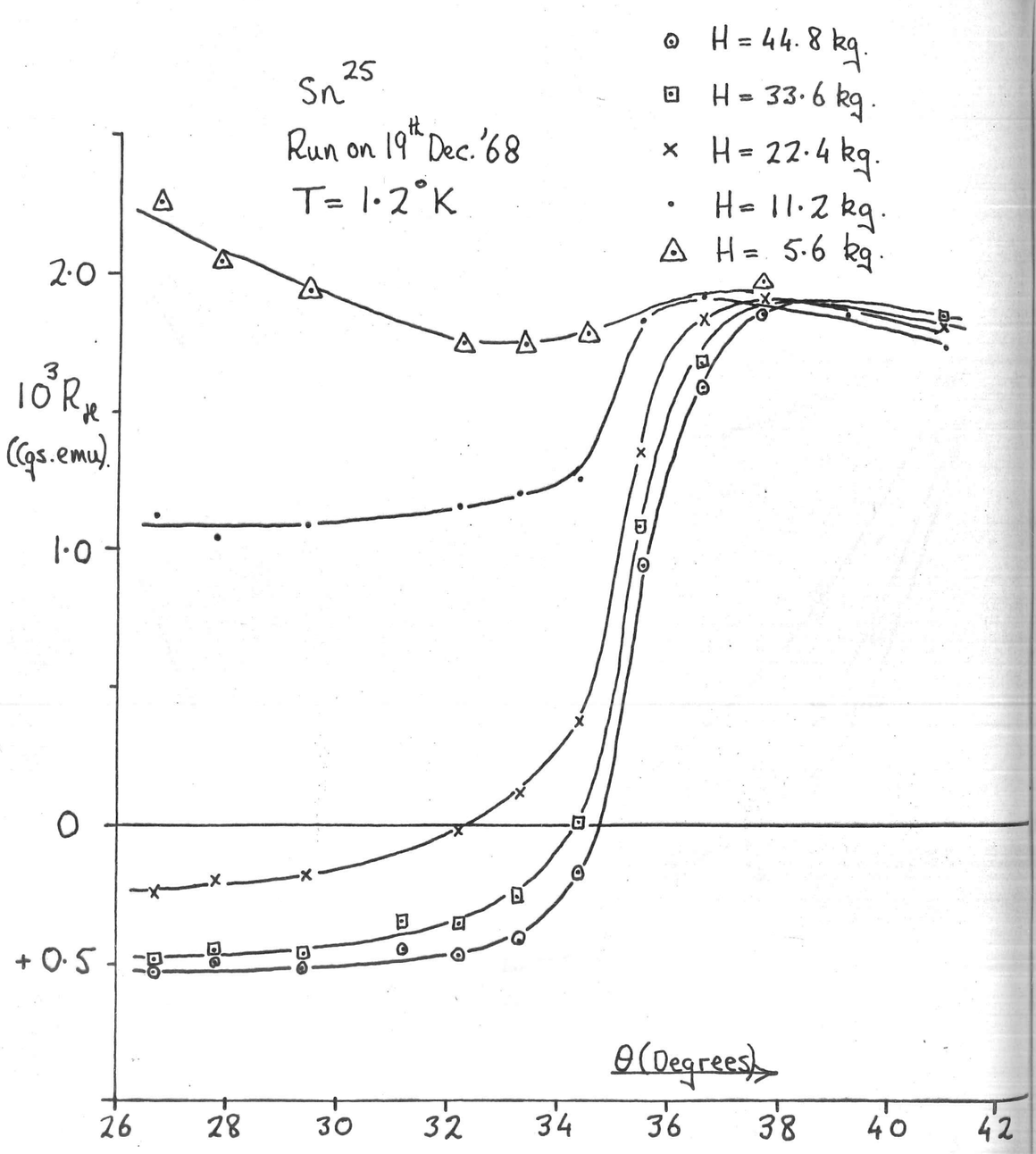

Fig. 5-8. Dependence of the Hall Coefficient on θ and H.

With the exception of anomaly I, the agreement between the observed and predicted positions of the anomalies is quite good. This indicates that the directions of the crystal axes determined by x-raying the crystals, and the allocation of θ values is not much in error.

5-2) Non-oscillatory behaviour of the Hall voltage.

The results were obtained using the three crystals Sn^{11}, Sn^{25} and Sn^{37}. The dependence of the mean value of the Hall coefficient, R_H, on H and θ is shown in fig. 5-4. The dependence of R_H on H and θ for $19^\circ < \theta < 24^\circ$ is shown in finer details in fig. 5-5. It was found that the transition region near $\theta = 37^\circ$ became much sharper when the temperature was reduced from $4.2^\circ K$ to $1.2^\circ K$. Figs. 5-6 and 5-7 show the results of two sets of measurements at $4.2^\circ K$ and fig. 5-8 shows the results obtained in a third experiment at $1.2^\circ K$.

Theory. 5-2a) The behaviour of R_H in the region $15^\circ > \theta > 9^\circ$.

When H is tipped away from [001], open orbits can occur on the fourth and fifth zone open surfaces. In the present case, measurements were made on Sn^{11} with H lying in the plane defined by J and [001], so that the open orbits are aperiodic and have a mean direction in k-space which makes an angle of about 11° with $[1\bar{1}0]$, as illustrated in the

stereogram below:-

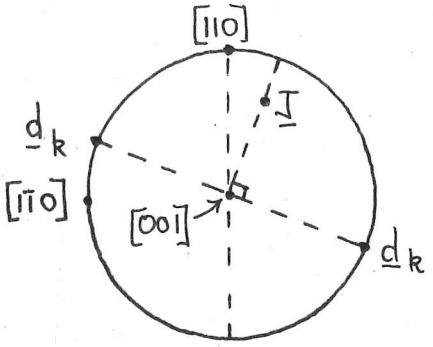

Fig. 5-9. The open orbit direction in k-space, $\underline{d}_k$, when H lies in the plane defined by J and [001]. (not to scale).

From equation (2-3) we have that, in the presence of open orbits whose direction in k-space is perpendicular to J, R_H is given by

$$R_H = \frac{(n_- - n_+)e}{\gamma'(n_-\gamma_- + n_+\gamma_+) + (n_- - n_+)^2 e^2} \qquad (5\text{-}1)$$

The dependence of R_H on H for $9° < \theta < 15°$ is similar to that observed for the [110] specimens for $\theta > \sim 2°$. No explanation for the behaviour has been found.

As the angle θ is increased, fewer electron orbits $\jmath$ and hole orbits λ can exist and more open orbits on the fourth and fifth zone open surface can occur. Thus n_- and n_+ decrease and γ' increases. It is not surprising, therefore, to find R_H changing slowly as θ changes. The decrease in $|R_H|$ as θ increases may be due to increasing value of γ', as this term occurs in the denominator of equation (5-1).

5-2b) The behaviour of R_H in the region $20.5^\circ > \theta \geq 15^\circ$

As can be seen from fig. 5-4, at $\theta = 16^\circ$, $|R_H|$ starts to decrease more rapidly than before with increasing field strength, H. The development with H leads one to expect that some magnetic breakdown process is responsible and, indeed, the angle between $\underline{H}$ and [001] at which this anomaly occurs is the same as that at the anomaly, III, observed by Young (4) in the transverse magnetoresistance. As shown in chapter one, this was explained in terms of the linking by magnetic breakdown of two open orbits on the fourth zone open surface via the closed orbit γ and two δ orbits to form a closed hole orbit. This mode of breakdown is referred to as mode C and is illustrated in fig. 1-18. This figure illustrates the case for periodic open orbits, but aperiodic open orbits can be linked in the same way to form extended hole orbits. This will lead to an increase in n_+ and also a decrease in n_- ; β' will also decrease. Since R_H is negative, implying that $n_- > n_+$, then from equation (5-1) we see that the decrease in $(n_- - n_+)$ can cause R_H to become less negative, as is observed.

Breakdown first occurs when it is just possible for the two open orbits and the closed orbit γ to lie in the same plane. Using the dimensions of Weisz' model we can thus calculate the height, k_z, above the central (001) plane at which breakdown first occurs. We get that $k_z = 0.17\ k_o$ where $k_o = 1.08 \times 10^8 cm^{-1}$. Also breakdown effects are first

noticeable in a field of about 22kg. Thus we expect the breakdown field at $k_z = 0.17k_o$ to be smaller than the value of about 150 kg. calculated previously, as this would yield a probability of breakdown of only about 10^{-3}.

The persistence of the strong development of R_H with H in the range $20.5^\circ > \theta \gtrsim 16^\circ$ indicates that breakdown linking the open orbits by mode C is continuing throughout this range, as is expected.

5-2c) The behaviour of R_H in the region $32^\circ > \theta \gtrsim 20.5^\circ$.

From fig. 5-5 we see that at $\theta = 20.5^\circ$, $|R_H|$ decreases with increasing H, for H < 23kg. more rapidly than before. Beyond about 23kg, however, the change in R_H with H is smaller than before and R_H appears to be heading towards saturation. One further point of interest is that at H greater than about 22kg., R_H reverses sign, and the value of θ at which this occurs decreases as the field is increased. The onset of this behaviour at $\theta = 20.5^\circ$ coincides with the appearance of anomaly II in the transverse magnetoresistance. We have seen in chapter one how anomaly II was explained in terms of the linking by magnetic breakdown of two open orbits on the fourth zone open surface via the δ orbit. When the open orbits are aperiodic as they are in the present case, then their linkage results in the formation of extended hole orbits as shown in fig.1-17c. This leads to a decrease in δ' and

an increase in n_+. Also if n_+ is increased to such an extent that n_+ becomes greater than n_- then from equation (5-1) we see that R_H will reverse sign.

As θ is increased it becomes possible for more aperiodic open orbits to occur on the fourth zone open surface, but because they are aperiodic in the limit of infinite relaxation time, they traverse all the arcs ζ (see fig.1-17) that are geometrically allowed. Thus each will be linked to another open orbit when it enters the breakdown zone which extends a distance h, say, above and below the central (001) plane. So long as it is geometrically possible for open orbits to exist on the fourth zone surface, they can be closed by breakdown by mode A. However, because the relaxation time is not infinite, it may not be possible for a particle starting on an open orbit near the top of the open surface to reach the breakdown zone where its behaviour becomes hole-like. Increasing the field causes the height, h, of the breakdown zone to increase and thus more open orbits will be linked by breakdown. At sufficiently high fields, h may become large enough for all particles on open orbits to reach the breakdown zone and thus all open orbits will become closed; when this happens we expect to see no more change in R_H.

All features of the dependence of R_H on H and θ in the range $32^\circ > \theta \geq 20.5^\circ$ have thus been explained.

5-2d) The behaviour of R_H in the region $51^\circ \geq \theta \geq 32^\circ$.

From fig. 5-8 we see that between about $\theta = 34^\circ$ and $\theta = 38^\circ$ there is a considerable change in the dependence of R_H on H and θ. Beyond $\theta = 37^\circ$ there is very little change in R_H when H changes and it only decreases slowly when θ increases. The anomaly I in the transverse magnetoresistance also occurs when H is 37° from [001] and except when the open orbit direction is close to parallel to [110], Young (4) interprets I as marking the limit of aperiodic open orbits on the fourth and fifth zone open surfaces. We have also mentioned in chapter one the evidence obtained by Hays and McLean (15) for the non-existence of aperiodic open orbits when the angle between H and [001] is greater than 37°. In the present measurements on R_H, the mean direction in k-space of the aperiodic open orbits makes an angle of $15^\circ \pm 1^\circ$ with [110] for the specimen Sn^{25} and an angle of $11^\circ \pm 1^\circ$ with [110] for the specimen Sn^{37}, so we might expect the anomaly to represent the limit of aperiodic open orbits on both open surfaces. Evidence for this is that beyond $\theta = 37^\circ$ R_H is almost independent of H, but if there were any aperiodic open orbits left on the fourth zone surface we would expect them to continue to get linked by breakdown with a consequent strong dependence of R_H on H. Also the fact that R_H shows only a weak dependence on θ for $\theta > 37^\circ$ indicates that $\theta = 37^\circ$ probably represents the limit of aperiodic open orbits on the fifth zone surface as well.

Thus we suppose that at low fields (H< about 5kg.) when the amount

of breakdown is small, once θ is greater than 37° all the aperiodic open orbits on the fourth zone hole surface become closed hole orbits and that all aperiodic open orbits on the fifth zone electron become closed electron orbits. Thus β' decreases and n_- and n_+ increase. At high fields (H about 45kg.) when almost all the open orbits on the fourth zone surface have already been closed by breakdown to form closed hole orbits, the effect of increasing θ above 37° is solely to cause β' to decrease and n_- to increase. Thus at high fields we might expect to see R_H becoming negative again, the change in R_H being greater at higher fields since the change in $(n_- - n_+)$ is greater. This behaviour is observed, as shown in figs. 5-6, 5-7, 5-8. Kachinskii (19), in measurements carried out at 6.9kg., also found that R_H became more negative when the angle between $\underline{H}$ and [001] increased from about 35° to 38°. The major objection to the above explanation of the behaviour is that when no open orbits are present i.e. $\beta' = 0$, then tin is compensated as found by Alekseevskii et al. (5) and evidence given in section 5-4b also indicates that this is the case. Thus from equation (5-1) we see that R_H should become zero for $\theta > 37°$, if this marks the limit of aperiodic open orbits or both open surfaces. No explanation for the non-zero value of R_H has been found.

At $\theta = 47°$ there appears to be a weak anomaly in R_H. The position of this coincides with that at which very large amplitude oscillations

appear in the transverse even voltage and more will be said about this in the next section on the oscillatory behaviour of the transverse voltage.

5-2e) The dependence of the sharpness of the transition region near $\theta = 37^{\circ}$ on the temperature.

The increase in sharpness with decrease in temperature is very evident when figs. 5-7 and 5-8 are compared. Now if $\theta = 37^{\circ}$ marks the limit of aperiodic open orbits on the fourth and fifth zone open surface then for θ just less than 37°, almost all the orbits on these surfaces will be open in low fields. Since they are aperiodic they will traverse all the arcs that are geometrically allowed. Thus at some time in the lifetime of a particle only a very small amount of scattering parallel to H will cause it to be shifted from an open orbit to the closed orbits $\int$ or λ. At high fields the situation is more complicated as now most of the aperiodic open orbits on the fourth zone surface have been linked to form extended hole orbits. Nevertheless it might be expected that since the open orbits are aperiodic, a small amount of scattering parallel to H would have the effect of altering the character of a large number of orbits and hence tend to smear out the transition region. Decreasing the temperature would decrease the amount of small angle scattering due to phonons and hence would be expected to increase the sharpness of the transition region.

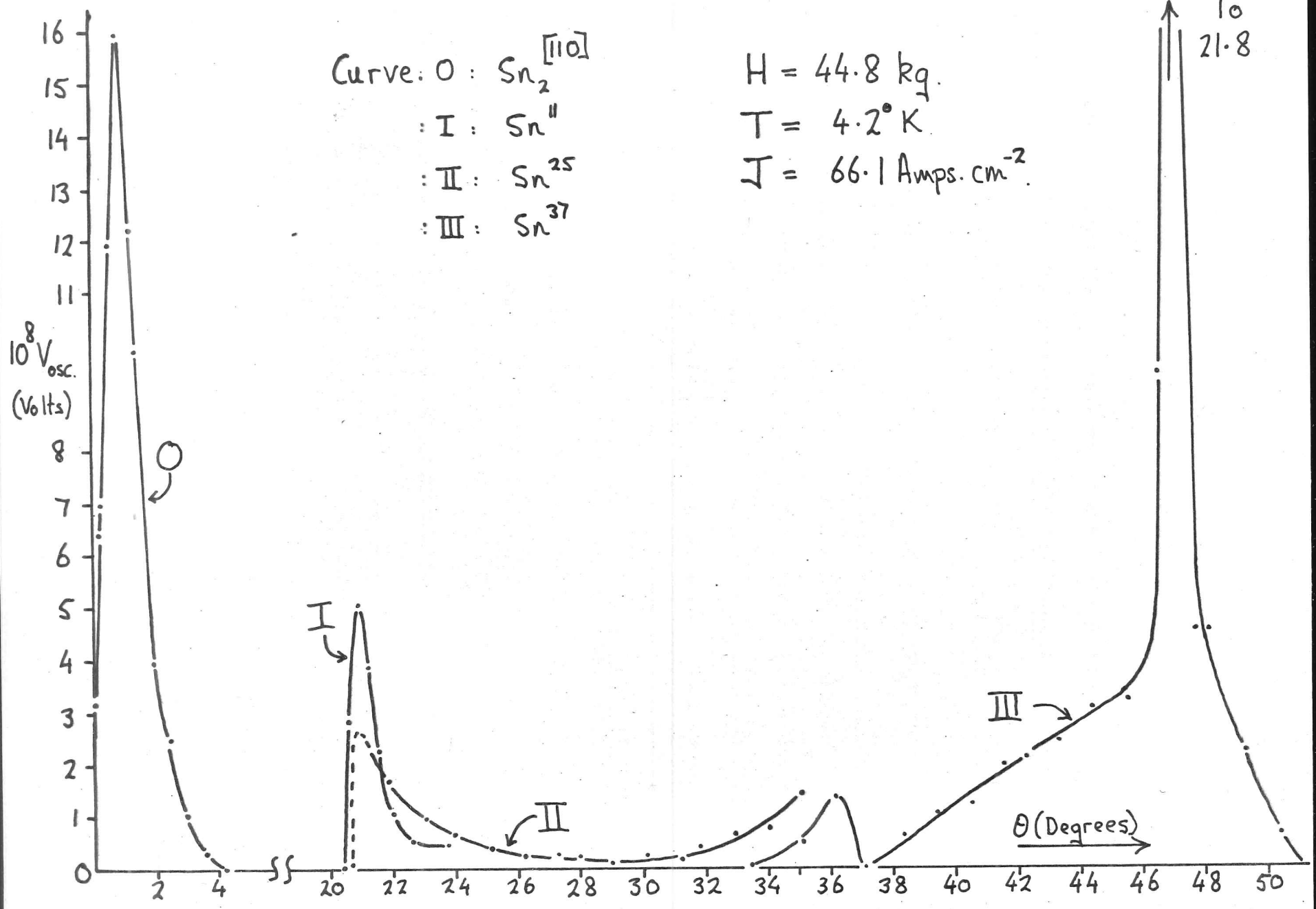

Fig. 5-10. Dependence of the amplitude of the oscillations in the transverse voltage on θ.

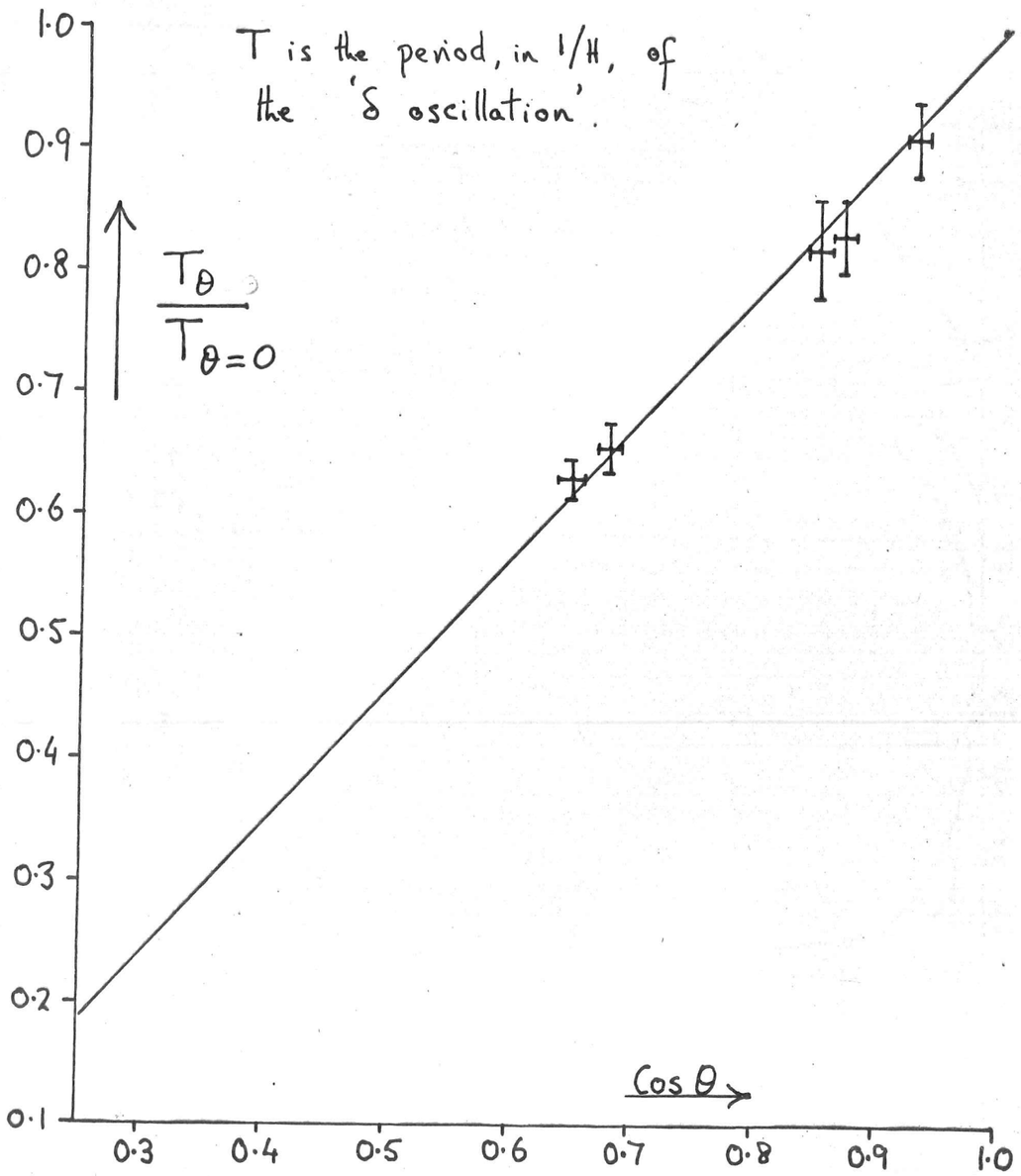

Fig. 5-11. Period of 'δ oscillation' relative to that for θ = 0 versus Cos θ.

5-3) Oscillatory behaviour of the Hall and transverse even voltages. Results.

The dependence of the oscillation amplitude of the transverse voltage on the angle θ is as shown in fig. 5-10. The amplitude shown is the mean value of the oscillation amplitude for two opposite directions of magnetic field. (H = 44.8kg.). The value of θ corresponding to the position at which the small peak occurred was arbitrarily chosen to be 21°. This is the fixed point referred to in chapter two when the determination of the angles θ was discussed. By fitting the curves shown in fig. 5-4 for Sn^{11}, Sn^{25} and Sn^{37}, the other values of θ could be determined. As we have seen, this choice of θ values is consistent with the transverse magnetoresistance, ρ_{xx}, data.

All the oscillations were periodic in 1/H having a period roughly proportional to Cos θ, as shown in fig. 5-11. This would indicate that the orbit responsible was on a cylindrical sheet. As mentioned in chapter four, the value of the period at θ = 0 corresponds to phase coherence around the δ orbit. Since the third zone hole surface is like a cylinder, it is reasonable to suppose that the oscillations which occur in the range $\theta = 20.5^{\circ}$ to $\theta = 51^{\circ}$ are also due to magnetic breakdown effects involving the δ orbit, with phase coherence around this orbit.

By comparing experimental traces of the transverse voltage against field strength for two opposite directions of field, the field being

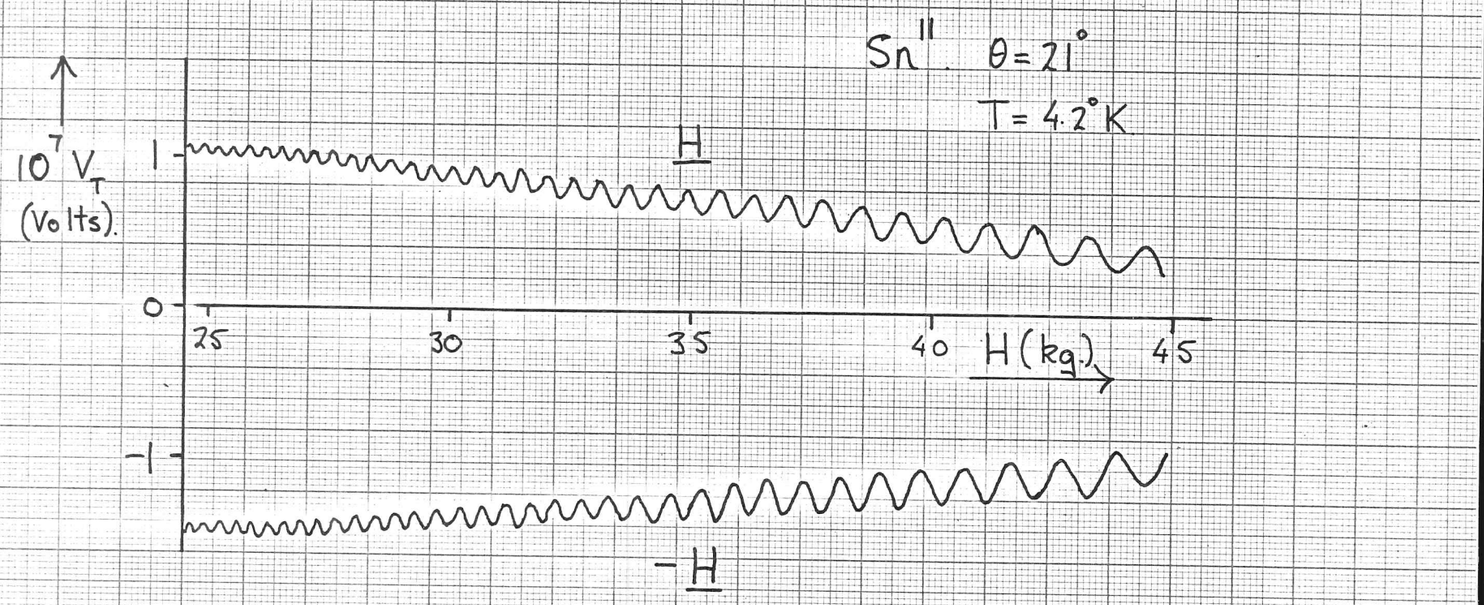

Fig. 5-12. Experimental record of transverse voltage versus magnetic field, showing how the phase of the oscillations reverses when $\underline{H}$ is reversed.

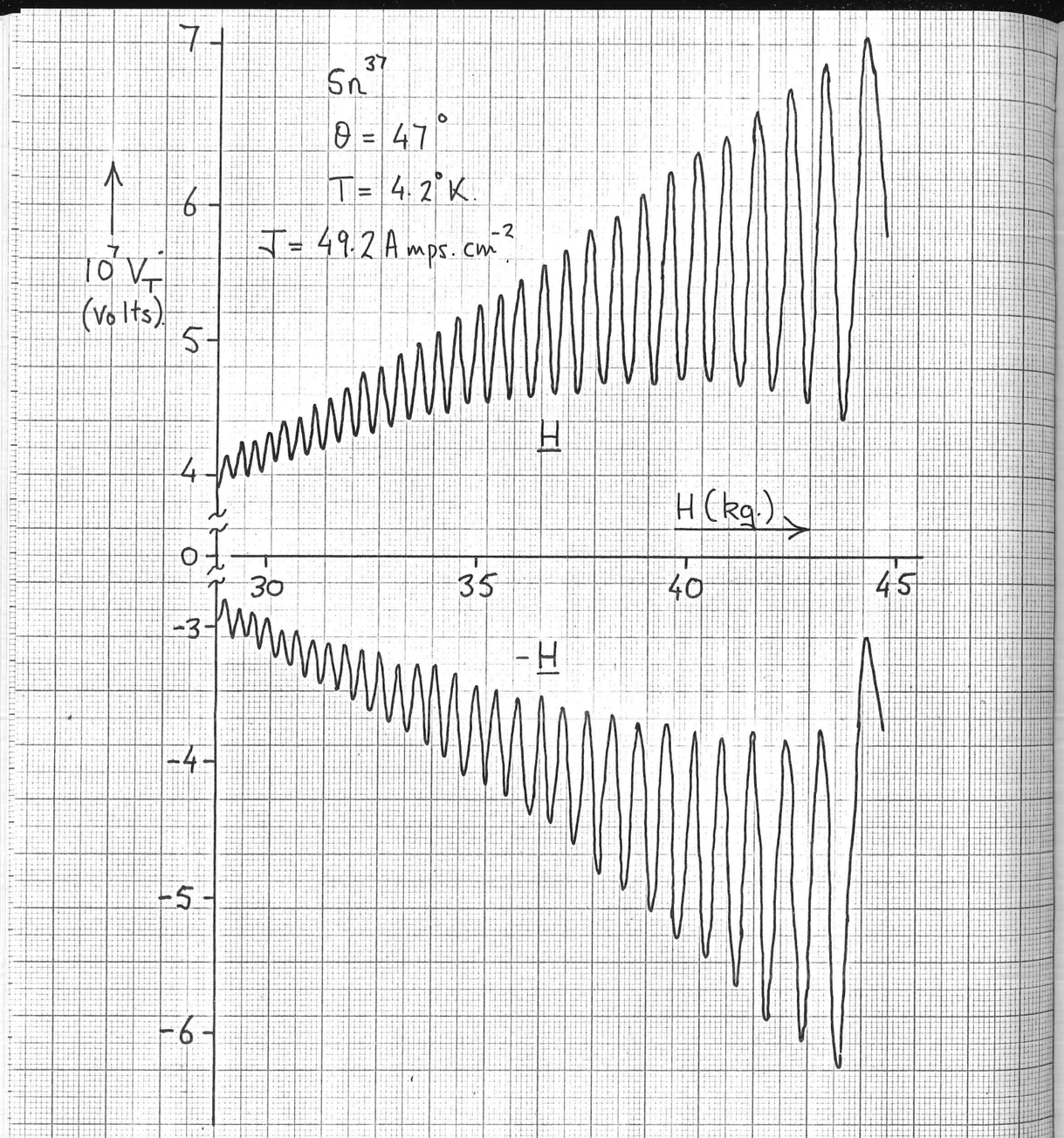

Fig. 5-13. Experimental record of transverse voltage, V_T, versus magnetic field showing that the phase of the oscillations remains unchanged when $\underline{H}$ is reversed.

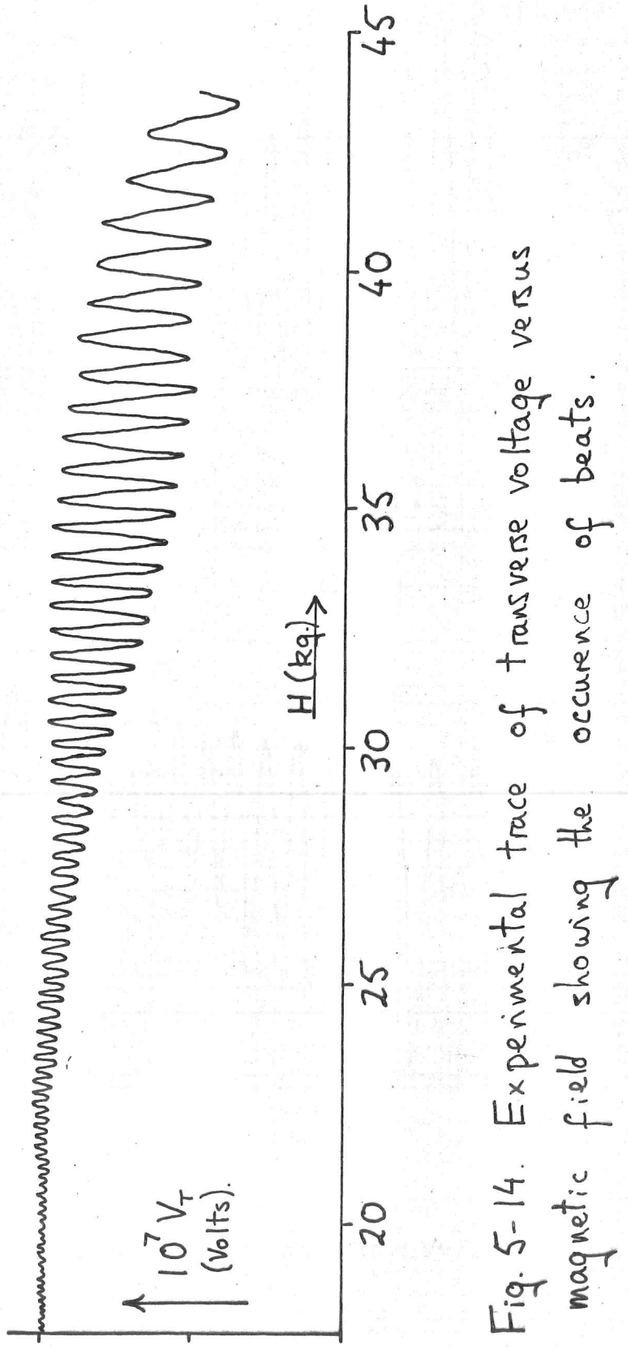

Fig. 5-14. Experimental trace of transverse voltage versus magnetic field showing the occurence of beats.

swept in the same direction in both cases, it was found that oscillations in the range $\theta = 20.5^\circ$ to $\theta = 37^\circ$ reversed phase when $\underline{H}$ was reversed. The phase of the oscillations in the range $\theta = 38^\circ$ to $\theta = 51^\circ$ remained unchanged when the field was reversed. Experimental traces for two opposite directions of field at $\theta = 21^\circ$ and $\theta = 47^\circ$ are shown in figs. 5-12 and 5-13. A further point of interest that is clear from figs. 4-7, 5-12, 5-13 is that the envelope of the oscillations at $\theta = 47^\circ$ has a different shape from those enclosing the oscillations at $\theta = 21^\circ$ or $\theta = 0.7^\circ$.

In the range $\theta = 26^\circ$ to $\theta = 37^\circ$, beats occur in the oscillations as illustrated in fig. 5-14. The two frequencies giving rise to the beats differ only by about 3%; for example, at $\theta = 29^\circ$, the two frequencies are $(0.210 \pm 0.004) \times 10^7$ g. and $(0.203 \pm 0.004) \times 10^7$ g. They both correspond closely to that expected for the δ orbit at $\theta = 29^\circ$.

Theory 5-3a) The occurence of oscillations, odd in $\underline{H}$, in the region $\theta = 20.5^\circ$ to $\theta = 37^\circ$.

The value of θ at which these oscillations first appear is close to that at which the linking of open orbits on the fourth zone surface via the δ orbits can first occur. Let us see whether this is capable of producing oscillations in ρ_{yx} which are odd in $\underline{H}$.

Let us consider first a linear chain of coupled hole orbits as shown in fig. 5-15. If an electric field, $\underline{E}$, is applied parallel to

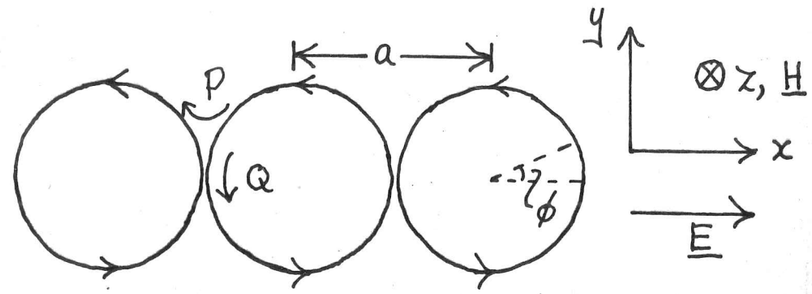

Fig. 5-15. A chain of linked hole orbits.

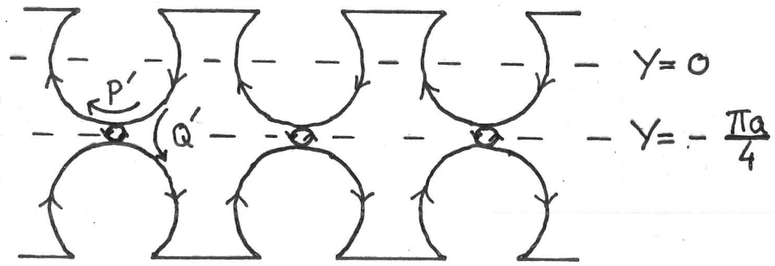

Fig. 5-16. The linking of two periodic open orbits to form a linear chain of linked hole orbits. To evaluate the conductivity we take as a model the chain of fig 5-15 but with P, Q replaced by P', Q', where

$$P' = \frac{2Q}{1+Q}, \quad Q' = \frac{P}{1+Q}$$ (Young (4)).

the x direction then electrons are "created" (23) at the point ϕ on the orbit at a rate proportional to E Sinϕ dϕ. If scattering is allowed for by including a relaxation time, τ, then Young (21) has shown that the effective paths in the x and y directions are given by

$$X = \frac{aP}{2Q} + \frac{a}{2\omega\tau}$$

$$Y \doteq \frac{-\frac{1}{2}aQ\omega\tau}{1 + 2Q\omega\tau/\pi} + O\left(\frac{1}{\omega\tau}\right) \qquad (5\text{-}2)$$

Now breakdown by mode A links two periodic open orbits on the fourth zone hole surface into a linear chain of coupled hole orbits as shown in fig. 5-16. Young (4) shows that if we ignore all phase coherence effects on the δ orbit, then it may be replaced by a transmission doefficient Q' = P/(1 + Q) and a reflection coefficient P' = 2Q/(1 + Q). The chain of coupled orbits in fig. 5-16 is thus the same as that of fig. 5-15 if we replace P by P' and Q by Q'. Thus from (5-2) we have that

$$X = \frac{aQ}{P} + \frac{a}{2\omega\tau}$$

$$Y \doteq \frac{-\frac{1}{2}a\omega\tau P}{1 + Q + 2P\omega\tau/\pi} + O\left(\frac{1}{\omega\tau}\right) \qquad (5\text{-}3)$$

X and Y determine the conductivity components σ_{xx} and σ_{yx} respectively. From (5-3) we see that when P = 0, Y = 0 to lowest order in $\frac{1}{H}$ but that when P = 1, Y = $-\frac{1}{4}\pi a$ and the particles have their mean terminal point on

the centre line as shown in fig. 5-16. Thus the linking of the open orbits to form closed orbits leads to a modified value of the Hall conductivity σ_{yx}. Also when phase coherence exists around the δ orbit the transmission and reflection coefficients will oscillate at the de Haas-van Alphen frequency of the orbit and thus σ_{yx} will oscillate. Similarly it is clear from (5-3) that the open orbit conductivity, determined by X, will oscillate. Now, when H is tipped some way from [001] so that the open orbit conductivity is large, then

$$(\rho_{yx})_{odd} = \frac{(n_- - n_+)\, e\, H}{\sigma'(n_-\gamma_- + n_+\gamma_+) + e^2(n_- - n_+)^2}$$

Thus when the open orbits are linked to form a linear chain of closed hole orbits we expect to see oscillations in the Hall voltage, due to the oscillations in n_+ and σ', which reverse phase when H reverses i.e. which are odd in H. This will clearly be so even if the open orbits are aperiodic.

The maximum in the oscillation amplitude at $\theta = 21^\circ$ occurs because it is only here that all the orbits get linked by breakdown in or very close to the central (001) plane where the cross-section of the δ orbit is an extremum. As θ is increased, breakdown can occur further from the central (001) plane and as we have seen before, the oscillatory properites vary with height above the central plane. This leads to a smearing out of the oscillations with a consequent reduction in amplitude. This also explains why no oscillations are seen at $\theta = 16^\circ$

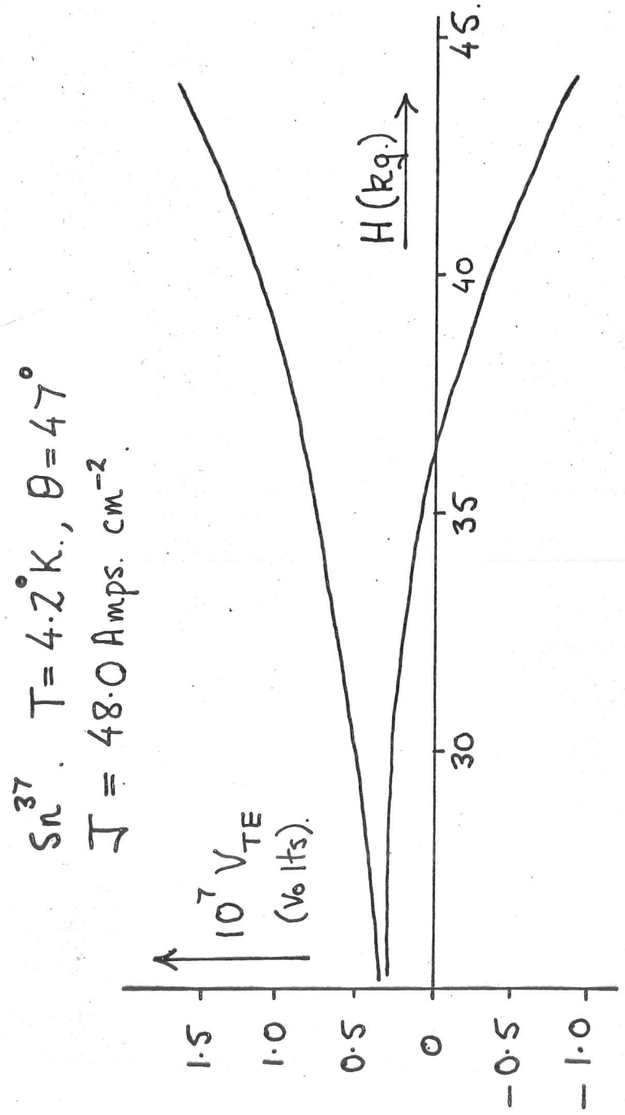

Fig. 5-17. The envelope of the oscillations in the transverse even voltage, V_{TE}.

where breakdown by mode C occurs. As is clear from fig. 1-18, breakdown occurs well away from the extremal cross-section of the orbit.

5-3b½ The occurrence of oscillations in the transverse voltage in the region $37^\circ < \theta \leq 51^\circ$.

The oscillations in this region reverse phase when H is reversed and hence must occur in the transverse even voltage. A graph showing the envelope of the oscillations in the transverse even voltage at $\theta = 47^\circ$ is shown in fig. 5-17 and it is seen that at the higher fields the sign of the transverse even voltage also oscillates. Now the transverse even field is given by

$$\frac{(P_{yx})_{even}}{J} = \frac{\delta' H^2 \sin\phi \cos\phi}{\delta'(n_- y_- + n_+ y_+) + e^2(n_- - n_+)^2}$$

where ϕ is the angle between the open orbit direction in real space and the projection of J on the plane perpendicular to H. Clearly the transverse even voltage will reverse sign when ϕ reverses sign. Thus the oscillations would be accounted for if there was some mechanism of breakdown involving the δ orbit, which led to the formation of open orbits whose mean direction was swung from side to side about the direction of J, as indicated below.

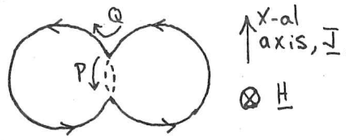

Fig. 5-19. Breakdown of an extended hole orbit to two coupled hole orbits.

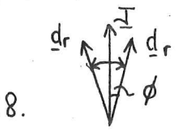

Fig. 5-18. The swinging of the open orbit direction, dr, in real space from side to side of the current direction (// to X-al axis).

However, the only breakdown that is expected to occur is that which occured in the range $\theta = 20.5^{\circ}$ to $\theta = 37^{\circ}$ except that for $\theta > 37^{\circ}$, the effect of this is solely to convert each extended hole orbit into two coupled hole orbits as illustrated above (fig. 5-19). Also, since for $\theta > 37^{\circ}$, R_H is almost independent of H, it seems that particles on extended hole orbits do behave as if they were on closed orbits not open orbits. Thus it does not seem possible that such a breakdown process could produce an oscillatory open orbit conductivity, let alone an open orbit whose direction swung from side to side of J. Thus the oscillations in the transverse even voltage in the region $37^{\circ} < \theta \leq 51^{\circ}$ remain unaccounted for.

The appearance of beats in the region $\sim 26^{\circ} < \theta < 37^{\circ}$ due to the occurence of oscillations of two frequencies, both very close to that of the δ orbit, is also unaccounted for.

Fig 5-20 Dependence of Transverse Magnetoresistance, ρ_{xx}, on $\angle\theta$.
$T = 4.2°K$ $J = 44.5$ Amps. cm^{-2}, $t = 0.6$ cm

• Sn^{11}
× Sn^{25}
⊙ Sn^{37}

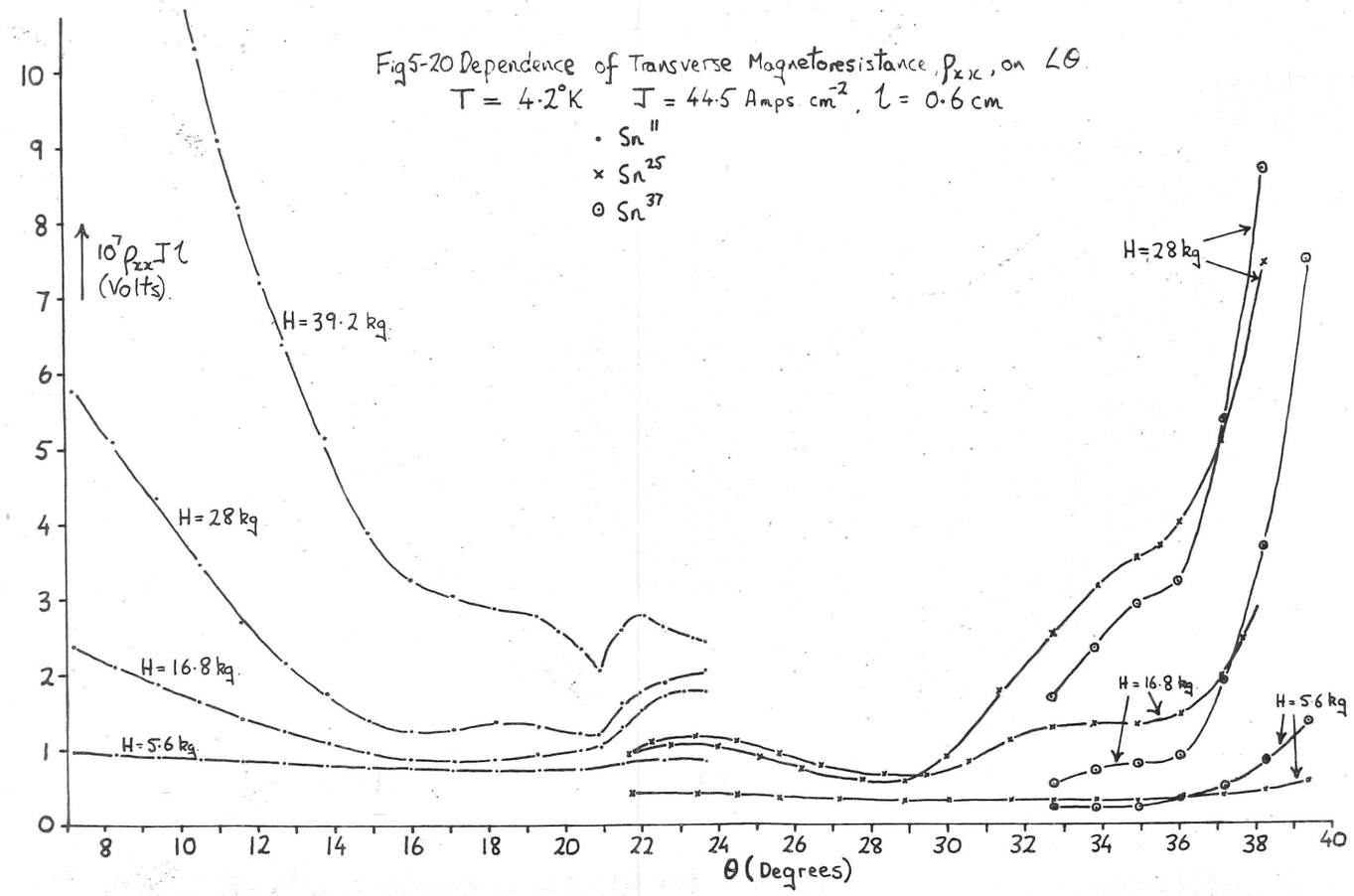

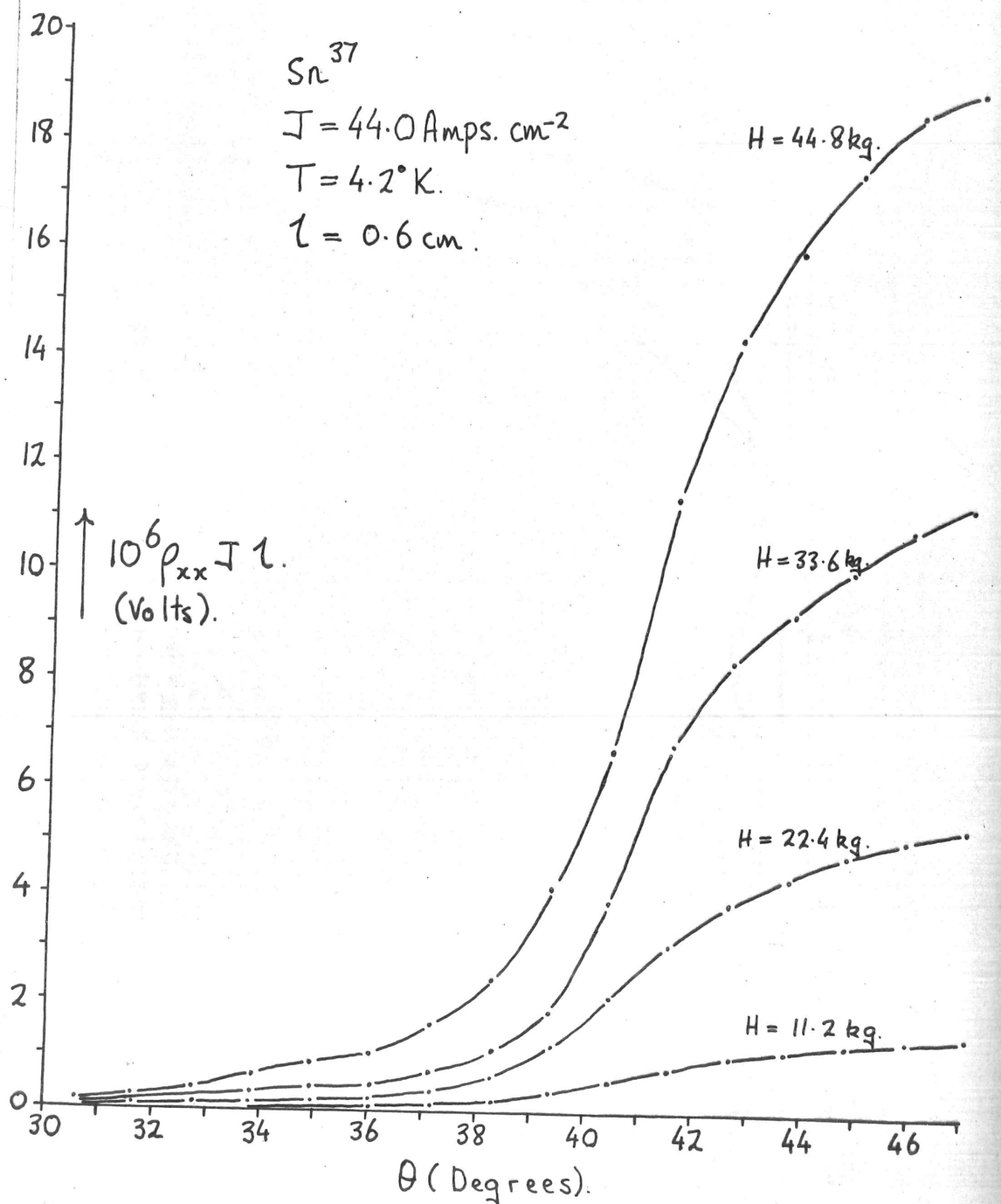

Fig. 5-21. Dependence of the transverse magnetoresistance on θ for various values of H.

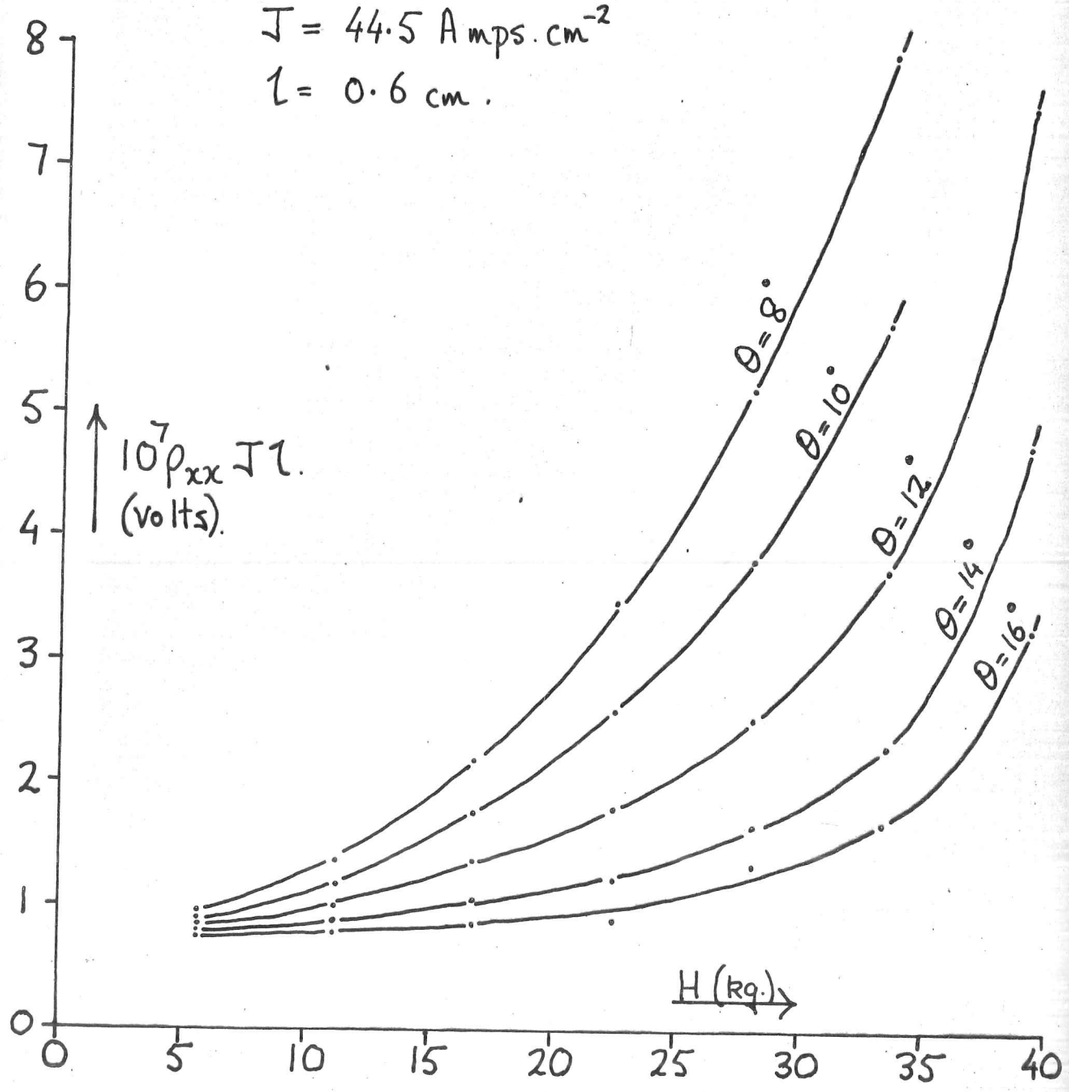

Fig. 5-22. Dependence of transverse magnetoresistance on H for various values of θ.

Sn^{25}

$T = 4.2°K.$

$J = 44.5$ Amps. cm^{-2}

$l = 0.6$ cm.

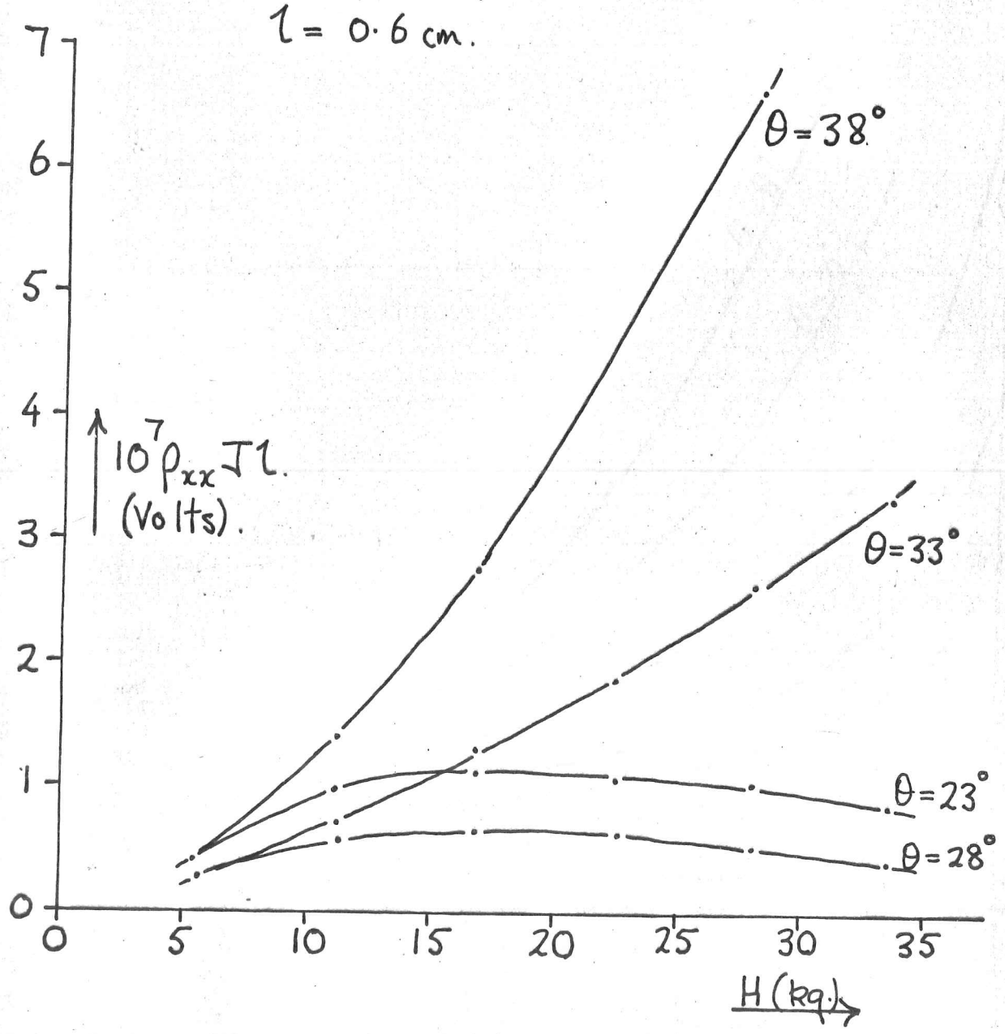

Fig. 5-23. Dependence of ρ_{xx} on H for various θ values.

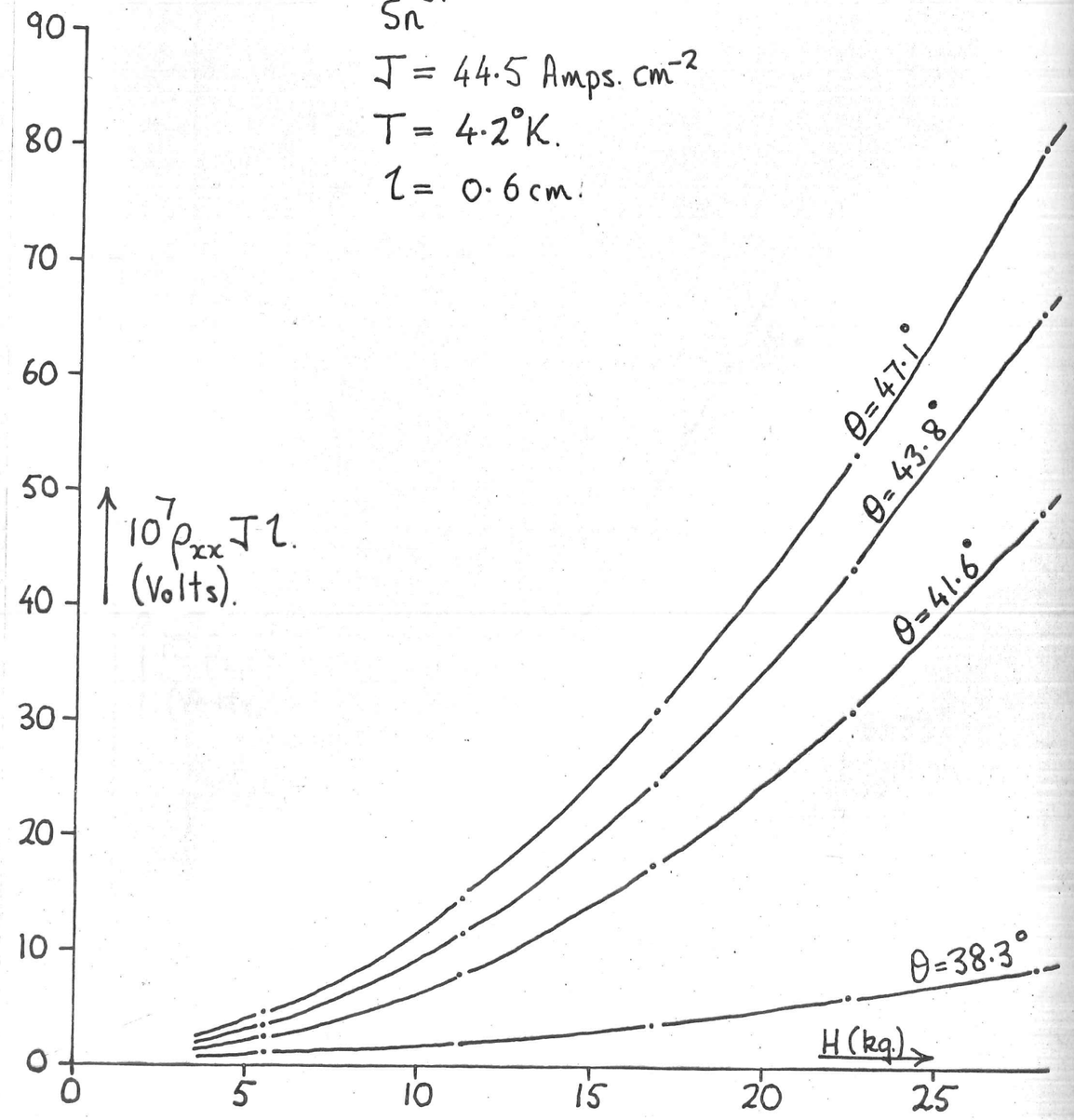

Fig. 5-24. Dependence of transverse magnetoresistance, ρ_{xx}, on H for various values of θ.

5-4) Dependence of the transverse magnetoresista nce, ρ_{xx}, on θ and H in the range $8^\circ \leq \theta \leq 47^\circ$.

The measurements were made on Sn^{11}, Sn^{25} and Sn^{37}. Each crystal was first oriented such that H lay close to, or in, the plane defined by J and [001]. Each crystal was then tipped about an axis approximately perpendicular to J and H. Thus H remained close (within about $\pm 1^\circ$) to the plane defined by J and [001], and so the angle between H and [001] may be taken to be approximately the same as the angle θ between [001] and the projection of H on the plane defined by J and [001].

Measurements of ρ_{xx} were made in constant magnetic field and for one direction of H only.

Figs. 5-20 and 5-21 show the dependence of ρ_{xx} on θ for various values of H, in the region $8^\circ \leq \theta \leq 47^\circ$. The dependence of ρ_{xx} on H for various values of θ is shown in figs. 5-22, 5-23, 5-24. It seems likely that there is a zero error of about 0.8×10^{-7} volts. in the values of $\rho_{xx} l J$ for Sn^{11}. This is shown up in fig. 5-22.

5-4a) Behaviour of ρ_{xx} in the region $8^\circ \leq \theta < 15^\circ$

In this region ρ_{xx} is approximately proportional to H^2 and its value at a given field decreases as θ increases. Now, H does lie exactly in the

plane defined by J and [001], so that we have from equation (1-4)

$$\rho_{xx} = \frac{(n_- \gamma_- + n_+ \gamma_+) + \gamma' H^2 \sin^2\phi}{\gamma'(n_- \gamma_- + n_+ \gamma_+) + e^2 (n_- - n_+)^2} \qquad (5\text{-}4).$$

ϕ will not be zero if H lies outside the plane, P, defined by J and [001] and ρ_{xx} will be proportional to H^2. Also we have seen in chapter 4 that increasing the angle θ causes the angle ϕ to decrease when H lies outside the plane P. Thus we expect ρ_{xx} to decrease as θ increases, as is observed.

5-4b) Behaviour of ρ_{xx} in the region $15^\circ \leq \theta \leq 47^\circ$.

In the region $15^\circ < \theta < 20^\circ$, ρ_{xx} increases very sharply with increasing H for H > 28kg. This is the region in which we expect breakdown by mode C to occur leading to a decrease in γ' and n_-, and an increase in n_+. In the region $20.5 \leq \theta \leq 37^\circ$ we expect breakdown by mode A to occur, causing a further decrease in γ' and increase in n_+. We expect the effects of this to be seen in fields greater than about 5kg, and to produce a change in ρ_{xx} similar to that produced in the region $15^\circ < \theta < 20^\circ$. However we see from fig. 5-23, that for H > 10kg, ρ_{xx} decreases slightly as H increases. It is difficult to see how these two forms of behaviour can be reconciled.

Beyond $\theta = 30^\circ$, ρ_{xx} starts increasing again with H but as is clear from fig. 5-20 it is only beyond about $\theta = 36^\circ$ that an H^2 dependence of

ρ_{xx} sets in. Now evidence has been found to suggest that the limit of aperiodic open orbits on the fourth and fifth zone surface occurs at $\theta \doteq 37^{\circ}$. Also when no open orbits occur, tin is compensated as confirmed by Alekseevskii et al. (5). It is well known (22) that for a compensated metal ρ_{xx} is proportional to H^2. Thus the present measurements confirm that $\theta \doteq 37^{\circ}$ marks the limit of aperiodic open orbits on both surfaces.

Conclusions.

When $\underline{H}$ is parallel to $[001]$, the oscillatory and non-oscillatory behaviour of the Hall voltage has provided evidence for the formation of a two dimensional network of coupled orbits and allowed us to estimate the variation of the breakdown field with height above the central (001) plane.

We have seen that when $\underline{H}$ is tipped away from $[001]$, oscillations can still occur in the Hall voltage provided the breakdown strip is wide enough and Pippard's theory accounts for this.

Good evidence for the occurence of breakdown by modes A and C, as proposed by Young (4), has been found and we have seen that the linking of two open orbits to form a linear chain of coupled orbits can produce oscillations in the Hall voltage. Evidence confirming the interpretation of anomaly I as marking the limit of aperiodic open orbits on both fourth and fifth zone surfaces has also been found.

Some results which remain unexplained are:-

1) The decrease in the Hall coefficient, R_H, with increasing field strength in the region $15^\circ > \theta > 2^\circ$.

2) The non-zero value of R_H in the region $51^\circ > \theta > 37^\circ$.

3) The occurence of two frequencies, both close to that for the δ orbit, in the oscillations in the region $37^\circ > \theta > 26^\circ$.

4) The occurence of oscillations in the transverse even voltage in the region $51^\circ > \theta > 37^\circ$, the amplitude of the oscillations having a very sharp maximum at $\theta = 47^\circ$.

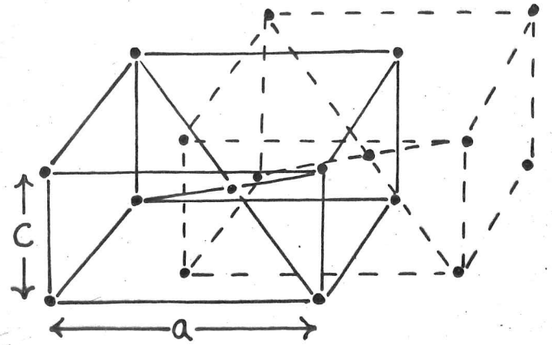

Fig. A1-1.

Real lattice structure of tin. (not to scale).

$a = 5.80$ Å, $c = 3.15$ Å.

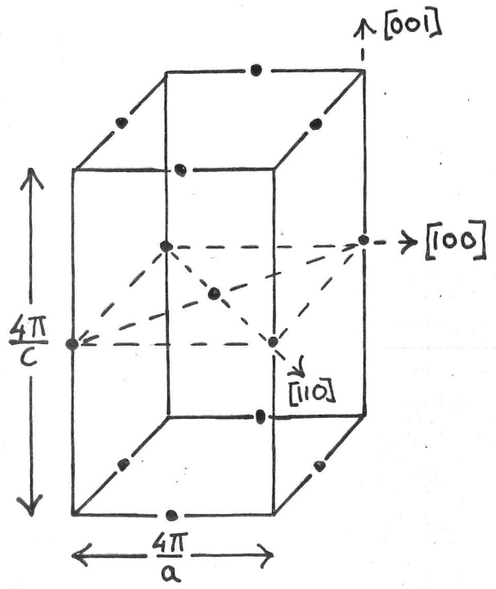

Fig. A1-2.

Reciprocal lattice structure of tin. (not to scale).

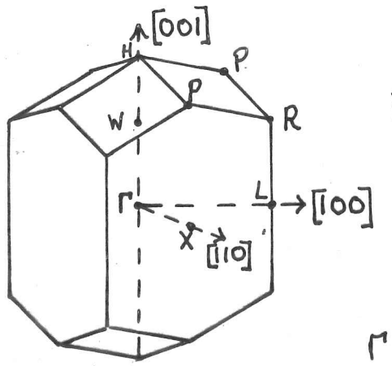

Fig. A1-3. The primitive Brillouin zone of tin. The coordinates of the points marked are as follows (in units of $2\pi/a$):-

Γ (0, 0, 0) ; L (1, 0, 0) ; H(0, 0, 1·19);
X (0·5, 0·5, 0); P (0·5, 0·5, 0·92).

Appendix I. Construction of the Fermi surface of tin.

A1-1) Harrison's method of constructing the Fermi surface.

This method is based on the principle that the energy in a given band is a continuous function of k with the period of the reciprocal lattice.

If the perturbing potential in the N.F.E. scheme is very small then the energy surfaces must be spheres. Thus, about each point of the reciprocal lattice is drawn a sphere of radius such that it accommodates all the electrons per smallest unit cell of the real lattice. Out of this pattern various parts are chosen that can be fitted together continuously to make surfaces that repeat in each zone. Each of these then constitutes a branch of the Fermi surface in the 1st, 2nd, zone etc. The zone number at any point is equal to the number of spheres in which that point lies.

To calculate the sphere radius we need to consider the real and reciprocal lattice structures for tin.

Real lattice structure.

The crystal structure can be regarded as being made up of two interpenetrating body-centred tetragonal unit cells as shown in fig. A1-1. Each b.c. tetragonal unit cell can in turn be constructed from unit cells each containing one atom. Thus, the smallest unit

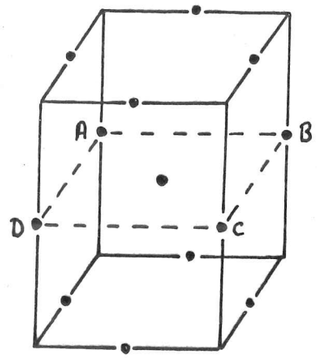

Fig.AI-4a. A unit cell of the reciprocal lattice structure. The dotted lines indicate the plane in which the section below is taken.

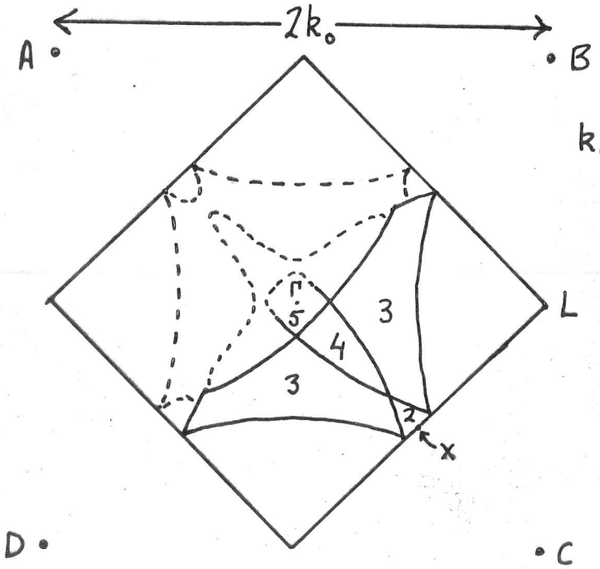

Fig.AI-4b. Zone contours in the (001) plane containing the points Γ, X, L. The dotted lines illustrate the effect of including the electrostatic lattice potential. The zone number in any region indicates the highest zone containing electrons there.

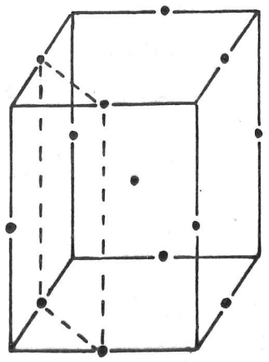

Fig.A1-5a. The reciprocal lattice structure. The dotted lines indicate the plane in which the section below is taken.

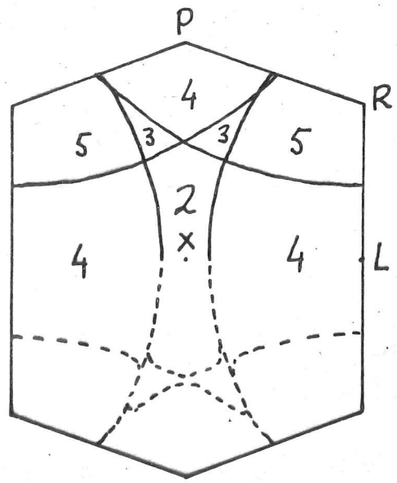

Fig.A1-5b.
Zone contours in the (110) section containing the points P, R, L, X.

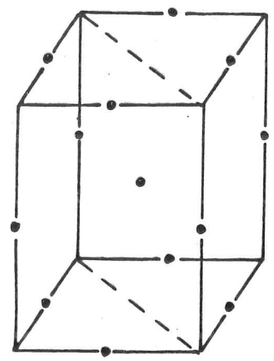

Fig.A1-6a. The dotted lines indicate the plane in which the section opposite is taken.

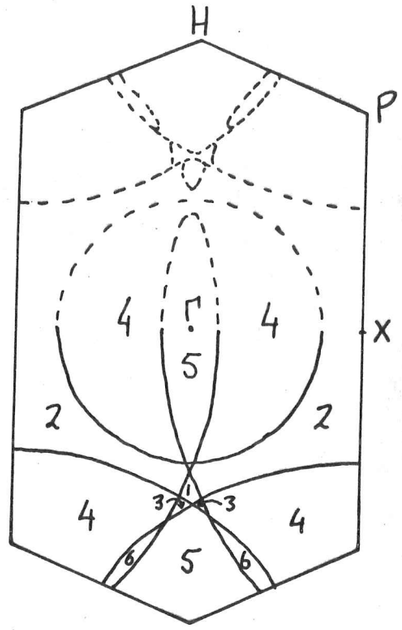

Fig.A1-6b. Zone contours in the (110) section containing H, P, X, Γ.

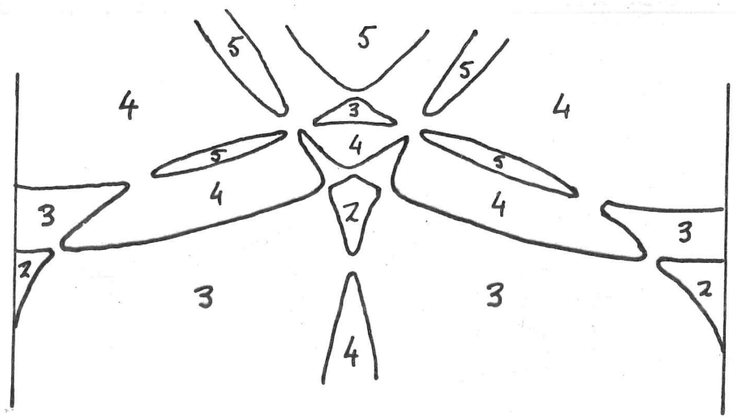

Fig. A1-6c. The region near W in the (110) section parallel to that above, but taken a distance $\frac{\pi}{5a}$ away from Γ. The corners have been rounded off.

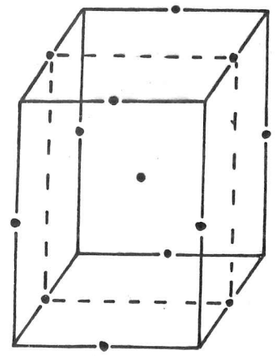

Fig. A1-7a. The dotted lines indicate the plane in which the section opposite is taken.

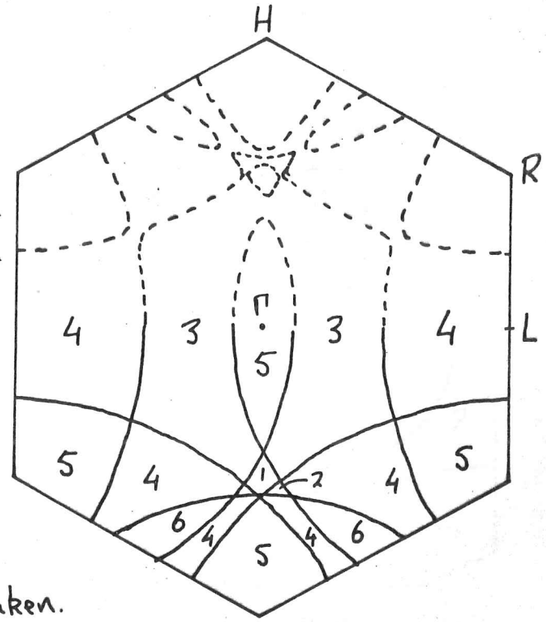

Fig. A1-7b. Zone contours in the (100) plane containing H, R, L, Γ.

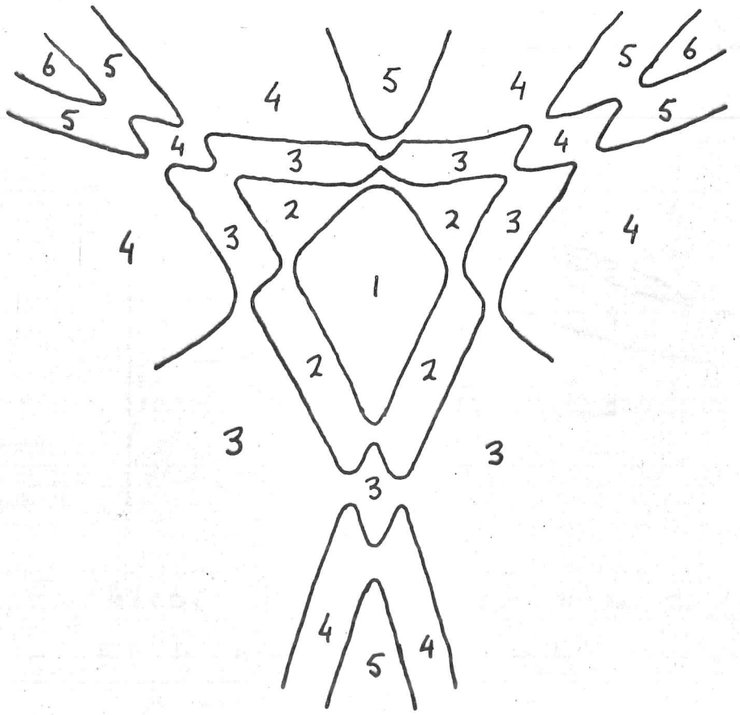

Fig. A1-7c. The region near W in the (100) section parallel to that above, but taken a distance $\frac{\pi}{20a}$ from Γ. The corners have been rounded off.

cell of the real lattice of tin will contain two atoms.

Reciprocal lattice structure and Brillouin zone.

Since the real lattice can be constructed from body-centred tetragonal unit cells, the reciprocal lattice can be made up of tetragonal face-centred unit cells as shown in fig. A1 -2. The Brillouin zone, being the Wigner-Seitz cell of the reciprocal lattice is thus as shown in fig. A1 -3, and its volume is $\frac{1}{4} \cdot \frac{a}{c}\left(\frac{4\pi}{a}\right)^3$. Now, the smallest unit cell of the real lattice contains two atoms, and the Brillouin zone can hold two electrons per smallest unit cell of this lattice. Tin has four valence electrons per atom and thus a sphere in K-space containing all the electrons per smallest unit cell of the real lattice will have a volume $\frac{a}{c}\left(\frac{4\pi}{a}\right)^3$ and hence a radius 0.75 $\frac{4\pi}{a}$. This sphere completely encloses the first zone so that the Fermi surface lies entirely in higher zones in the extended zone scheme.

Figs. A1 -4 to A1 -7 show the patterns produced in various cross sections through the Brillouin zone when spheres of the above radius are drawn about the reciprocal lattice points. These figures illustrate how the various surfaces shown in fig. 1 -1 arise and how they fit together. In fig. 1 -1, sharp corners have been rounded off as would be expected to be the case, due to the mixing of states associated with Fourier components of the potential.

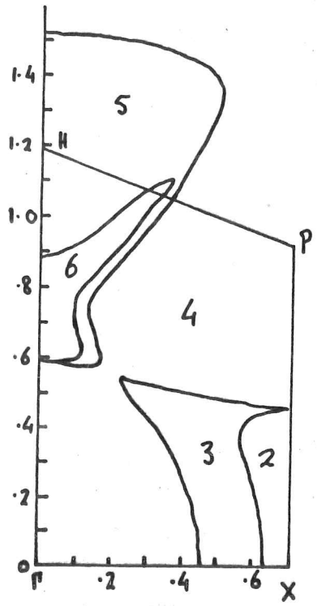

Fig. A1-8. Zone contours in the Γ X P H plane, according to Weisz (2). The dimensions are in units of 2π/a.

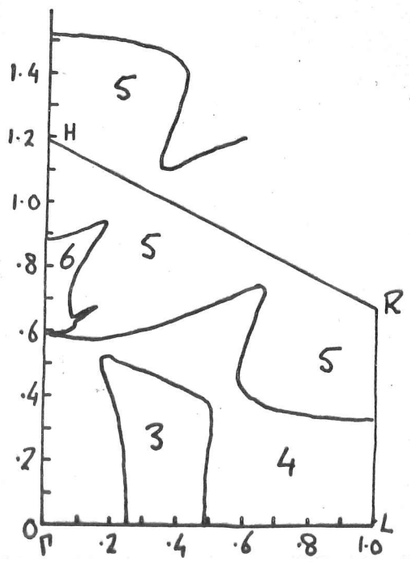

Fig. A1-9. Zone contours in the Γ L R H plane, according to Weisz.

A1-2) Weisz' model of the Fermi surface.

Weisz (2) has calculated the Fermi surface using an orthogonalized-plane-wave approach. He found it to differ from the N.F.E. model shown in fig. 1 -1 in the following ways:-

i. Zone 2: the hole surface at W is removed.

ii. Zone 3: the hole cylinders extending from W are destroyed, leaving only cylinders extending along lines XP

iii. Zone 4: electrons are introduced along ΓH near W so that there is a region connecting the electrons of the forth zone electron surface (double pancake) to those outside the open forth zone hole surface.

iv. Zone 5: The 'cigar' around Γ is removed.

v. Zone 6: The 'cigar' around V is removed and the 'cigars' near W are amalgamated into a vertical shape of square cross section with slight prongs in the direction of the original cigars.

Some contours of the Fermi surface, deduced by Weisz, are shown in figs. A1 -8 and A1 -9.

Appendix 2. An expression for the conductivity in terms of the effective path.

The conductivity of random networks where phase relationships may be ignored, can be calculated by the effective path method of Pippard (23). In this method the steady displacement of the distribution function in k-space by an electric field is replaced by the continuous generation of new particles at the Fermi surface. An element of Fermi surface $d\underline{S}$ by its displacement sweeps out a volume $e\underline{E} \cdot d\underline{S} / \hbar$ in unit time and generates new particles at a rate $e\underline{E} \cdot d\underline{S} / (4\pi^3 \hbar)$. These particles then move through the metal and are scattered, ultimately travelling a distance $\underline{L}$ from their point of origin. $\underline{L}$ is the effective path, and the current set up by $\underline{E}$ may be written

$$\underline{J} = \frac{e^2}{4\pi^3 \hbar} \int \underline{L} \, (\underline{E} \cdot d\underline{S})$$

Clearly,

$$\sigma_{ij} = \frac{J_i}{E_j} = \frac{e^2}{4\pi^3 \hbar} \int L_i \, dS_j$$

References

1. A. V. Gold and M. G. Priestley, Phil. Mag. 5, 1089, (1960)

2. G. Weisz, Phys. Rev. 149, 504, (1966)

3. V. F. Gantmaker, Zh.Eksperim, i. Teor. Fiz. 44, 811 (1963). 46, 2028, (1964) English transls. Soviet Phys.-JETP, 17, 549, (1963); 19, 1366, (1964)

4. J. G. Anderson and R. C. Young, Phys. Rev. 168, 696, (1968)

5. N. E. Alekseevskii, Yu.P.Gaidukov, I. M. Lifshitz, V. G. Pechanskii, Zh. Eksperim. i.Teor. Fiz. 39, 1201, (1960) English transl. Soviet Phys - JETP. 12, 837,(1961)

6. R. W. Stark and L. M. Falicov, Prog. in Low Temp. Physics 5, 20 (1968)

7. A. A. Slutskin Zh. Eksperim.i.Teor.Fiz. 53, 767, (1967) English transl: Soviet Phys.-JETP 26,474, (1968).

8. J. M. Ziman. Principles of the theory of solids (C.U.P.)

9. A. B. Pippard. Proc. Roy.Soc. A270, 1, (1962).

10. A. B. Pippard. Phil.Trans. A256, 317, (1964)

11. A. B. Pippard, Proc. Roy.Soc. A287, 165, (1965)

12. J. O. Ström-Olsen, To be published.

13. R. W. Stark and J. E. Craven, Phys. Rev. 168, 849, (1968)

14. R. C. Young, Phil Mag. 18, 201, (1968)

15. D. Hays and W. L. McLean, Phys. Rev. 168, 755, (1968)

16. W. C. Dash, J.Appl. Phys. 30, 459, (1959)

17. C. Elbaum, Phil. Mag. 5, 669, (1960)

18. S. Howe and C. Elbaum, Phil.Mag. 6, 1227, (1961)

19. V. N. Kachinskii, Zh. Eksperim.i.Teor.Fiz. 43, 1158, (1962)
English transl.:Soviet Phys - JETP 16,818 (1963)

20. R. C. Young, Phys.Rev. 152, 659, (1966)

21. R. C. Young Phys.Rev. 163, 676, (1967)

22. E. R. Fawcett, Advances in Physics 13, 139, (1964)

23. A. B. Pippard, Proc.Roy.Soc. A282, 464, (1964).